THE RHEOLOGY AND PHASE SEPARATION KINETICS OF MIXED-MATRIX MEMBRANE DOPES

A Dissertation
Presented to
The Academic Faculty

by

Kayode Olaseni Olanrewaju

In Partial Fulfillment
of the Requirements for the Degree
Doctor of Philosophy in the
School of Chemical & Biomolecular Engineering

Georgia Institute of Technology
May 2011

THE RHEOLOGY AND PHASE SEPARATION KINETICS OF MIXED-MATRIX MEMBRANE DOPES

Approved by:

Dr. Victor Breedveld, Advisor
School of Chemical & Biomolecular Engineering
Georgia Institute of Technology

Dr. David Bucknall
School of Materials Science and Engineering
Georgia Institute of Technology

Dr. William J. Koros
School of Chemical & Biomolecular Engineering
Georgia Institute of Technology

Dr. Martha Grover
School of Chemical & Biomolecular Engineering
Georgia Institute of Technology

Dr. Carson Meredith
School of Chemical & Biomolecular Engineering
Georgia Institute of Technology

Date Approved: January 4, 2011

In loving memory of my father
John Diran Olanrewaju
(June 5, 1941- April 14, 2002)

Daddy, this one is for you!

ACKNOWLEDGEMENTS

The completion of this thesis work is a consequence of the encouragements, support and guidance I have received from several people.

I am very grateful to my thesis advisor, Dr. Victor Breedveld, for his support both professionally and personally throughout my graduate studies under him. I was privileged to have unparalleled access to him through the various philosophies I pondered while in residence. His wisdom and dedication to his art served as a catalyst to my mastery of the tools our trade. I am grateful to Dr. Bill Koros for unlimited access to his lab's resources and for his insightful and practical advice which I found very helpful in the construction of my thesis. I am also grateful to my other thesis committee members; Dr. Carson Meredith, Dr. David Bucknall, and Dr. Martha Grover for their invaluable advice. Their suggestions and insights helped improved my thesis. I am very grateful to Dr. Sven Behrens who made his lab resources available to me, in addition to the many discussions we had on colloidal phenomena. I count myself very fortunate to have had this association with him. I am indebted to Dr. Vikram Prasad of The Dow Chemical Company who was a postdoctoral fellow in our lab during my graduate studies. His friendship in good and bad times and experience in the lab was a great catalyst to my research progress.

I am grateful to past lab colleagues: Dr. Jae-Kyu Cho, Dr. Balamurali Balu and Dr. Santosh Rahane for their assistance and encouragement especially during those crucial first few research semesters in residence. I am also grateful to Tracie Owens, Emily

Peterson, Kyung-Hee Oh, Lester Li for their companionship in the lab. I would also like to acknowledge Yichen Fang and Ryan Collins; undergraduate research students who worked with me on PSK and Rheology experiments respectively.

David Kadjo, Biodun Otolorin, Lateef Yusuf, Ogechi Nnadi, Ikpeme Erete, Babajide Olanrewaju, Moyin Abiodun, Mercy Changwesha, Leye Alabi, Travis Hoskins, Omoyemen Esekhile, Dr. Leonard Nyadong, Dr. Dhaval Bhandari and Dr. Quinta Nwanosike and many other friends provided the necessary break from work which kept me positive and happy in good and trying times.

I am forever grateful to my parents, John and Sarah Olanrewaju who nurtured me and supported my dreams all these years. Although, they had very limited formal education they spared no expense in starting and supporting me on this path of academic achievements. The unwavering love and sacrifices of my parents and siblings; Wale, Iyabo, Sanya, Bisi, Jimmy and Seun Olanrewaju kept me solid and focused.

Finally, to the Creator and Omniscient God, the one who knew me before I was formed in my mother’s womb; this is Your doing and it is marvelous in my sight.

TABLE OF CONTENTS

LIST OF TABLES

LIST OF FIGURES

LIST OF SYMBOLS AND ABBREVIATIONS

η	viscosity
$[\eta]$	intrinsic viscosity
η_r	relative viscosity
ρ	density
α	solvent absorption coefficient
φ	volume fraction
w	weight fraction
$1/\kappa$	Debye length
ζ	zeta potential
U_e	electrophoretic mobility
χ	interaction parameter
D_{eff}	effective diffusion coefficient
D_{self}	self diffusion coefficient
a	particle radius
r_o	particles center to center distance
δ	hydrodynamic thickness or boundary layer

PSK	Phase separation kinetics
MMMs	mixed-matrix membranes
MMX	mixed-matrix

SUMMARY

Mixed-matrix hollow fiber membranes are being developed to offer more efficient gas separations applications than what the current technologies allow. Mixed-matrix membranes (MMMs) are membranes in which molecular sieves incorporated in a polymer matrix enhance separation of gas mixtures based on the molecular size difference and/or adsorption properties of the component gases in the molecular sieve. The major challenges encountered in the efficient development of MMMs are associated with some of the paradigm shifts involved in their processing, as compared to pure polymer membranes. For instance, mixed-matrix hollow fiber membranes are prepared by a dry-wet jet spinning method. Efficient large scale processing of hollow fibers by this method requires knowledge of two key process variables: the rheology and kinetics of phase separation of the MMM dopes. Predicting the rheological properties of MMM dopes is not trivial; the presence of particles significantly affects neat polymer membrane dopes. Therefore, the need exists to characterize and develop predictive capabilities for the rheology of MMM dopes. Furthermore, the kinetics of phase separation of polymer solutions is not well understood. In the case of MMM dopes, the kinetics of phase separation are further complicated by the presence of porous particles in a polymer solution. Thus, studies on the phase separation kinetics of polymer solutions and suspensions of zeolite particles in polymer solutions are essential. Therefore, this research thesis aims to study the rheology and phase separation kinetics of mixed-matrix membrane dopes.

In our research efforts to develop predictive models for the shear rheology of suspensions of zeolite particles in polymer solutions, it was found that MFI zeolite suspensions have relative viscosities that dramatically exceed the Krieger-Dougherty predictions for hard sphere suspensions. Our investigations showed that the major origin of this discrepancy is the selective absorption of solvent molecules from the suspending polymer solution into the zeolite pores. Consequently, both the viscosity of the polymer solution and the particle contribution to the suspension viscosity are greatly increased. A predictive model for the viscosity of porous zeolite suspensions incorporating a solvent absorption parameter, α, into the Krieger-Dougherty model was developed. We experimentally determined the solvent absorption parameter and our results are in good agreement with the theoretical pore volume of MFI particles. In addition, fundamental studies were conducted with spherical nonporous silica suspensions to elucidate the role of colloidal and hydrodynamic forces on the rheology of mixed-matrix membrane dopes.

Also in this thesis, details of a novel microfluidic device for measuring the phase separation kinetics of membrane dopes are presented. We have used this device to quantify the phase separation kinetics (PSK) of polymer solutions and MMM dopes upon contact with an array of relevant nonsolvent. For the polymer solution, we found that PSK is governed by the micro-rheological and thermodynamic properties of the polymer solution and nonsolvent. For the MMM dopes, we found that the PSK may increase with increase in particles surface area due to surface diffusion enhancement. In addition, it was found that the dispersed particles alter the thermodynamic properties of the dope based on the hydrophilicity and porosity of the particle.

CHAPTER 1

INTRODUCTION

A membrane can be defined as a selectively-permeable barrier that enables the separation of components in a multicomponent mixture based on differences in transport rates through the membrane. Polymeric membranes have been developed for a variety of industrial applications [1,2], including microfiltration, ultrafiltration, reverse osmosis and gas separations. Each application imposes specific requirements on the material and structure of the membrane. For instance, the separation efficiency in microfiltration and ultrafiltration is determined by membrane porosity and pore sizes, while gas separation efficiency is determined by the permeability and selectivity.

Gas separation by polymeric membranes is one of the fastest growing fields in membrane separations [3]. The great interest in membrane separations is a result of the economical advantages derived from membrane-based gas separations and the fact that gases are important feed stocks in most chemical industries. Lower capital and operating costs, lower process energy requirements and the general ease of operation of polymeric membrane separation units [4,5] are some of the incentives cited for membrane separation. Current industrial applications of membrane-based gas separations include oxygen and nitrogen enrichment, hydrogen recovery and natural gas separations. However, existing polymeric membranes are inadequate to fully exploit the full range of potential applications on an industrial scale. In polymeric membrane-based gas separations, enhancement of permeability is typically achieved at the expense of selectivity and vice versa [6,7].

Inorganic membranes formed from metals, ceramics or pyrolyzed carbon [8,9], are increasingly being explored for gas separation because of higher gas fluxes and selectivities compared to polymeric membranes. For inorganic membranes, a lot of the attention has been directed towards zeolites and carbon molecular sieves which possess significantly higher diffusivity enhanced selectivity than polymeric materials. The superior selectivity stems from the very narrow pore size distribution of molecular sieves which furnishes precise size and shape discrimination for the gas molecules in a mixture [14]. Zeolites can be classified based on different pore size regimes available for separations. The various classes, which include zeolites with large pores (Y-type, β [10,11]), medium pores (ZSM-5, FER [12,13]) and small pores (A-type, SAPO-44 [14-18]) are suitable for different gas pair separations. Despite the good selectivities associated with inorganic membranes, these materials are often brittle with poor mechanical properties, and thus very difficult to assemble into modules for industrial applications. To resolve some of the inherent disadvantages of the different classes of membranes, a lot of research in recent years has focused on the development of hybrid membranes that are composed of inorganic molecular sieves and organic polymers.

1.1 Mixed-matrix (MMX) hollow fiber membrane

The trade-off between selectivity and permeability in polymeric membranes mentioned in the previous section implies that an upper limit exists on the performance of polymeric membranes for gas separations; this was first predicted by Robeson [6] in 1990 and just recently revisited [7]. In order to improve the selectivity of polymeric membranes, hybrid membranes with zeolite particles dispersed in a polymer matrix have been prepared to achieve selectivities and permabilities that exceed the Robeson's curve limitation. Such

hybrid membranes are known as mixed matrix (MMX) membranes [19-28]. MMX membranes combine the excellent selectivities of inorganic sieves with the processability and mechanical strength of polymers. For MMX membranes, the hollow fiber configuration is usually desired because of the high surface area per unit volume it furnishes for separation and the resulting throughput per unit volume. Dual layer design is usually desired in order to minimize wastage of expensive inorganic particulates while creating a cheap support layer with better mechanical strength. Dual layer mixed matrix hollow fiber membranes (Figure 1.1) possess an outer selective layer (thickness up to 50 μm) made of zeolites dispersed in a polymer matrix, supported by a pure polymer layer (thickness up to 150 μm). The dope formulation for the selective layer therefore consists of zeolite particles dispersed in a polymer solution, while the support layer is created from a neat polymer solution. The spinning of dual layer MMXs dopes into hollow fibers of desired geometry and dimensions entails the tailoring of the rheology of the composite membrane dope formulations to achieve this goal. In fact, as will become apparent later, one the major goal of this thesis is to measure and establish model predictions for the rheology of MMX membrane dopes. The viscosity measurements are then used to inform the choice for important process variables [29,30] like the extrusion rate and draw ratio in hollow fiber spinning shown in Figure 1.2.

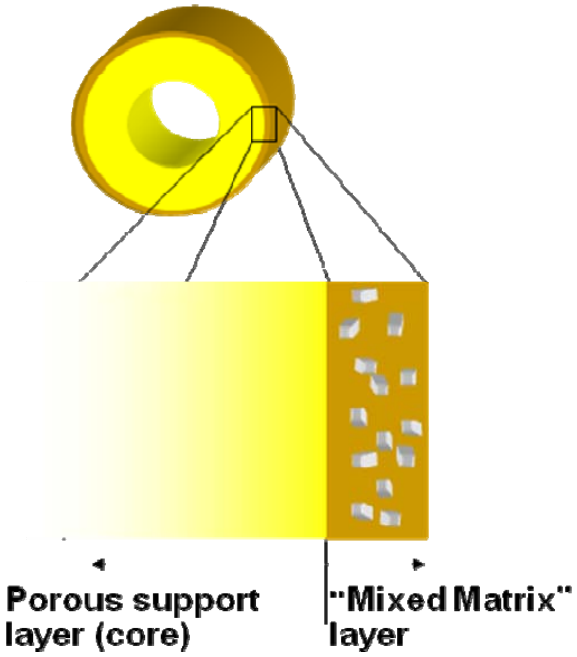

Figure 1.1 Schematic of a dual layer MMX membrane with a thick porous support layer underneath the selective layer.

1.2 Membrane formation by phase inversion processes

The techniques employed in preparing polymeric membranes include sintering, stretching and phase inversion processes. Despite the plurality of methods for membrane fabrication, majority of polymeric membranes are prepared by a controlled phase separation into two phases: a polymer-rich phase and a polymer-lean phase. The polymer-rich phase subsequently solidifies into the solid part of the membrane. Several methods have been employed to induce controlled phase separation during the preparation of polymeric membranes. ***Thermally induced phase separation (TIPS)*** [31-

35] is based on a decreasing solubility by decreasing polymer solution temperature. After demixing is induced by changing the solution temperature, the solvent can be removed by extraction, evaporation or freeze drying. ***Air-casting*** [36,37] of a polymer solution has also been used, and this entails dissolving polymers in a mixture of volatile solvent and less volatile nonsolvent. As the solvent vaporizes, the solubility of polymer decreases and phase separation is induced. ***Immersion precipitation*** [38] entails immersing an extruded or cast membrane dope into a liquid nonsolvent bath. Phase separation then occurs when the good solvent in the membrane dope is exchanged for nonsolvent from the bath. ***Dry-wet jet spinning*** (see Figure 1.2) is the preferred method for the spinning of MMX hollow fiber membrane. It is a combination of air-casting and immersion precipitation. The dope is often prepared so that a volatile component in the solvent mixture partially evaporates in the air gap to promote skin formation, while complete phase inversion into a solid fiber is completed in the nonsolvent bath. In this process, it is crucial that phase separation into solid fiber walls is complete before the fiber contacts the take-up drum in order to avoid crushing due to the high normal stress at take-up. Another important objective of this thesis is to develop methods to reliably quantify the time required for the phase separation of membrane dopes of desired thickness.

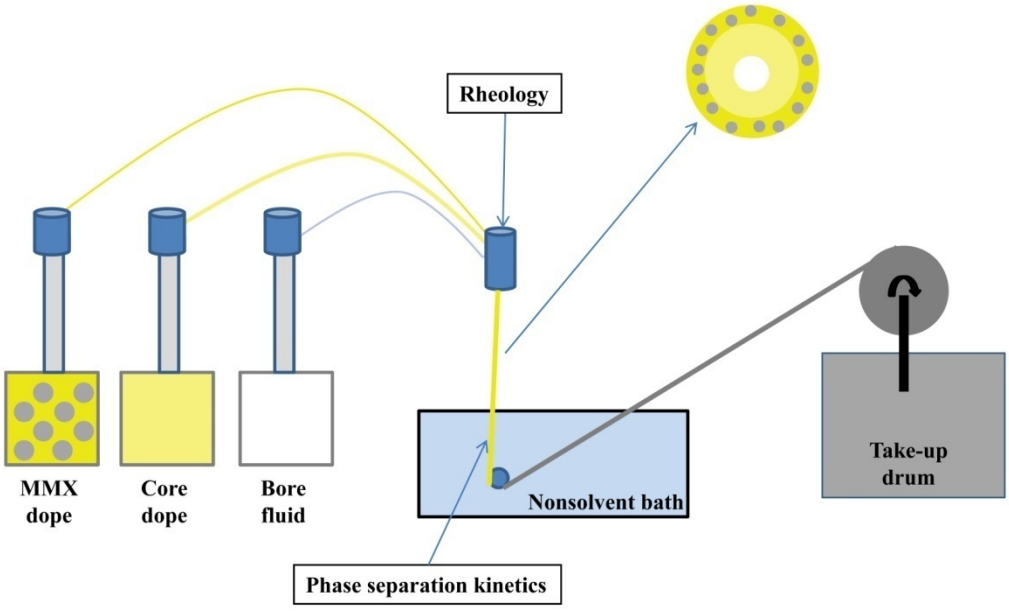

Figure 1.2 Spinning process of dual layer MMX hollow fiber membranes, indicating the role of dope rheology and phase separation kinetics.

1.3 Important theoretical and practical aspects of hollow fiber spinning

The consensus in the membrane literature is that the thermodynamic stability of membrane dopes with respect to phase separation determines the overall porosity of a polymeric membrane, while the kinetics of phase separation controls the average pore size and pore size distribution [2,39-49]. The subsections 1.3.1 and 1.3.2 provide a review of the thermodynamics and kinetics of phase separation in relation to membrane formation via phase separation of polymer solutions.

An efficient process design for the spinning of hollow fibers membrane requires quantification of the dope rheology, which is an important process design variable. The

rate of dope extrusion and draw ratio determine the thickness and outer diameter of hollow fibers. In subsection 1.3.3, the rheology of suspensions of dispersed particles is reviewed.

1.3.1 Thermodynamics of phase inversion of polymeric membrane solutions

Phase diagrams offer a convenient depiction of the thermodynamics of membrane dopes. They are used to predict if the solution of a polymer in a certain solvent is suitable for membrane formation via phase separation. A ternary system is required for air-casting and immersion precipitation. Equilibrium phase diagrams can be used to predict which phase transitions are thermodynamically favorable. A number of phase separation phenomena have been observed in polymer solutions [39,41,50-54]. They include liquid-liquid phase separation, crystallization of the polymer and gelation.

Liquid-liquid phase separation [51,52,55] occurs when a homogeneous polymer solution becomes unstable, due to the loss of solvent quality either by the introduction of a nonsolvent for the polymer or by lowering solution temperature. Subsequently, the unstable solution mixture can lower its free energy of mixing by separating into two liquid phases of different compositions; a polymer-rich phase and a polymer-lean phase. The liquid-liquid phase separation of polymer solutions can occur either through nucleation and growth or by spinodal decomposition. In the metastable state, there is a thermodynamic barrier to nucleation of a new phase. Nuclei smaller than some critical size are metastable and tend to redissolve into the homogeneous phase. However, a nucleus starts to grow when it exceeds the critical size and if the free energy decrease associated with phase separation is enough to overcome the energy barrier. Nucleation and growth could occur in the polymer-lean phase or polymer-rich phase depending on

the concentration of the original polymer solution. If the starting polymer solution concentration exceeds the "critical-point" composition, nucleation and growth of the polymer-lean phase occurs. On the other hand, below the critical-point, nucleation and growth of the polymer-rich phases occurs. Polymeric membranes are generally made from polymer solutions that exceed the critical-point concentration (~10 wt.%), so that the norm in polymeric membranes is the nucleation and growth of a polymer-lean phase. During spinodal decomposition, the two phases diffuse to equilibrium composition spontaneously with no thermodynamic barrier to phase separation. For these compositions, the solution is unstable with respect to infinitesimal concentration fluctuations and thus separates spontaneously by molecular diffusion into interconnected regions of high and low polymer concentrations to form stable polymer-rich and polymer-lean phases. However, spinodal decomposition is highly improbable in membrane solutions because nucleation and growth kinetics are generally completed before the required composition for spinodal decomposition is attained in the high concentration polymer solutions used as membrane solutions. As a result, nucleation and growth of the polymer lean phase is the most frequently observed liquid-liquid phase separation mechanism in membrane dopes.

Crystallization [39,56-58] occurs when polymer molecules form ordered agglomerates as the solvent quality of a polymer solution decreases, either by decreased temperature, introduction of a nonsolvent for the polymer or by the loss of solvent. However, the formation of such ordered structures depends on the ability of the macromolecules to crystallize within the relevant timescales. For instance, for a polymer solution at some intermediate concentration where both crystallization and liquid-liquid phase separation

are thermodynamically feasible, crystallization is often surpassed by the kinetically more favorable liquid-liquid phase separation. The order of events might very well be reversed by increasing the polymer concentration, so that the rate of heterogeneous nucleation for crystallization is substantially increased while the rate of liquid-liquid phase separation remains largely unchanged. Hence, very high initial polymer concentration in membrane dopes tends to promote phase separation by crystallization.

For crystallization of polymer solutions at intermediate and high concentrations, the solution will contain numerous submicroscopic ordered regions due to the increased rate of nucleation but limited growth. These submicroscopic ordered regions act as physical crosslinks in the polymer solution and thus a thermo-reversible polymer gel is formed.

1.3.2 Kinetics of phase inversion of polymeric membrane solutions

The kinetics of phase separation determines the extent to which thermodynamically favorable transitions occur. This means that the details of the microstructure of a membrane can be controlled by the kinetics of phase separation. Qualitative mechanisms of structure formation in polymer membranes formed by immersion precipitation are detailed in the reports by Strathmann *et al.* and from the Smolders group [45,46,54,59,60]. In these studies, it was proposed that the skin layer is formed by gelation and that the porous sub-layer is formed as a result of the liquid-liquid demixing via nucleation and growth. The primary factor responsible for the type of structure formed is the local polymer concentration at the instant of phase separation. In the first moments of immersion in a nonsolvent bath, the rate of outflow of solvent is greater than the rate of inflow of nonsolvent (due to diffusion aided by stirring in the bath); this then leads to an increased polymer concentration at the polymer solution/nonsolvent bath

interface so that the gel boundary is crossed (path 1 in Figure 1.3). The resulting thin dense top layer becomes the skin of the membrane. The presence of the skin then decreases the rate of solvent outflow from the layers underneath the skin. As a consequence, phase separation in the inner layers occurs at lower polymer concentrations, leading to liquid-liquid demixing by nucleation and growth of the polymer-lean phase which results in the formation of the porous substructure (path 2 in Figure 1.3). The nucleation and growth of the polymer-lean phases will continue until the solidification of the polymer-rich regions around them prevents further growth due to very high viscosity attained. Membrane pore size is therefore determined by the extent of growth of the polymer-lean phases.

As a measure of the kinetics of phase separation, the nonsolvent penetration distance over time can be followed and an effective diffusion coefficient, D_{eff} of nonsolvent in the dope can be determined, as demonstrated by Strathmann [45].

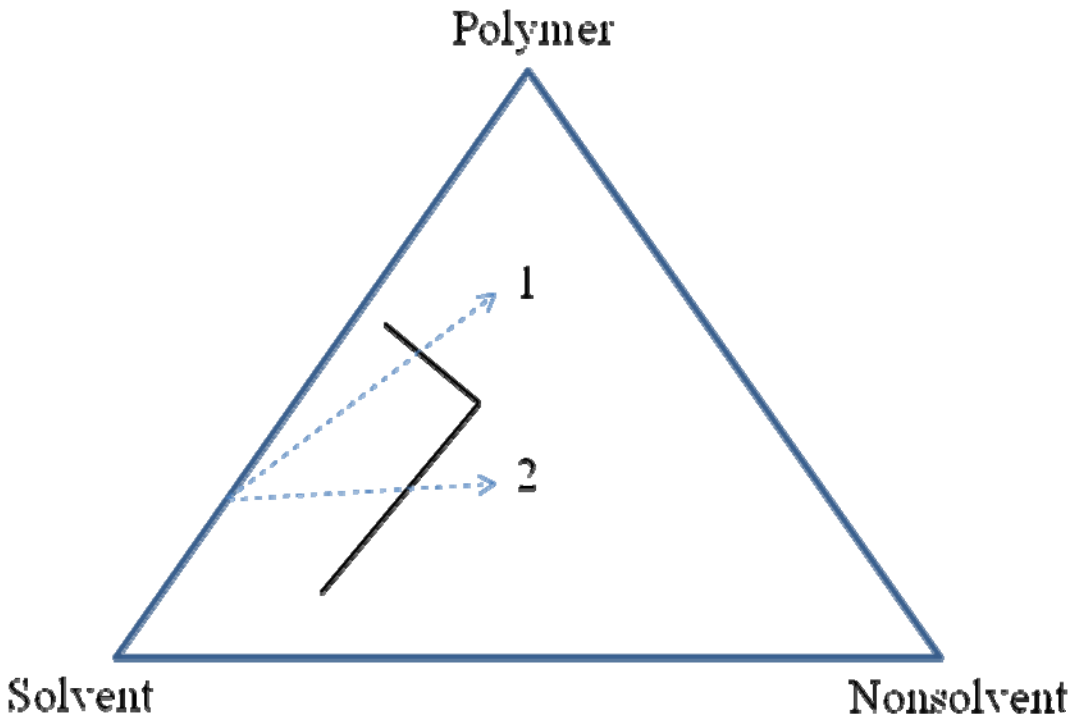

Figure 1.3 A ternary phase diagram; illustrating different paths to phase separation: gelation (1) and liquid-liquid demixing (2).

Other, more detailed mass transfer models for immersion precipitation are available in the literature [61-66]. However, they are often limited in applications and scope due to the assumptions that are necessary for solving the set of partial differential equations involved. These limitations of the mass transfer models and unreliable measuring techniques of phase separation kinetics in our opinion have slowed progress in fundamental understanding of controlling the pore size formation in membranes made by immersion precipitation. We believe that improvements in the measurement and prediction of phase separation kinetics of membrane dopes are still very much needed in

membrane development. Therefore, this thesis seeks to develop a novel device for measuring the phase separation kinetics of membrane dopes upon contact with a nonsolvent.

1.3.3 The rheology of membrane dopes

The rheology of membrane dopes can be discussed from two perspectives, *i.e.* the rheology of pure polymer solutions and the rheology of suspensions of zeolite particles in polymer solutions. The former has received much attention in the literature already and there is a well-established knowledge base on the rheology of polymer solutions. As far as we know, the latter topic has received little or no treatment in the public domain literature. Although many studies have been reported on the rheology of colloidal suspensions since the classic work of Einstein [67,68], it is our opinion that the rheology of suspension of porous zeolite particles in polymer solutions deserves special attention, especially in light of the marked observed deviations of their viscosity (measured in our lab) in comparison with traditional model suspensions.

The emphasis in this thesis will not be on the rheology of polymer solutions; it shall be on the rheology of suspensions of porous and nonporous siliceous nanoparticles in polymer solutions. To concentrate our focus on the particle contribution to the rheology of composite membrane dopes, we mostly discuss the relative viscosity, η_r, which is defined as the ratio of suspension viscosity to suspending medium viscosity. The simplest shear viscosity model for dilute suspensions of non-interacting hard spheres from the classic work of Einstein [67,68], is expressed in terms of the volume fraction, φ, as

$$\eta_r = \left(1 + 2.5\varphi\right) \tag{1.1}$$

The ratio of suspension viscosity to solvent viscosity is the relative viscosity, η_r. As particle loading in a suspension is gradually increased, the hydrodynamic spheres of the particles start to overlap and interact. Hence, for particle volume fractions up to about 0.1, it is necessary to include a second order corrective term in the Einstein relation. This contribution was first computed by Batchelor [69,70] for hard spheres:

$$\eta_r = \left(1 + 2.5\varphi + 6.2\varphi^2\right) \tag{1.2}$$

As the particle volume fraction increases above 0.1, the interactions between the hydrodynamic volumes of the Brownian particles becomes even more pronounced and multi-particle interactions must be accounted for. A more general, semi-empirical expression that works well for suspension viscosity at both low and high volume fractions is the Krieger-Dougherty model. For Brownian hard spheres, the maximum particle packing fraction, $\varphi_m \cong 0.63\text{-}0.64$ and the intrinsic viscosity, $[\eta]=2.5$. The Krieger-Dougherty equation [71] for Brownian hard spheres is then expressed as:

$$\eta_r = \left(1 - \frac{\varphi}{\varphi_m}\right)^{-[\eta]\varphi_m} \tag{1.3}$$

For particles with surface modification or roughness, the hydrodynamic radius may be larger than their physical radius, *a,* by a layer thickness δ. In that case, the effective volume fraction of particles in suspension must be adjusted as given in equation (1.4), where *a* is the physical particle radius and φ_o is the volume fraction of the bare particles:

$$\varphi = \varphi_o \left(1 + \frac{\delta}{a}\right)^3 \tag{1.4}$$

For nonspherical particles, the value of φ_m can be much smaller than for spherical particles. For instance, $\varphi_m = 0.44$ for rough crystals with aspect ratio close to unity [72]. In a recent paper by Mueller *et al.*[73], a correlation for the maximum packing fraction in axisymmetric particles as a function of particle aspect ratio, r_p, was established

$$\varphi_m = \frac{2}{0.321\, r_p + 3.02} \tag{1.5}$$

Because the aspect ratio of some zeolite particles depends on their size, the viscosity of zeolite particles may depend on size, in contrast to predictions for hard spheres that solely depend on volume fraction.

Another important phenomenon fundamentally altering the rheology of zeolite particles suspensions is the large electroviscous effects that they exhibit, as will be shown in this thesis. This work to our knowledge is the first attempt to study the electroviscous effects

in suspensions of zeolites. Surface charges are not typically expected for inorganic particles suspended in an organic medium. However, the work of several authors [74-76] established a mechanism of surface charge acquisition by particles suspended in aqueous as well as non-aqueous media. When silica particles and zeolites are dispersed in a polar aprotic medium, they invariably become negatively charged due to the dissociation of the surface silanol groups and release of hydrogen ions into the aprotic medium. As a result, the particles may become highly charged with zeta potentials exceeding 50 mV. This high surface charge and the rather long Debye length expected for a salt-free polar liquid enhance the electroviscous effects in this system. Consequently, dilute suspensions of siliceous particles with surface silanol groups may possess intrinsic viscosities greater than the Einstein value of 2.5. In addition, for charged spheres the effective collision diameter may be greater than that for hard spheres due to the greater sphere of influence of a charged sphere. Consequently, the value of the maximum random packing fraction, φ_m is much lower than for hard spheres. The equation relating φ_m to the effective hard sphere diameter, r_0, are given below:

$$\varphi_m = 0.63\left(\frac{2a}{r_0}\right)^3 \tag{1.6}$$

$$r_0 \approx \kappa^{-1} \ln\{\alpha / \ln[\alpha / \ln(\ln\alpha / \ln ...)]\} \tag{1.7}$$

Where $\alpha = \left[\frac{4\pi\varepsilon\kappa(a\zeta)^2 \exp(2\kappa a)}{k_B T} \right]$, a is the particle radius, κ^{-1} the Debye screening length, and ζ the zeta potential.

1.4 The component materials in MMX membrane dopes

The components of an MMX dope are carefully chosen to satisfy a complex set of conditions. In choosing the components, the thermodynamics and kinetics of phase separation, rheology and stability of dope must all be taken into consideration. The polymer, solvent, cosolvents and zeolite particles are must fulfill certain constraints.

The polymer used for all experiments reported in this thesis is polyetherimide, PEI (Ultem 1000, MW ~ 61,000) purchased from GE Plastics. The solvent of choice for the Ultem polymer is NMP purchased from Sigma-Aldrich. The zeolite particles used are 150 nm synthesized by research collaborators at Georgia Tech [28]. The size and shape of the MFI particles were estimated from SEM images (an example is shown in Figure 1.4). MFI is nonporous in the uncalcined form with density 1.99 $g \cdot cm^{-3}$ [77]. The microporous form is obtained by calcination in air at 500-600 ^{o}C, which leads to thermal decomposition of the organic templates that was used during the synthesis and yields porous MFI of a lower density.

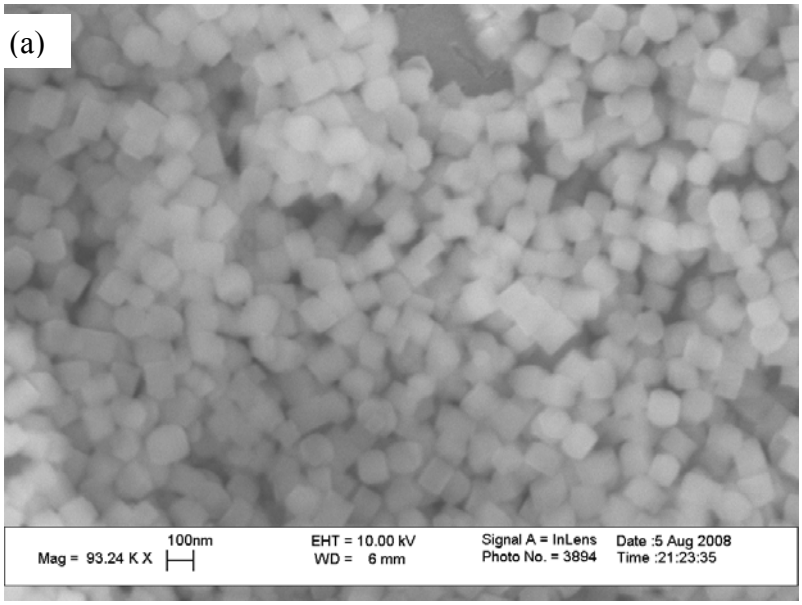

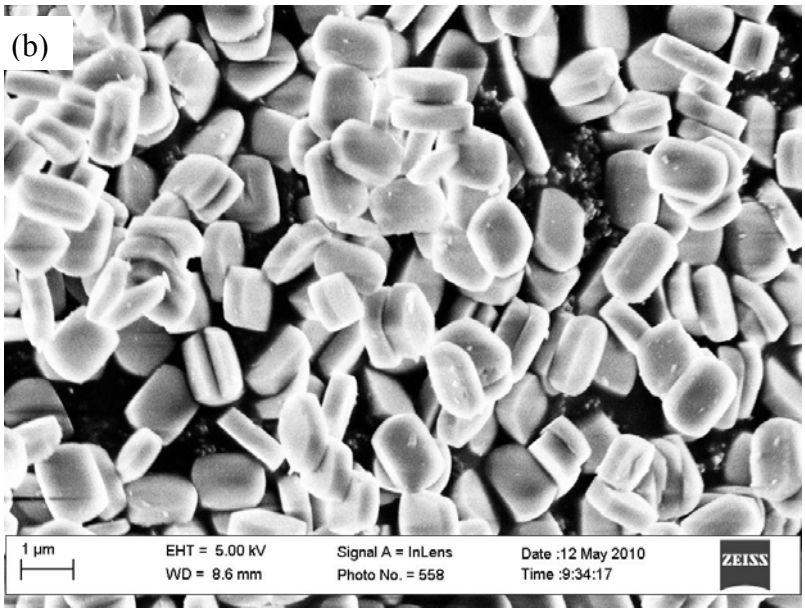

Figure 1.4 SEM image of (a) 150 nm and (b) 2 µm MFI zeolite particles.

The zeolite particles are functionalized in order to facilitate dispersion of the particles in the polymer solution and to promote adhesion between polymer and the zeolite particles. Three surface treatments employed on the MFI particles were reported previously [27]. The first method is the 'silane surface treatment' (ST) of particles, which involves the chemical reaction of surface silanol groups with a silane agent (APDMES) to yield 'ST MFI'. It is believed that the chemically bonded silane groups on the zeolite surface create a steric barrier against particle aggregation. The second surface treatment is 'Ultem-sizing' (USZ); it involves the chemical coupling of Ultem polymer chains to the free ends of silane groups (from a preceding silane treatment of particles step) whose other end is bonded to the zeolite surface to form 'USZ MFI'. In this case, particle aggregation is also prevented by steric stabilization as a result of the macromolecules grafted to the surface of the MFI particles. A schematic reaction pathway of these two surface treatments is shown in Figure 1.5. Although silane treatment and Ultem-sizing do improve the stability of zeolite particles suspension with respect to aggregation, they do not eliminate the poor adhesion between zeolite particles and the polymer matrix. To solve this problem, a third surface treatment was used to modify the surface of zeolite particles. The method was developed by researchers in the Koros group at Georgia Tech. It involves growth/deposition of high aspect ratio Mg $(OH)_2$ nano-whiskers on the surface of zeolite particles [78,79]. This method is known as the "Grignard treatment" (GT). It is believed that the process improves the adhesion between particles and polymer by decreasing the tendency of the zeolite particles to act as hydrophilic nucleation centers for the nonsolvent. In addition, it has been proposed that some degree of entanglement of polymer coils around the whiskers may promote adhesion.

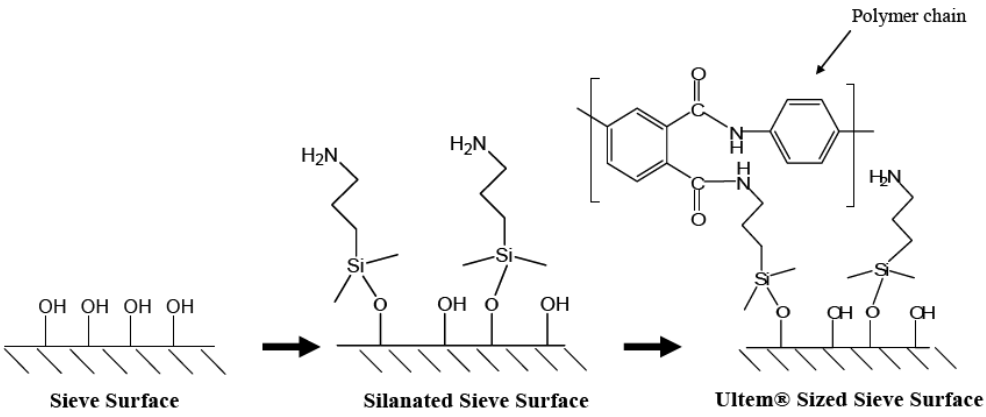

Figure 1.5 Schematic of MFI particle silane treatment and Ultem-sizing.

1.5 Research objectives

The objective of this research thesis is to provide measures for process parameters that play a key role in the efficient processing of polymer/zeolite composite membrane dopes into mixed-matrix hollow fiber membranes. This overarching objective is subdivided into the following sub-aims to address different aspects of hollow fiber membrane formation:

I. ***To characterize the rheology and develop predictive models for the viscosity of membrane dopes***

During the extrusion and drawing of membrane dopes into fibers, membrane dopes are compelled to flow under the influence of strong shear and elongational stresses. A mixed-matrix membrane dope is a composite dope, comprised of porous zeolite particles dispersed in a polymer solution. The rheology of such composite membrane dopes differs greatly from model suspensions and has not

been subject of any detailed study in the open literature. It will be shown in this thesis that the major origins of the discrepancies with model suspension predictions are: solvent absorption within porous zeolite particles, electroviscous effects and tunable boundary layers around these particles. These effects conspire to significantly increase the measured viscosities of composite membrane dopes above values obtained from simple model predictions. The first half of this thesis will address the rheology and structure of composite membrane dope with the ultimate aim of developing predictive capabilities for zeolite suspension viscosities.

II. To develop a method to measure phase separation kinetics of membrane dopes

The average pore size and pore size distribution in polymer membranes for various filtration applications is controlled by the kinetics of phase separation of polymer solutions. However, there is still much unknown about the process of porous structure formation in membrane literature. Models developed to date are inadequate because of simplifying assumptions that are necessary to make membrane formation mass transfer problems mathematically tractable. Most techniques described in literature to measure phase separation kinetics (PSK) of polymer solutions are unreliable and inefficient. Moreover, available methods used to measure the kinetics of phase separation of polymer solutions are challenging to extend to composite membrane dopes. Hence, this thesis also aims to develop a new method to reliably measure the kinetics of phase separation of membrane dopes, which is equally applicable for the quantification of the PSK of dopes with dispersed zeolite particles.

III. To determine measurable and/or predictable parameters from which phase separation kinetics of membrane dopes can be predicted

This research thesis also seeks to establish correlations between the kinetics of phase separation and measurable and/or predictable properties of membrane dopes. Such correlations can offer invaluable insights into the interplay between PSK, microstructure and thermodynamics of membrane dopes. In addition to the predictive power of such models, we fully expect enhanced ability to predict PSK to be of great utility in the process design of membrane hollow fiber spinning by phase inversion in a nonsolvent bath.

IV. To determine the effect of porous and nonporous particles on the phase separation kinetics of membrane dopes

MMX membranes are a relatively new class of membranes being developed and the effect of particle addition to the kinetics of phase separation is yet to be explored in any quantitative manner. This thesis will provide some quantitative measures of the effect of porous and nonporous particles on the kinetics of phase inversion of membrane dopes. Qualitative descriptions of how the degree of hydrophilicity of zeolite particles suspended in a polymer solution alters phase separation kinetics will be proposed. In addition, the effect of zeolite porosity to components in the membrane formation process will be discussed. These fundamental studies on the PSK of MMX membrane dopes described constitutes one of the unique contribution of this thesis as no data is available in literature on these phenomena.

1.6 Thesis overview

Chapter 2 of this thesis deals with the rheology of suspensions of silica-type spheres in a polar organic solvent. This chapter endeavors to get at some of the fundamental colloidal and structural forces on the particle scale which dictates the observed bulk rheology of silica-type materials suspended in organic solutions. We have chosen to study the rheology of silica particles suspensions as a model system because MFI zeolite is a porous, non-spherical form of silica. These studies provide insight into the colloidal and structural forces in play and their impact on the intrinsic viscosities and long range interactions of siliceous particles with either pure NMP solvent or Ultem/NMP polymer solutions as the suspending phase. Furthermore, a concentrated suspension of silica in NMP is used to show that the maximum random packing fraction of siliceous particles is much less than the value obtained for hard spheres. The practical implication of this is that due to the high double layer charge and low salt content in NMP mediated suspensions of siliceous particles, the suspension viscosity diverges at much lower maximum random packing fractions than the classic value of 0.63 for hard spheres. Chapter 3 deals with the rheology of real composite membrane dopes that are composed of porous zeolite particles in a polymer solution. Here, solvent absorption effects on the rheology of composite membrane dopes will be examined. In addition, findings from Chapter 2 are used to explain some of the complex composite membrane dope rheology observed for MFI zeolite particles suspensions. Chapter 4 addresses the measurement of phase separation kinetics of membrane dopes in a novel microfluidic device that I developed in the course of this thesis. Using this microfluidic device, the role of polymer solution microstructure and the thermodynamics of membrane dope components are

investigated. In Chapter 5, the effect of addition of zeolite particles on phase separation kinetics will be investigated. The effect of porosity of particles to membrane dope solvent and nonsolvent is explored as well. Furthermore, the effect the phase separation kinetics and thermodynamics of membrane dope components in relation to macrovoids elimination will be investigated. Finally, conclusions and recommendations based on the investigations and findings reported are discussed in Chapter 6.

1.7 References

1. Lonsdale HK: **The growth of membrane technology.** *Journal of Membrane Science* (1982) **10**(2-3):81-181.

2. Pusch W, Walch A: **Synthetic membranes - preparation, structure, and application.** *Angewandte Chemie-International Edition in English* (1982) **21**(9):660-685.

3. Dunkel J: **Applications of membrane separation technology in the chemical-industry.** *Chemische Technik* (1988) **40**(9):407-407.

4. Strathman H, Bell CM, Kimmerle K: **Development of synthetic membranes for gas and vapor separation.** *Pure and Applied Chemistry* (1986) **58**(12):1663-&.

5. Hensema ER: **Polymeric gas separation membranes.** *Advanced Materials* (1994) **6**(4):269-279.

6. Robeson LM: **Correlation of separation factor versus permeability for polymeric membranes.** *Journal of Membrane Science* (1991) **62**(2):165-185.

7. Robeson LM: **The upper bound revisited.** *Journal of Membrane Science* (2008) **320**(1-2):390-400.

8. Morooka S, Kusakabe K: **Microporous inorganic membranes for gas separation.** *Mrs Bulletin* (1999) **24**(3):25-29.

9. MunozAguado MJ, Gregorkiewitz M: **Preparation of silica-based microporous inorganic gas separation membranes.** *Journal of Membrane Science* (1996) **111**(1):7-18.

10. Kusakabe K, Kuroda T, Morooka S: **Separation of carbon dioxide from nitrogen using ion-exchanged faujasite-type zeolite membranes formed on porous support tubes.** *Journal of Membrane Science* (1998) **148**(1):13-23.

11. Tuan VA, Li SG, Falconer JL, Noble RD: **In situ crystallization of beta zeolite membranes and their permeation and separation properties.** *Chemistry of Materials* (2002) **14**(2):489-492.

12. Yan YS, Davis ME, Gavalas GR: **Preparation of zeolite zsm-5 membranes by in-situ crystallization on porous alpha-al2o3.** *Industrial & Engineering Chemistry Research* (1995) **34**(5):1652-1661.

13. Nishiyama N, Ueyama K, Matsukata M: **Synthesis of fer membrane on an alumina support and its separation properties.** In: *Progress in zeolite and microporous materials, pts a-c.* 105. Chon H, Ihm SK, Uh YS (Eds), (1997):2195-2202.

14. Aoki K, Kusakabe K, Morooka S: **Gas permeation properties of a-type zeolite membrane formed on porous substrate by hydrothermal synthesis.** *Journal of Membrane Science* (1998) **141**(2):197-205.

15. Poshusta JC, Tuan VA, Falconer JL, Noble RD: **Synthesis and permeation properties of sapo-34 tubular membranes.** *Industrial & Engineering Chemistry Research* (1998) **37**(10):3924-3929.

16. Poshusta JC, Tuan VA, Pape EA, Noble RD, Falconer JL: **Separation of light gas mixtures using sapo-34 membranes.** *Aiche Journal* (2000) **46**(4):779-789.

17. Li SG, Falconer JL, Noble RD: **Sapo-34 membranes for co2/ch4 separation.** *Journal of Membrane Science* (2004) **241**(1):121-135.

18. Li SG, Martinek JG, Falconer JL, Noble RD, Gardner TQ: **High-pressure co2/ch4 separation using sapo-34 membranes.** *Industrial & Engineering Chemistry Research* (2005) **44**(9):3220-3228.

19. Mahajan R, Koros WJ: **Factors controlling successful formation of mixed-matrix gas separation materials.** *Industrial & Engineering Chemistry Research* (2000) **39**(8):2692-2696.

20. Mahajan R, Koros WJ: **Mixed matrix membrane materials with glassy polymers. Part 1.** *Polymer Engineering and Science* (2002) **42**(7):1420-1431.

21. Mahajan R, Koros WJ: **Mixed matrix membrane materials with glassy polymers. Part 2.** *Polymer Engineering and Science* (2002) **42**(7):1432-1441.

22. Kulprathipanja S: **Mixed matrix membrane development.** In: *Advanced membrane technology*. 984. Li NN, Drioli E, Ho WSW, Lipscomb GG (Eds), (2003):361-369.

23. Jiang LY, Chung TS, Cao C, Huang Z, Kulprathipanja S: **Fundamental understanding of nano-sized zeolite distribution in the formation of the mixed matrix single- and dual-layer asymmetric hollow fiber membranes.** *Journal of Membrane Science* (2005) **252**(1-2):89-100.

24. Li Y, Chung TS, Cao C, Kulprathipanja S: **The effects of polymer chain rigidification, zeolite pore size and pore blockage on polyethersulfone (pes)-zeolite a mixed matrix membranes.** *Journal of Membrane Science* (2005) **260**(1-2):45-55.

25. Husain S: **Mixed matrix dual layer hollow fiber membranes for natural gas separation.** In: (2006).

26. Chung TS, Jiang LY, Li Y, Kulprathipanja S: **Mixed matrix membranes (mmms) comprising organic polymers with dispersed inorganic fillers for gas separation.** *Progress in Polymer Science* (2007) **32**(4):483-507.

27. Husain S, Koros WJ: **Mixed matrix hollow fiber membranes made with modified hssz-13 zeolite in polyetherimide polymer matrix for gas separation.** *Journal of Membrane Science* (2007) **288**(1-2):195-207.

28. Liu JQ, Bae TH, Qiu WL, Husain S, Nair S, Jones CW, Chance RR, Koros WJ: **Butane isomer transport properties of 6FDA-DAM and MFI-6FDA-DAM mixed matrix membranes.** *Journal of Membrane Science* (2009) **343**(1-2):157-163.

29. Ekiner OM, Vassilatos G: **Polyaramide hollow fibers for hydrogen methane separation - spinning and properties.** *Journal of Membrane Science* (1990) **53**(3):259-273.

30. Ekiner OM, Vassilatos G: **Polyaramide hollow fibers for h-2/ch4 separation - ii. Spinning and properties.** *Journal of Membrane Science* (2001) **186**(1):71-84.

31. Berghmans M, Thijs S, Cornette M, Berghmans H, Deschryver FC, Moldenaers P, Mewis J: **Thermoreversible gelation of solutions of syndiotactic poly(methyl methacrylate) in toluene - a 2-step mechanism.** *Macromolecules* (1994) **27**(26):7669-7676.

32. Tan HM, Moet A, Hiltner A, Baer E: **Thermoreversible gelation of atactic polystyrene solutions.** *Macromolecules* (1983) **16**(1):28-34.

33. Schneider T, Wolf BA, Kasten H, Kremer F: **Thermoreversible gelation and vitrification of highly concentrated polymer-solutions under poor thermodynamic conditions.** *Macromolecules* (1991) **24**(19):5387-5392.

34. Yang YC, Geil PH: **Morphology and properties of pvc solvent gels.** *Journal of Macromolecular Science-Physics* (1983) **B22**(3):463-488.

35. Guenet JM, Klein M: **Structures in polystyrene solutions - their origins and their implications on physical gelation.** *Makromolekulare Chemie-Macromolecular Symposia* (1990) **39**(85-98.

36. Goodfellow BJ, Wilson RH: **A fourier-transform ir study of the gelation of amylose and amylopectin.** *Biopolymers* (1990) **30**(13-14):1183-1189.

37. Hikmet RM, Callister S, Keller A: **Thermoreversible gelation of atactic polystyrene - phase-transformation and morphology.** *Polymer* (1988) **29**(8):1378-1388.

38. Aubert JH, Clough RL: **Low-density, microcellular polystyrene foams.** *Polymer* (1985) **26**(13):2047-2054.

39. Broens L, Altena FW, Smolders CA, Koenhen DM: **Asymmetric membrane structures as a result of phase separation phenomena.** *Desalination* (1980) **32**(33-45.

40. Hong PD, Huang HT: **Effect of polymer-solvent interaction on gelation of polyvinyl chloride solutions.** *European Polymer Journal* (1999) **35**(12):2155-2164.

41. Wijmans JG, Kant J, Mulder MHV, Smolders CA: **Phase-separation phenomena in solutions of polysulfone in mixtures of a solvent and a nonsolvent - relationship with membrane formation.** *Polymer* (1985) **26**(10):1539-1545.

42. Frommer MA, Lancet D: **Mechanism of membrane formation .5. Structure of membranes and its relation to their preparation conditions.** *Abstracts of Papers of the American Chemical Society* (1971) NSEP):32.

43. Matz R: **Structure of cellulose-acetate membranes .1. Development of porous structures in anisotropic membranes.** *Desalination* (1972) **10**(1):1-15.

44. Kang YS, Kim HJ, Kim UY: **Asymmetric membrane formation via immersion precipitation method .1. Kinetic effect.** *Journal of Membrane Science* (1991) **60**(2-3):219-232.

45. Strathmann H, Kock K, Amar P, Baker RW: **Formation mechanism of asymmetric membranes.** *Desalination* (1975) **16**(2):179-203.

46. Strathmann H, Kock K: **Formation mechanism of phase inversion membranes.** *Desalination* (1977) **21**(3):241-255.

47. Saier HD, Strathmann H, Mylius UV: **Mechanism of asymmetric membrane formation.** *Angewandte Makromolekulare Chemie* (1974) **40**:391-404.

48. Strathma.H, Scheible P: **Formation mechanism of asymmetrical cellulose acetate membranes.** *Kolloid-Zeitschrift and Zeitschrift Fur Polymere* (1971) **246**(2):669-679.

49. Strathma.H, Scheible P, Baker RW: **Rationale for preparation of loeb-sourirajan-type cellulose acetate membranes.** *Journal of Applied Polymer Science* (1971) **15**(4):811-820.

50. Broens L, Altena FW, Smolders CA, Koenhen DM: **Asymmetric membrane structures as a result of phase-separation phenomena.** *Desalination* (1980) **32**(1-3):33-45.

51. Broens L, Koenhen DM, Smolders CA: **Mechanism of formation of asymmetric ultrafiltration and hyperfiltration membranes.** *Desalination* (1977) **22**(1-3):205-219.

52. Koenhen DM, Mulder MHV, Smolders CA: **Phase separation phenomena during formation of asymmetric membranes.** *Journal of Applied Polymer Science* (1977) **21**(1):199-215.

53. Altena FW, Smolders CA: **Phase-separation phenomena in solutions of cellulose-acetate .1. Differential scanning calorimetry of cellulose-acetate in mixtures of dioxane and water.** *Journal of Polymer Science-Polymer Symposia* (1981) 69):1-10.

54. Bokhorst H, Altena FW, Smolders CA: **Formation of asymmetric cellulose-acetate membranes.** *Desalination* (1981) **38**(1-3):349-360.

55. Vanaarts.Jj, Smolders CA: **Light scattering of polymer solutions during liquid-liquid phase separation.** *European Polymer Journal* (1970) **6**(8):1105-&.

56. Kubo S, Wunderli.B: **Unit cell of poly-p-xylylene and structure of solution-grown crystals.** *Makromolekulare Chemie* (1972) **162**(NDEC):1-&.

57. Treiber G, Melillo L, Wunderli.B: **Effect of solvent concentration on crystallization of polyethylene under elevated pressure.** *Journal of Polymer Science Part C-Polymer Letters* (1973) **11**(7):435-440.

58. Smolders CA, Vanaarts.Jj, Steenber.A: **Liquid-liquid phase separation in concentrated solutions of non-crystallizable polymers by spinodal decomposition.** *Kolloid-Zeitschrift and Zeitschrift Fur Polymere* (1971) **243**(1):14-&.

59. Wijmans JG, Baaij JPB, Smolders CA: **The mechanism of formation of microporous or skinned membranes produced by immersion precipitation.** *Journal of Membrane Science* (1983) **14**(3):263-274.

60. Smolders CA, Reuvers AJ, Boom RM, Wienk IM: **Microstructures in phase-inversion membranes .1. Formation of macrovoids. 73**:Abs 259-275.

61. Cohen C, Tanny GB, Prager S: **Diffusion-controlled formation of porous structures in ternary polymer systems.** *Journal of Polymer Science Part B-Polymer Physics* (1979) **17**(3):477-489.

62. Reuvers AJ, Vandenberg JWA, Smolders CA: **Formation of membranes by means of immersion precipitation .1. A model to describe mass-transfer during immersion precipitation.** *Journal of Membrane Science* (1987) **34**(1):45-65.

63. Tsay CS, McHugh AJ: **Mass-transfer modeling of asymmetric membrane formation by phase inversion.** *Journal of Polymer Science Part B-Polymer Physics* (1990) **28**(8):1327-1365.

64. Tsay CS, McHugh AJ: **An improved numerical algorithm for ternary diffusion with a moving interface.** *Chemical Engineering Science* (1991) **46**(4):1179-1187.

65. McHugh AJ, Tsay CS, Barton BF, Reeve JL: **Comments on a model for mass-transfer during phase inversion.** *Journal of Polymer Science Part B-Polymer Physics* (1995) **33**(15):2175-2179.

66. Cheng LP, Soh YS, Dwan AH, Gryte CC: **An improved model for mass-transfer during the formation of polymeric membranes by the immersion-precipitation process.** *Journal of Polymer Science Part B-Polymer Physics* (1994) **32**(8):1413-1425.

67. Einstein A: **A new determination of the molecular dimensions.** *Annalen Der Physik* (1906) **19**(2):289-306.

68. Einstein A: **A new determination of the molecular dimensions (vol 19, pg 289, 1906).** *Annalen Der Physik* (1911) **34**(3):591-592.

69. Batchelor GK: **Brownian diffusion of particles with hydrodynamic interaction.** *Journal of Fluid Mechanics* (1976) **74**(MAR9):1-29.

70. Batchelor GK: **Effect of brownian-motion on bulk stress in a suspension of spherical-particles.** *Journal of Fluid Mechanics* (1977) **83**(NOV):97-117.

71. Krieger IM, Dougherty TJ: **A mechanism for non-newtonian flow in suspensions of rigid spheres.** *Transactions of the Society of Rheology* (1959) **3**(137-152.

72. Kitano T, Kataoka T, Shirota T: **An empirical-equation of the relative viscosity of polymer melts filled with various inorganic fillers.** *Rheologica Acta* (1981) **20**(2):207-209.

73. Mueller S, Llewellin EW, Mader HM: **The rheology of suspensions of solid particles.** *Proceedings of the Royal Society a-Mathematical Physical and Engineering Sciences* (2010) **466**(2116):1201-1228.

74. Vanderhoeven PHC, Lyklema J: **Electrostatic stabilization in nonaqueous media.** *Advances in Colloid and Interface Science* (1992) **42**(205-277.

75. Labib ME, Williams R: **The effect of moisture on the charge at the interface between solids and organic liquids.** *Journal of Colloid and Interface Science* (1987) **115**(2):330-338.

76. Labib ME: **The origin of the surface-charge on particles suspended in organic liquids.** *Colloids and Surfaces* (1988) **29**(3):293-304.

77. Flanigen EM, Bennett JM, Grose RW, Cohen JP, Patton RL, Kirchner RM, Smith JV: **Silicalite, a new hydrophobic crystalline silica molecular-sieve.** *Nature* (1978) **271**(5645):512-516.

78. Shu S, Husain S, Koros WJ: **A general strategy for adhesion enhancement in polymeric composites by formation of nanostructured particle surfaces.** *Journal of Physical Chemistry C* (2007) **111**(2):652-657.

79. Shu S, Husain S, Koros WJ: **Formation of nanostructured zeolite particle surfaces via a halide/grignard route.** *Chemistry of Materials* (2007) **19**(16):4000-4006.

CHAPTER 2

THE RHEOLOGY OF SUSPENSIONS OF SILICEOUS PARTICLES IN POLAR ORGANIC MEDIA

2.1 Introduction

The overarching goal of the rheological measurements in this thesis is to develop predictive models for the viscosity of MMX membrane dopes. The most convenient approach to determine relative viscosity of these dopes would be to predict it from existing suspension rheology models. Unfortunately, as will be shown below, that would result in erroneous predictions since membrane dope suspensions are rheologically different than suspensions for which successful rheological models exist. The reasons for these differences are multifarious and may vary from one MMX dope to another depending on the specific physical and chemical properties of the components. For instance, the aspect ratio of MFI [1-3] zeolite particles increases with increasing particle size; based on this fact alone, the viscosity of a suspension of 500 nm MFI particles should exceed that for 100 nm MFI particles at the same volume fraction. Moreover, zeolite particles invariably acquire surface charges in aqueous and non-aqueous media the same way like silica particle does [4-7]. When this occurs, electroviscous effects [8-13] arise, which may be quite significant in organic solvents where the concentration of dissolved salt is usually very low. Another complicating effect for suspended particles in polymer solutions is that macromolecules may become adsorbed on particle surfaces, leading to enhanced suspension viscosity due to the increased excluded volume of the particles.

In view of all these non-idealities that potentially complicate the analysis of the rheology of zeolite particle suspensions, we considered it desirable to study a simplified model system that retains essential features of the targeted MMX membrane dope system. For such a model system, we have chosen suspensions of silica spheres in NMP solvent, with and without dissolved polymer. The systematic study described in this Chapter progresses from the most simplified model system to increasingly complex systems, thus enabling a stepwise, comprehensive analysis of the relevance of various system properties on the rheology of MMX membrane dopes.

2.2 Materials and methods

Three aqueous silica sols are the sources of the silica particles used in the studies described in this Chapter: (i) two commercial products of Bangs Lab (Fisher, IN): one with mean particle size of 320 ± 10 nm, hereafter referred to as the S2 sample; and another with mean particle size 540 ± 20 nm (sample S3), and (ii) a commercial product of Nissan Chemical America (Houston, TX) with mean particle size of 100 ± 10 nm (sample S1). The dried form of the particles is obtained by centrifugation of the sols to collect the particles. This step is followed by two washing steps in DI water which entails suspending particles in DI water followed by centrifugation. The particles are then re-suspended in IPA, followed and collected by centrifugation. The collected particles are then dried at 120 ^{o}C for at least 10 hours. The physicochemical properties of these particles are listed in Table 2.1. The particle size and distribution were estimated from SEM images and are in good agreement with the nominal size provided by the supplier. The SEM images of these particles are shown in Figure 2.1.

Table 2.1 The physicochemical properties of three different silica nanoparticles.

	S1	S2	S3
Diameter (nm) (SEM)	100±10	320±10	540±10
Density (g/ml)	2.35	-	2.31
Zeta potential, ζ in NMP (mV)	59±5	72±5	89±5

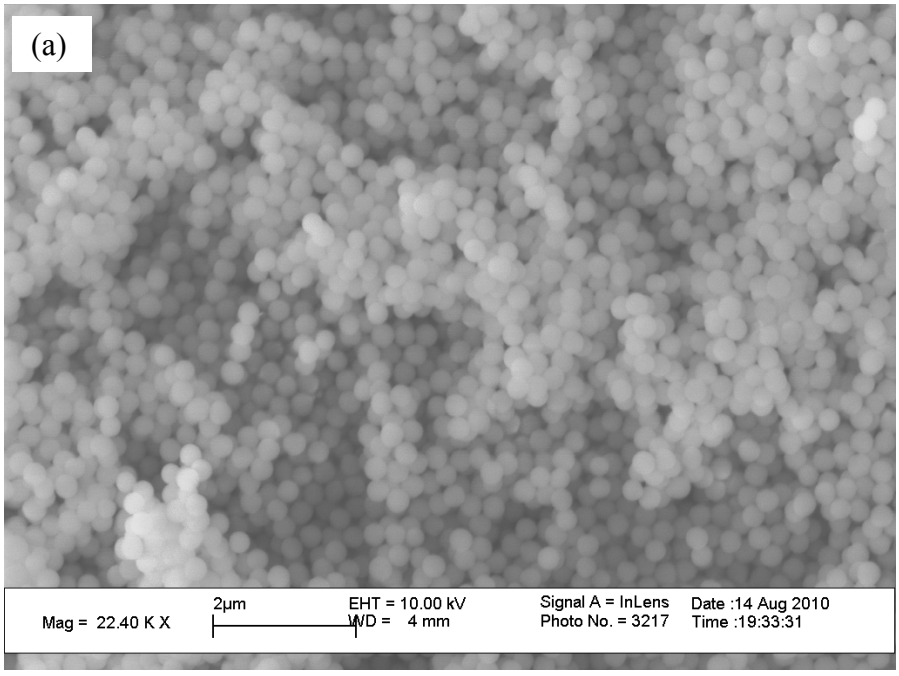

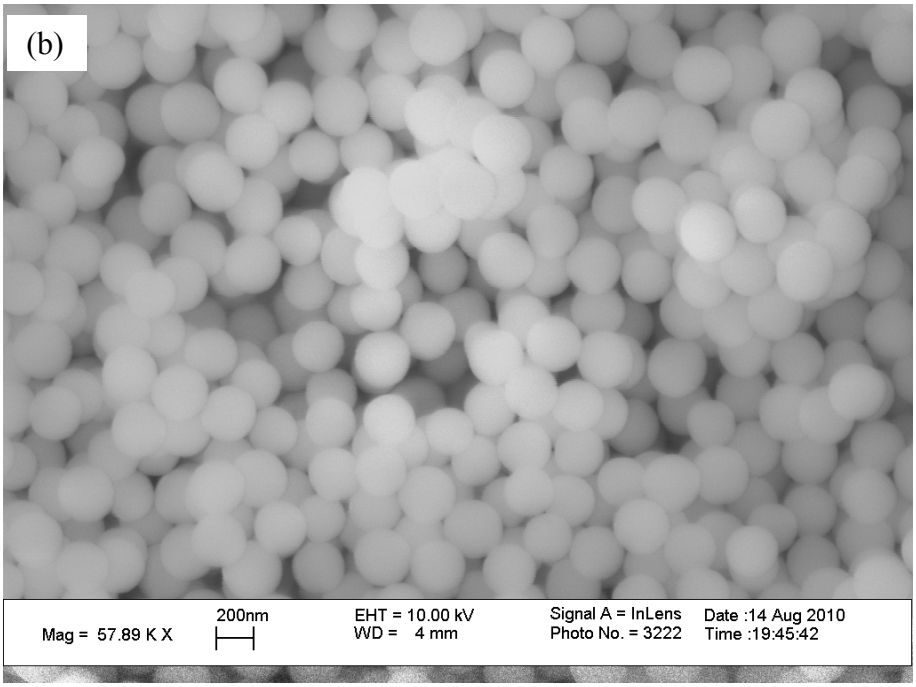

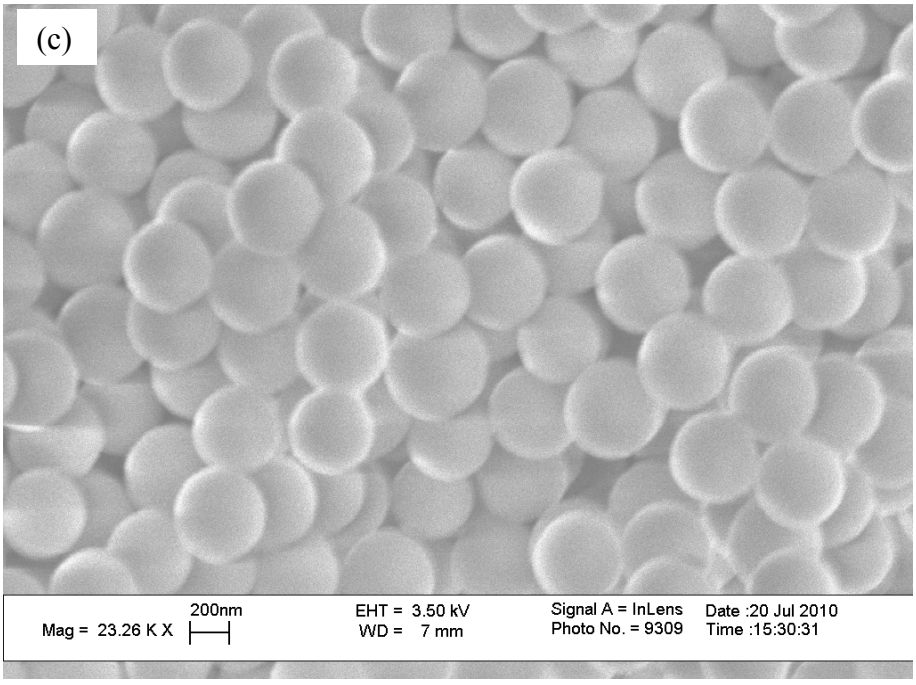

Figure 2.1 Scanning electron micrographs of (a) 100 nm (S1), (b) 320 nm (S2), (c) 540 nm (S3) silica particles used in this study.

In addition to the untreated as-received silica particles, two additional Ultem-sized versions of S1 and S2 were used in these studies, which are referred to as ^{UZ}S1 and ^{UZ}S2, respectively. The Ultem-sizing of particles involves the chemical grafting of Ultem macromolecules to the particle surfaces, as described in detail in Section 1.4.

The densities of the particles S1 and S3 were determined by pycnometer measurements of concentrated silica suspensions, using the known volume of the pycnometer, the density of the suspending fluid and the weights of particles and fluid as input parameters for the calculations. Because of the excellent agreement for these two samples, S2 was not subjected to this test.

The electrophoretic mobility, U_e /zeta potential, ζ of these particles in NMP and water-NMP mixtures was determined using a Malvern Nano-ZS90 zetasizer. In addition, the conductivity of NMP with and without dissolved salts is determined using the same instrument. The zeta potential of ^{UZ}S1 and ^{UZ}S2 in NMP was respectively measured as 57 ± 10 mV and 67 ± 10 mV; within experimental errors this is the same as the measured value for the corresponding untreated S1 and S2 particles, 59 ± 5 mV and 72 ± 5 mV, respectively.

The viscosity of the suspensions and suspending media were measured over a range of shear rates (0.1 - 20 s^{-1}) at 20 ^{o}C with a stress-controlled rheometer (MCR 300, Anton Paar) and Couette geometry (CC17; cup inside diameter 18.071 mm and bob outer diameter 16.660 mm). The viscosities for the NMP/water suspending media and dilute suspensions are reported at 10 s^{-1}, because these systems are Newtonian. At higher particle concentrations, were the onset of shear thinning is noticeable within the range of applied shear rates; the viscosity is reported at shear rates lower than 10 s^{-1}, before the

onset of shear-thinning. The viscosity of the polymer solutions and suspensions in polymer solutions were also measured over a range of shear rates (0.1 - 100 s^{-1}) at 20 ^{o}C, but with a different Couette geometry (CC10; cup inside diameter 10.845 mm and bob outer diameter 10.000 mm); the higher viscosities of the polymer solutions enabled use of the less sensitive geometry, which requires smaller sample volumes. The viscosities of polymeric samples reported in this paper are at a shear rate of 0.2 s^{-1}, which is below the onset of shear-thinning in all samples.

2.3 Dilute suspension*s* in aqueous liquids

The rheology of dilute suspension of silica particles in different media without dissolved polymer was investigated first. The aim here was to understand how the silanol surface chemistry of siliceous particles and the acid-base properties of the suspending liquid medium (NMP) impact the intrinsic viscosity of the suspension. Below, a series of viscosity, electrophoretic mobility and conductivity measurements are reported for S3 particles in NMP. It will be shown that the intrinsic viscosity significantly exceeds the Einstein value of 2.5 and that it may be tuned by changing the chemical composition of the suspending medium. The structural and colloidal forces that play key roles in the experimentally observed deviations of intrinsic viscosity from Einstein's prediction are identified and explained.

Figure 2.2 shows the relative viscosity versus particle volume fractions in NMP at several dissolved salt concentrations. For silica particles in pure NMP, we found $[\eta] = 6.24 \pm 0.16$ compared to the Einstein prediction of intrinsic viscosity of 2.5 for suspensions of hard spheres. Electrophoretic mobility measurements of very dilute

suspensions of silica particles in NMP (< 0.05 wt.%) show that the silica particles becomes negatively charged in NMP with zeta potential value of 89 ± 5 mV. An explanation for this observation is that NMP is more basic than the silica surface, thus enhancing the deprotonation of silica surface silanol groups to create a negatively charged surface, *i.e.* $SiOH \leftrightarrow SiO^- + H^+$. The greater the number of dissociated silanol groups on the surface of a silica particle, the greater its surface charge and, consequently, the greater its electrophoretic mobility/zeta potential.

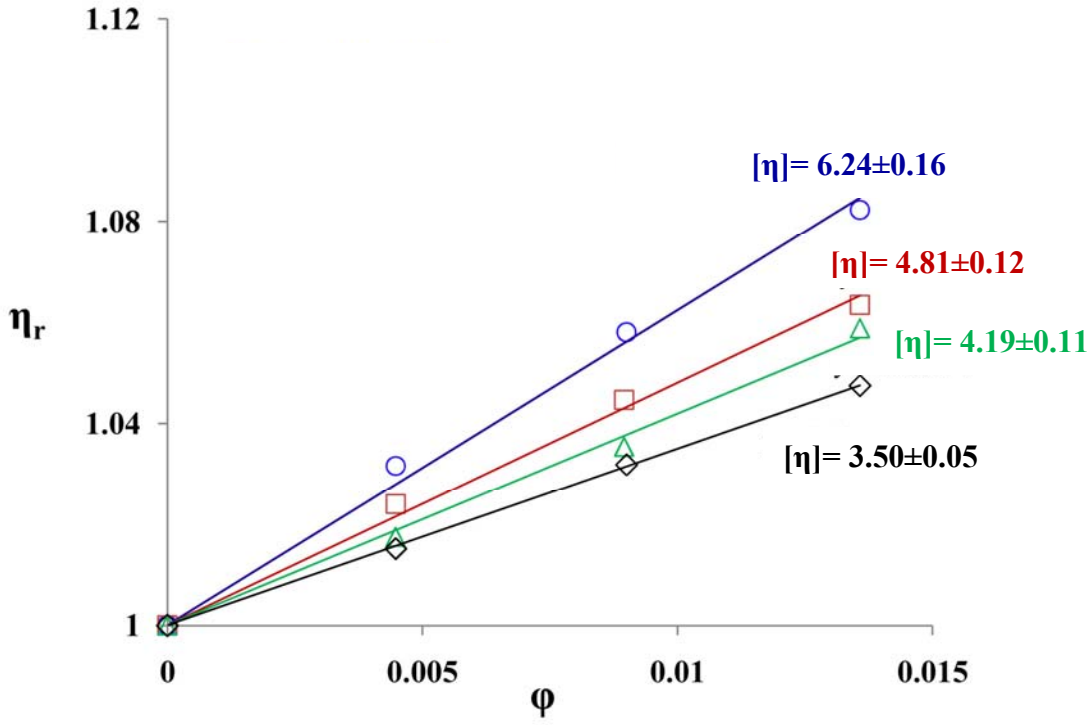

Figure 2.2 Relative viscosity of suspensions of S3 versus particle volume fraction at different $LiNO_3$ salt concentrations in NMP. ○ S3-NMP; □ S3-2mM $LiNO_3$-NMP; Δ 10mM $LiNO_3$-NMP; ◊ 20mM $LiNO_3$-NMP.

The mechanism of charging of particles in an aqueous/organic medium is described in several literature sources [5,6]. Since NMP is an organic liquid, the concentration of dissolved salt in as-purchased NMP is low and the implication is that charges on the silica particles are only minimally screened. Therefore, the measured viscosity of spherical siliceous particles in NMP should be enhanced as a result of the additional viscous dissipations associated with distortions of the electric double layer around the silica particles in a flow field. This enhancement of intrinsic viscosity for suspensions of charged spheres is known as the primary electroviscous effects and has been a subject of investigation by many authors [8,10]. Our claim that electroviscous effects are primarily responsible for the observed deviations of the intrinsic viscosity of silica/NMP solutions from the Einstein model is bolstered by the fact that the intrinsic viscosity decreases with increases in $LiNO_3$ salt concentration, as shown in Figure 2.2 and Figure 2.3. $LiNO_3$ is soluble in NMP and often used as an additive in membrane dopes [14]. This drop in intrinsic viscosity as a result of added salt is due to the screening of charges in suspensions of charged particles. It should be noted that the first data point in Figure 2.3 suggests a dissolved $LiNO_3$ concentration of ~0.1 mM in pure NMP. In fact, this concentration should be interpreted as an equivalent $LiNO_3$ concentration, which was estimated from the conductivity measurements shown in Figure 2.4; in reality, we expect that trace amounts of other ions than Li^+ and NO_3^- are present in as-purchased NMP.

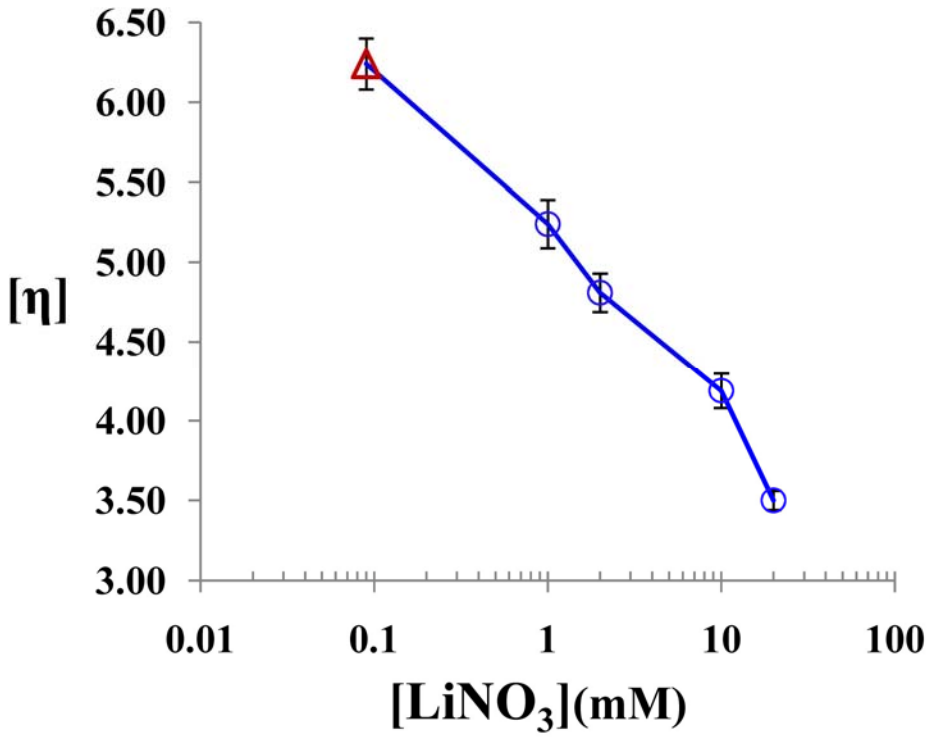

Figure 2.3 Intrinsic viscosity of suspensions of S3 silica particles in NMP at different dissolved salt concentration.

Figure 2.4 shows a plot of conductivity of NMP/$LiNO_3$ solutions versus $LiNO_3$ concentration. This graph shows that the solution conductivity is proportional to the amount of salt added to NMP. This observation makes us conclude that the $LiNO_3$ salt is completely dissolved and dissociated in NMP for the concentration range shown. For salt concentrations greater than 50 mM, it was found that the conductivity shows a plateau, an indication of limited solubility. As alluded to above, this plot can be extrapolated in the low salt regime towards the conductivity of pure NMP (horizontal line in the graph) to determine the equivalent dissolved salt concentration in "pure" NMP, which was found to

be 0.09 mM. Subsequently, the Debye length, 1/κ in NMP was calculated as 20.4 nm from equation (2.1) assuming only monovalent ions. However, as the particle concentration is increased into the semi-dilute and concentrated suspensions regimes, the excluded volume of particles and counter ion effects must be accounted for as demonstrated by Russel *et al.* [15]. They proposed equation (2.2) to account for the modified Debye length, $1/\kappa_{\varphi}$. Therefore, equation (2.2) may be used to calculate the modified Debye length for semi-dilute and concentrated suspensions of charged silica particles. These equations assume symmetrical electrolytes with ions of valency z; n_b is the bulk ionic concentration, φ is the volume fraction of particles of radius a, and surface charge density, σ_0. The zeta potential may be used to approximate the surface charge density, if data for charge density is unavailable.

$$\frac{1}{\kappa} = \left(\frac{2z^2 n_b e^2}{\varepsilon\varepsilon_0 k_B T} \right)^{-\frac{1}{2}} \tag{2.1}$$

$$\frac{1}{\kappa_{\varphi}} = \left\{ \left(\frac{e^2}{\varepsilon\varepsilon_0 k_B T} \right) \frac{\left[2z^2 n_b - \left(\frac{3\sigma_0 z\varphi}{ae} \right) \right]}{(1-\varphi)} \right\}^{-\frac{1}{2}} \tag{2.2}$$

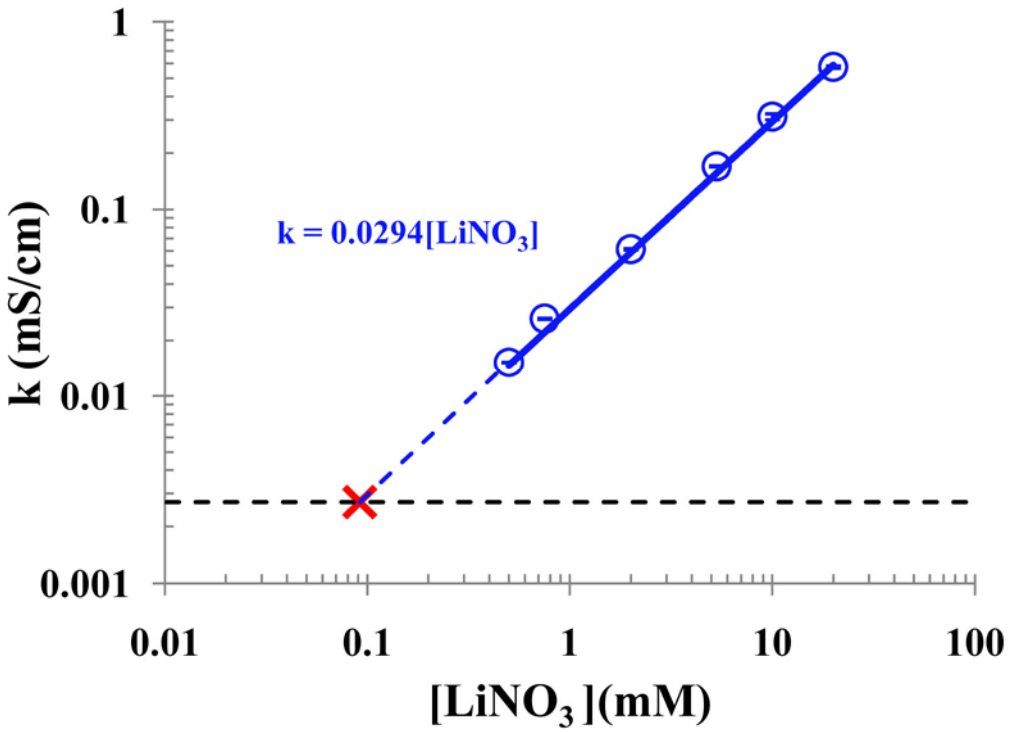

Figure 2.4 Conductivity *k* of solutions of [$LiNO_3$] in NMP at different dissolved salt concentrations, with extrapolation to determine the amount of dissolved salt in 'pure' NMP.

In order to interpret our results, we first compare them with the results of Watterson and White [8] for primary electroviscous effects. These researchers reported comprehensive numerical calculations of the primary electroviscous effects, *p* for reduced zeta potential, (eζ/kT) and *κa* values, *a* being the particle radius and *ζ* is the zeta potential. In this treatment, the effect of the primary electroviscous effect, $p(\zeta, \kappa a)$ on the viscosity of dilute suspensions of charged particles can be captured in equation (2.3) or (2.4) below.

$$\eta_r = \eta_0 \left[1 + \frac{5}{2} \varphi \left(1 + p\left(\zeta, \kappa a \right) \right) \right] \tag{2.3}$$

$$[\eta] = \frac{5}{2} \left(1 + p\left(\zeta, \kappa a \right) \right) \tag{2.4}$$

The primary electroviscous coefficient, p is a function of electrostatic potential ζ at the slipping plane that defines the hydrodynamic radius of the particle, and of the properties of the electrolyte ions captured in the Debye length, κ^{-1}. The theoretical prediction of p values calculated for the S3 particles in this study based on the numerical calculations of Watterson and White (*i.e.*, p_{calc}) are shown in Figure 2.5, together with our experimental values (*i.e.*, p_{exp}) determined from Figure 2.3 and equation (2.4). p_{calc} is determined by interpolation from the numerical solutions plots of Watterson and White using the reduced zeta potential ($e\zeta/kT$) and κa values of the suspensions of S3 particles in NMP at different [$LiNO_3$] as input variables and a constant ζ of 90 mV. Figure 2.5 reveals a large discrepancy between our experimental data and the theoretically predicted primary electroviscous coefficient, p_{calc}. Consequently, we believe the primary electroviscous effect alone may not account for the observed deviation from Einstein's hard sphere prediction. However, the fact that the experimental data in Figure 2.3 show sensitivity to the salt concentration suggests that the effect is electrostatic in nature. Since all viscosities reported above are for dilute suspensions ($\eta_r < 1.08$), secondary electroviscous effects that account for second order interparticle interactions [12,13] are not in play and thus cannot explain the observed deviations at these low particle volume fractions. In the

face of all the experimental data presented so far in relation to theoretical models, we must seek a different model to account for the observed substantial deviations from hard sphere and primary electroviscous effects theories. Still, we pursue a model that is electroviscous in nature, because of the observed salt effects. We refer to the experimentally observed electroviscous effect as p_{exp} and the calculated primary electroviscous effect as p_{calc} .

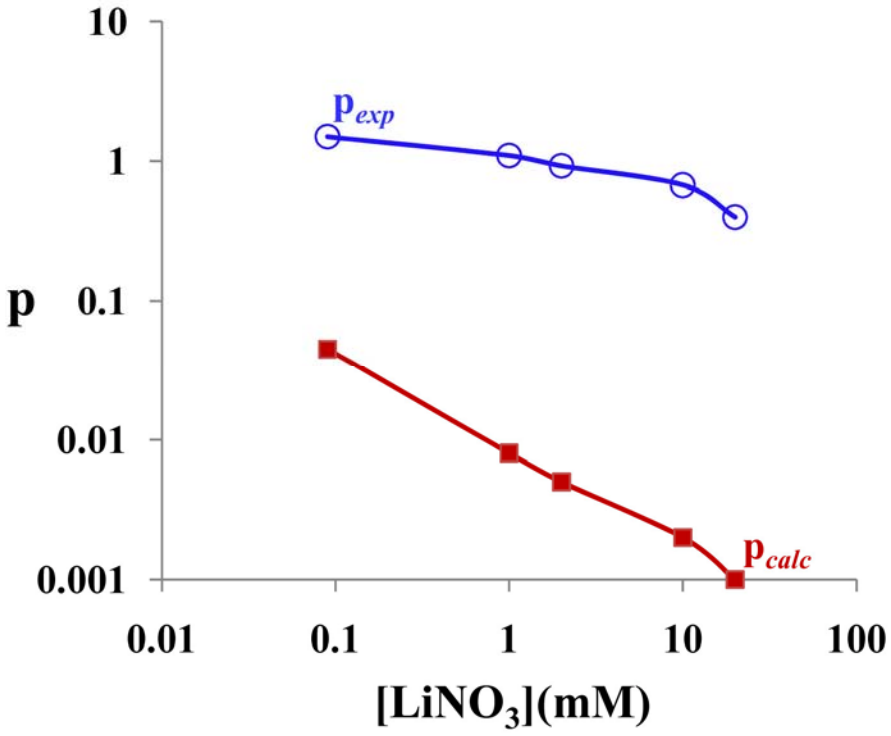

Figure 2.5 Comparison of experimental and theoretical 1st electroviscous effect for silica particles in NMP at different salt concentrations.

Tertiary electroviscous effect treatments [16] typically assume polyelectrolyte of thickness, δ is adsorbed from solution on to particle surface. Thus the effective particle size in solution is greater than the dry particle size. Just like for adsorbed polymers, the effective volume fraction occupied by particles in solution is related to the dry particle volume fraction, φ by the relation given in equation (2.5).

$$\varphi_{eff} = \varphi\left(1+\frac{\delta}{a}\right)^3 \tag{2.5}$$

Invoking a tertiary electroviscous model in our case study requires that a boundary layer of thickness δ is associated with the silica particles. Using this relation, δ for the 540 nm silica particles in pure NMP was determined as 94 nm. However, there are no dissolved species of this size in our suspensions. Therefore, the observed effective hydrodynamic radius, $a + \delta$, must be some kind of effective, immobile boundary layer around the particle, which is composed of constituents of the suspending medium: NMP, ions and other trace impurities. This analysis begs the question: what forces are capable of sustaining structures of such long range (*i.e.* 94 nm)? We hypothesize that a boundary layer of such range is possible in a situation where strong hydrogen bonding, poorly screened surface charges and a hydrophilic surface coexist.

In order to further explore the nature and structure of the boundary layer around the particle, we next consider how composition and structural changes in the suspending medium affect the rheology of silica particle suspensions. To do this, we measured the viscosity of dilute suspensions of S3 and the electrophoretic mobility of these particles in

NMP-water mixtures of different compositions. Figure 2.6 shows the relative viscosity of silica particles as function of particle volume fraction for various water concentrations in NMP; linear fits to these data show the intrinsic viscosity, which decreases with increasing water mole fractions from 0 to 0.55. In Figure 2.7, the intrinsic viscosity and electrophoretic mobility are both plotted as a function of water mole fraction in the NMP/water mixtures. At low concentrations, both quantities decrease strongly with increasing water content and an upturn occurs for water mole fractions greater than 0.55. The correlation between [η] and electrophoretic mobility support our established trend that electroviscous effects are in play. However, the changes in intrinsic viscosity again cannot be solely accounted on the basis of primary electroviscous effects because the corresponding changes in the Debye length of the medium cannot account for the effect of water addition. If these results are instead interpreted within the framework of the tertiary electroviscous model of an adsorbed boundary layer around the particles, the conclusion must be that the range of the adsorbed boundary layer can be changed significantly by varying the water content in NMP.

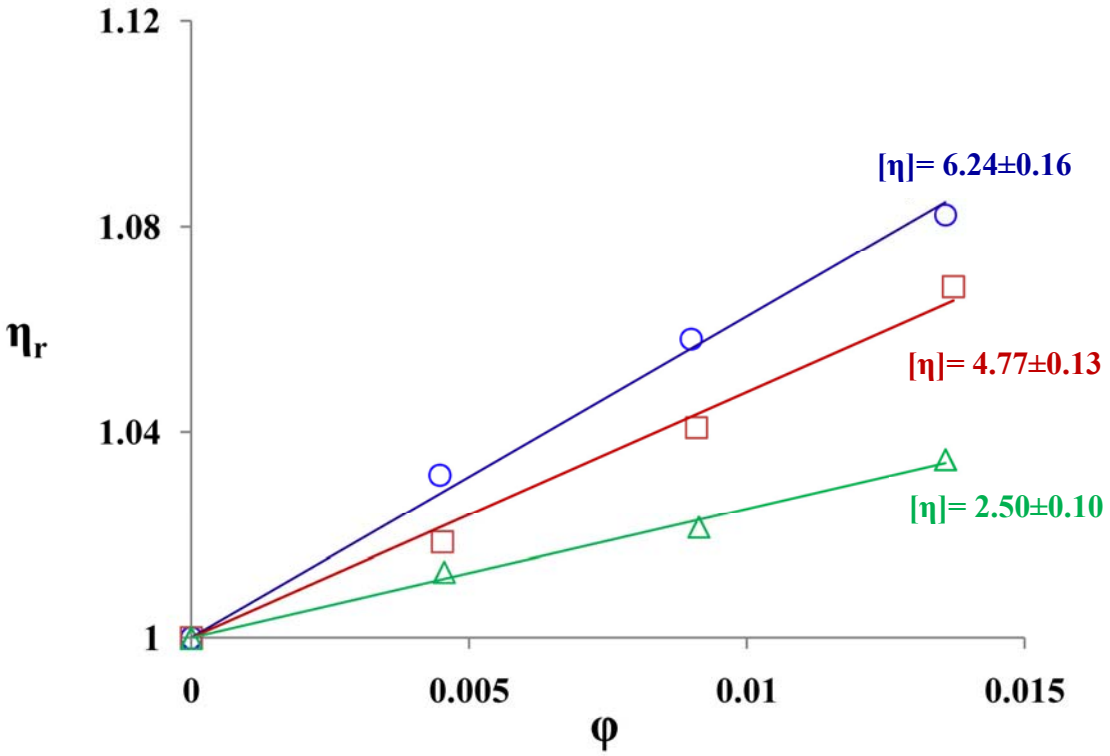

Figure 2.6 The relative viscosity for different water composition in NMP versus particle volume fraction. ○**S3-NMP**; □ **S3- [water-NMP] (10-90 vol.%)**; Δ **S3- [water-NMP] (20-80 vol.%)**.

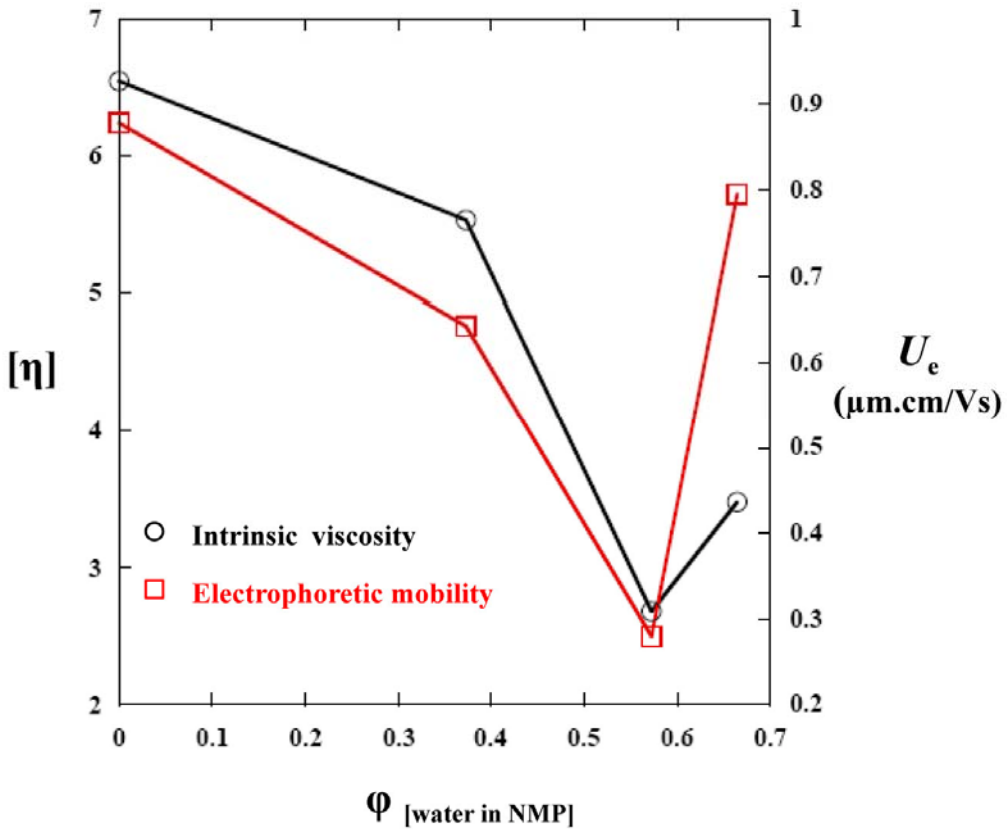

Figure 2.7 The intrinsic viscosity and electrophoretic mobility of suspensions of S3 particles as functions of mole fraction of water in NMP.

Consider our case study of hydrophilic silica particles suspended in aqueous NMP. It is well-known that water-NMP mixtures contain polar hydrogen bonded NMP-$(H_2O)_2$ complexes[17]. It is feasible that some of these complexes undergo hydrogen bonding with the hydrophilic silica surface or surrounding water molecules. Once this primary structure is formed, more NMP-$(H_2O)_2$ complexes, water, and NMP molecules may continue to form by the alignment of the polar molecules in the suspending medium to form contiguous hydrogen bonds; with the alignment power being some function of the

range of the field due to the electric double layer. That is, the assembling of the boundary layer will be limited only by the distance from the particle surface where the field strength becomes insufficient to confine structural units of the medium to the boundary layer against the diffusive force of Brownian motion. The strength and range of the electric field due to the electric double layer of the particle at any distance from its surface will depend on the dipole moment of the hydrogen-bonding in the medium, ζ and κ^{-1}. Unfortunately, there are no available models for calculating this dependence because of the difficulties associated with the theory of the liquid state and liquid boundary layers. The existence of boundary layers of water on surfaces was first reported in the 1930s by Derjaguin and Kussakov.[18] Derjaguin showed that the overlap of structurally modified boundary layers when the interlayer becomes thinner and the surfaces approach each other give rise to structural forces. He argued that structural forces are the third component of disjoining pressure, alongside the two other well known components: Van-der Waals and electric double layer forces. This has been experimentally confirmed in the reports by Kitchener and other authors [19-21]. Despite the experimental veracity of structural forces very little interest has been paid to it due to the remarkable success of the DLVO stability theory, which focuses exclusively on electrostatic and molecular forces as the only two components of disjoining pressure.

This trend of unexpectedly high intrinsic viscosity we have described here for suspensions of silica particles in NMP has been reported for aqueous dispersions of silica in water by other authors [22-26]. To explain their results, Laven and Stein[22] interpreted the high intrinsic viscosity as been due to a porous polyelectrolyte gel-like structure [27-30] of silica particles or at least their surface layer. They hypothesize that

the silica gel behaves like a swollen polyelectrolyte network; the size of the network may be greater than the dry particle and it shrinks as the isoelectronic point (IEP) is approached at high ionic strengths. We think this model is improbable because we have shown that just by increasing the concentration of DI water in NMP; the intrinsic viscosity goes through drastic changes that can't be accounted on the basis of the modest [screening ions] changes involved. Thus we think that our model of an immobilized boundary layer around the particles (which is a function of the particles interaction with the components of the suspending medium) is a more realistic physical model for our experimental observations on dilute suspensions of siliceous particles in NMP.

2.4 Semi-dilute and concentrated suspensions in aqueous liquids

In Section 2.2, it was established that siliceous particles acquire surface charges in NMP. It was also shown that the acquired charges contribute to electroviscous effects in dilute suspensions of silica, resulting in intrinsic viscosities that are much greater than the Einstein value. In these dilute suspensions, the particles were assumed to be so far apart that adjacent particles do not interact hydrodynamically or through overlap boundary layers or double layers. However, as the particle concentration is gradually increased, the particles will inevitably start to interact, raising the need to include a second order corrective term for interparticle interactions in the viscosity model. For uncharged hard spheres this correction was first computed by Batchelor [31] as expressed in equation (1.2) in Chapter 1.

For charged particles, the secondary interaction term may be greatly enhanced above 6.2; such observations have been reported in numerous sources, including the classic work of

Russell on the secondary electroviscous effects of charged spheres [12]. The relative viscosity expression capturing the secondary electroviscous effects for particles of radius, a with center-to-center distance, r_0 is given by

$$\eta_r = 1 + [\eta]\varphi + \left[2.5 + \frac{3}{40}\left(\frac{r_0}{a} \right)^5 \right] \varphi^2 \qquad (2.6)$$

For suspensions of silica spheres in NMP or water, equation (2.6) should be more relevant for predicting the viscosity than equation (1.2), since silica particles become charged in NMP or DI water. Consequently, one would measure coefficients of the secondary term that are much greater than the Batchelor value of 6.2. The S1 silica particles are used here; they are 100 nm in diameter and specific gravity of 2.35.

Figure 2.8 shows the relative viscosity of S1 particles in NMP and in water as a function of particle volume fraction. The zeta potential in NMP and water were measured as 59 ± 5 mV and 60 ± 5 mV, respectively, which implies that one should measure similar secondary electroviscous coefficients in NMP and in water, as can indeed be seen in Figure 2.8. For these 100 nm silica particles (S1), the secondary term coefficient is almost an order of magnitude greater than the Batchelor coefficient. The secondary electroviscous effect primarily stems from an increase in the particles' effective collision diameter due to the range of the electric double layer around them. It is possible to predict the secondary coefficient from equation (2.6) using an appropriate Debye length, to calculate r_0.

$$r_0 \approx 2a + \frac{5}{\kappa} \tag{2.7}$$

In the previous section, the Debye length in "pure" NMP was estimated to be 20 nm. As the particle concentration is increased, the double layer ions of the particles will start to contribute significantly to the charge screening potential of the medium. For particle volume fractions up to 0.05 in NMP, the Debye length of the medium decreases to ~16.7 nm; calculated by equation (2.2). Using this value in equations (2.7) and (2.6), the secondary term coefficient can be calculated as 51.76, in good agreement with the experimental fitted value of 51.7 for suspensions of S1 in NMP according to Figure 2.8. At these semi-dilute concentrations, using the estimated Debye length of 16.7 nm for φ = 0.05, in equation (2.7), the effective charged sphere diameter for S1 is 154 nm.

It should be noted that the intrinsic viscosity fitted to data in the dilute regime differs from the linear coefficient found if viscosity data at higher concentrations in the semi-dilute regime are included as well. For S1 particles in NMP, for instance, the fitted intrinsic viscosity decreases from 5.98 to roughly 4.26 if data in the semi-dilute concentration regime are included. This observation we think is due to charge regulation; whose net effect is to decrease the surface charge density. Charge regulation [32,33] occurs when charged surfaces come in very close proximity such that the electric double layers of charged surfaces start to overlap. Electric double layer overlap is important in semi-dilute suspensions of charged particles.

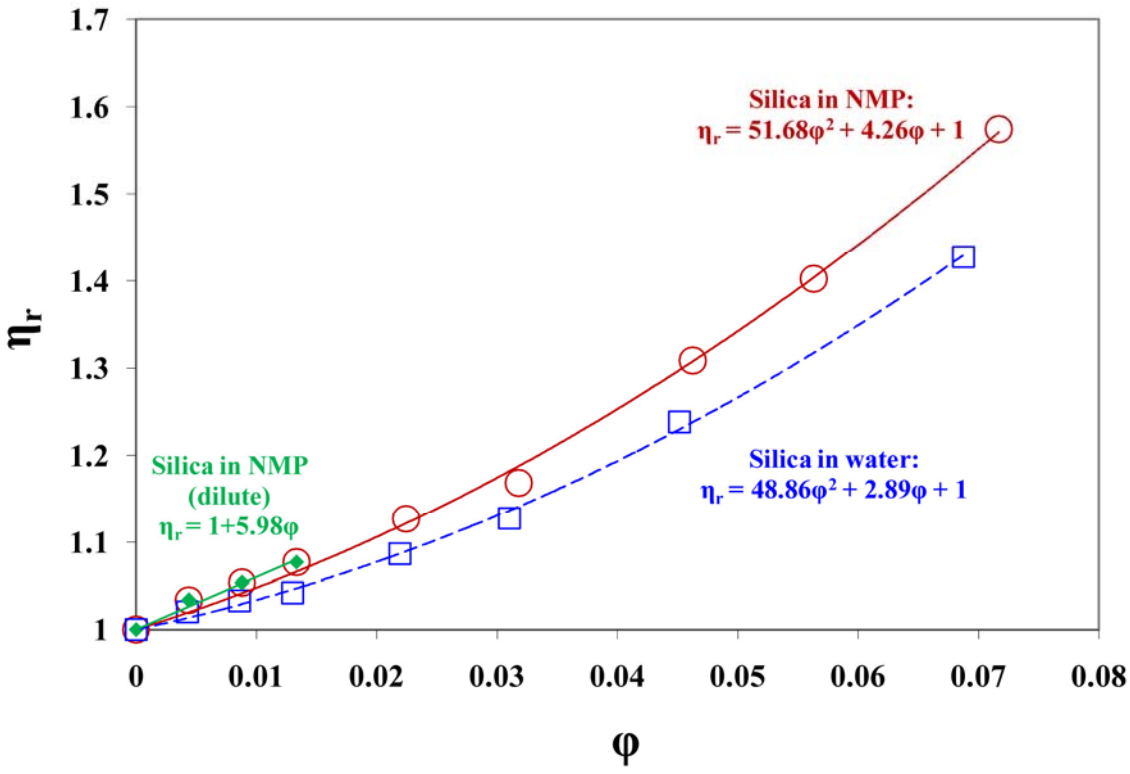

Figure 2.8 Relative viscosity as function of S1 particles volume fractions for semi dilute concentrations of silica in NMP and water.

As the particle concentration is increased from the semi-dilute regime to even higher concentrations, multi-body interactions and higher order contribution terms begin to dominate the rheology of the suspension.

Figure 2.9 shows the graph of relative viscosity as a function of S1 particle volume fraction in NMP up to the concentrated regime. The graph (note the logarithmic scale) shows that the viscosity of silica in NMP diverges at around 17 vol.% of particles in the suspension; this is in sharp contrast with the maximum random packing fraction of 63 vol.% expected for hard sphere suspensions. Our experimental observation actually

shows good agreement with theoretical predictions of concentrated charges particles suspensions. For hard spheres the effective collision diameter would be greater than for hard spheres due to the repulsion associated with the double layer overlap. This means that in a suspension, charged particles cannot be packed as closely as uncharged particles. Consequently, the maximum packing fraction, φ_m for charged spheres is less than for hard spheres. One would expect the equation relating φ_m to the effective center-to-center hard sphere diameter, r_0, to depend on the magnitude of the zeta potential and the Debye length of the suspending medium. The relevant equations are expressed in equations (1.6), (1.7) and (2.8):

$$\varphi_m = 0.63\left(\frac{2a}{r_0}\right)^3 \tag{1.6}$$

$$r_0 \approx \kappa^{-1} \ln\{\alpha / \ln[\alpha / \ln(\ln\alpha / \ln ...)]\} \tag{1.7}$$

$$\alpha = \left[\frac{4\pi\varepsilon\kappa(a\zeta)^2 \exp(2\kappa a)}{k_B T}\right] \tag{2.8}$$

a is the particle radius, κ^{-1} the Debye screening length, and ζ the zeta potential. Using these equations, φ_m is calculated as 0.162, in good agreement with the experimentally observed value of 0.17, determined from the divergence of the curve of Figure 2.9. This is a consequence of the fact that the effective collision diameters of the charged S1 silica

particles in NMP significantly exceed their actual hard sphere diameter by a thickness, 2δ. It is possible to estimate the charged spheres diameter, $r_0 = 2(a + \delta)$ from equation (1.7), as shown below for particle radius, a = 50nm:

$$0.63 = 0.17\left(1+\frac{\delta}{a}\right)^3$$

For 100 nm silica particles, δ = 27.5 nm. The result implies that the 100 nm silica particles appear to have a charged sphere diameter of about 155 nm in the concentrated suspension regime. This value is smaller than the r_0 = 183 nm, charged sphere diameter value observed at φ = 0.05, in the semi-dilute regime. This decrease of effective diameter from semi-dilute to concentrated suspensions is reasonable if charge regulation in concentrated suspension, arising from the increased double layer overlap, decreases the surface charge density.

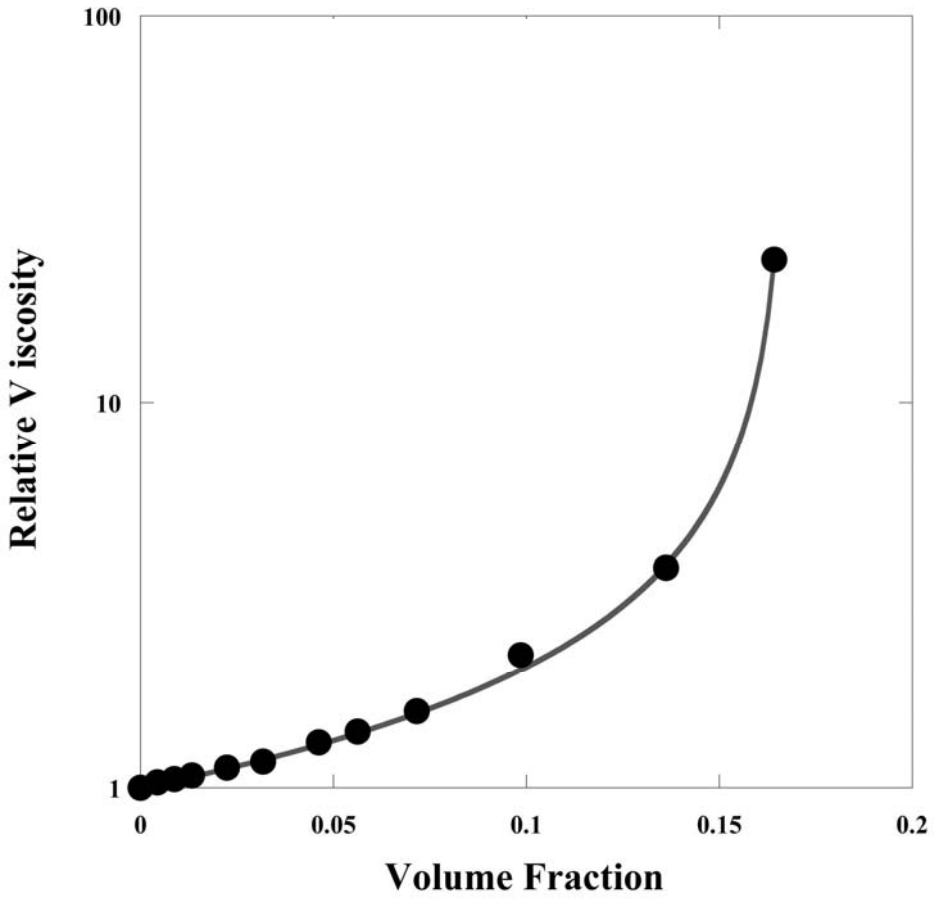

Figure 2.9 Relative viscosity as a function of particle volume fraction in concentrated suspension of silica particles in NMP.

2.5 Silica particles suspension with dissolved polymer in solution

In this section, the rheology of silica particles in the presence of dissolved polymer is investigated. This system is important because mixed-matrix membranes are made from suspensions of zeolite particles in polymer solutions. When bare silica particles are suspended in Ultem-NMP solutions, it was found that at particle concentrations greater than 2 wt. % the suspension becomes unstable with respect to aggregation of particles. This aggregation is the result of depletion flocculation [34], because Ultem polymer does not adsorb onto the silica surface. However, when silica particles were Ultem-sized by the method described in Section 1.4, we were able to prepare stable suspensions of silica particles in Ultem-NMP solutions over a wide range of particle concentrations; the grafted polymer layer provides a steric barrier against aggregation. In order to compare the rheology of bare silica with Ultem-sized silica, we assume a low Ultem polymer grafting density on silica particles, so that changes in the particle density and the surface electrical characteristics can be neglected. The latter is in part justified by the fact that the measured zeta potential values of Ultem-sized silica and bare silica are statistically the same in the light of the data presented in Section 2.2. Figure 2.10 showing flow curves comparing the viscosity of suspensions of ^{UZ}S1 in comparison to S1 particles in NMP shows that their rheology is essentially the same. The main reason for this observation is that the rheology of these suspensions is controlled by the thickness of the electric double-layer (κ^{-1} = 20 nm in pure NMP) and the surface charges on the particles. The range of the double layer and the boundary layer around siliceous particles exceeds the radius of gyration of the grafted Ultem polymer (R_g ~ 10 nm). Hence, one would expect the rheology of both bare particles and Ultem sized particles to be governed by surface

potential, which is roughly the same for bare and Ultem-sized silica particles. This is another supporting evidence for our earlier conclusion that the rheology of siliceous particles in aqueous media is dominated by the structure and range of the boundary layer and/or electric double layer of the suspending medium around each particle.

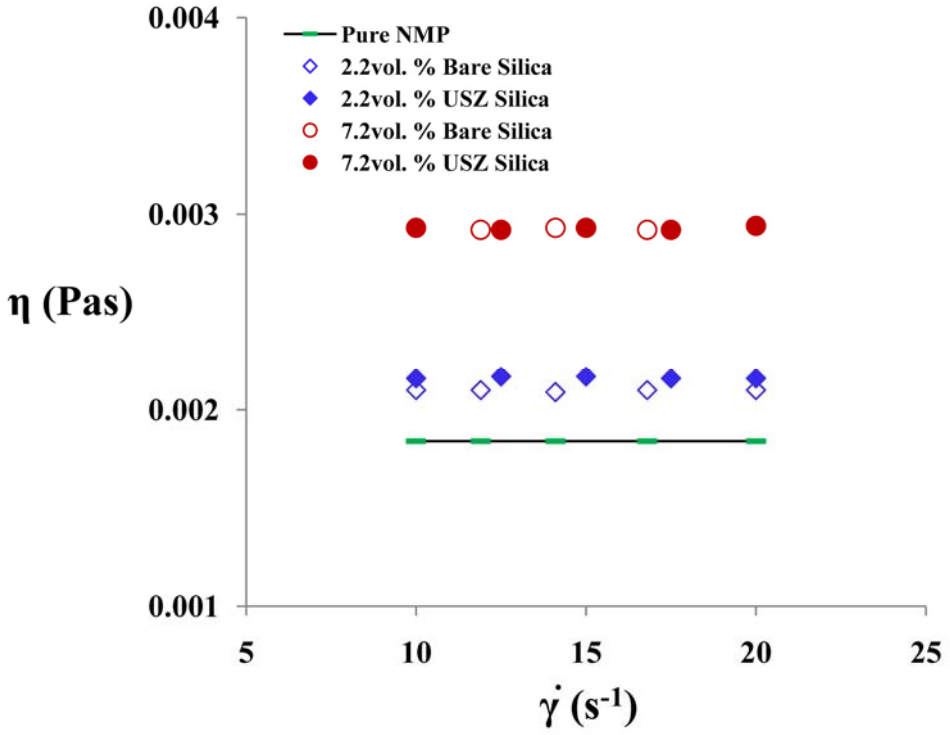

Figure 2.10 Flow curves comparing the viscosities of equal volume fractions of S1 and ^{UZ}S1 in NMP.

Since it has been shown that the rheology of well dispersed and stable siliceous particle suspensions is roughly the same for bare and Ultem-sized silica, the emphasis hereafter will be on Ultem-sized particles, because the grafted polymer layer helps to avoid depletion flocculation and to ensure that particles are well dispersed in solution.

Here, data is reported to compare the rheology of 100nm Ultem-sized silica particles (^{UZ}S1) suspended in (a) 30 wt.% Ultem/NMP solution and (b)'pure' NMP in Figure 2.11. The graph shows relative viscosity as a function of particle volume fraction. It can be seen that the viscosity of particles suspended in Ultem/NMP is significantly greater than for the pure NMP solvent at corresponding particle concentrations, especially in the dilute and semi-dilute regimes. These data suggest that the intrinsic viscosity of suspensions of ^{UZ}S1 in a polymer solution significantly exceeds the intrinsic viscosity for suspensions of ^{UZ}S1 in pure solvent. This observation is contrary to hard spheres prediction; intrinsic viscosity should be independent of the nature of suspending medium. However, we showed in Section 2.3 that changing composition of NMP by increasing [H_2O] in NMP significantly changes the intrinsic viscosity. Thus one may envisage a scenario in which the dissolved macromolecules in solution also significantly affect the structure and range of the immobilized boundary layer around particles. The enhanced viscosity observed for these suspensions in polymer solutions may be also be partly due to entanglements between polymer chains grafted on particles and entangled polymer coils in the concentrated bulk polymer solution. For suspensions in pure NMP this entanglement effect would be absent since there are no dissolved macromolecules in solution.

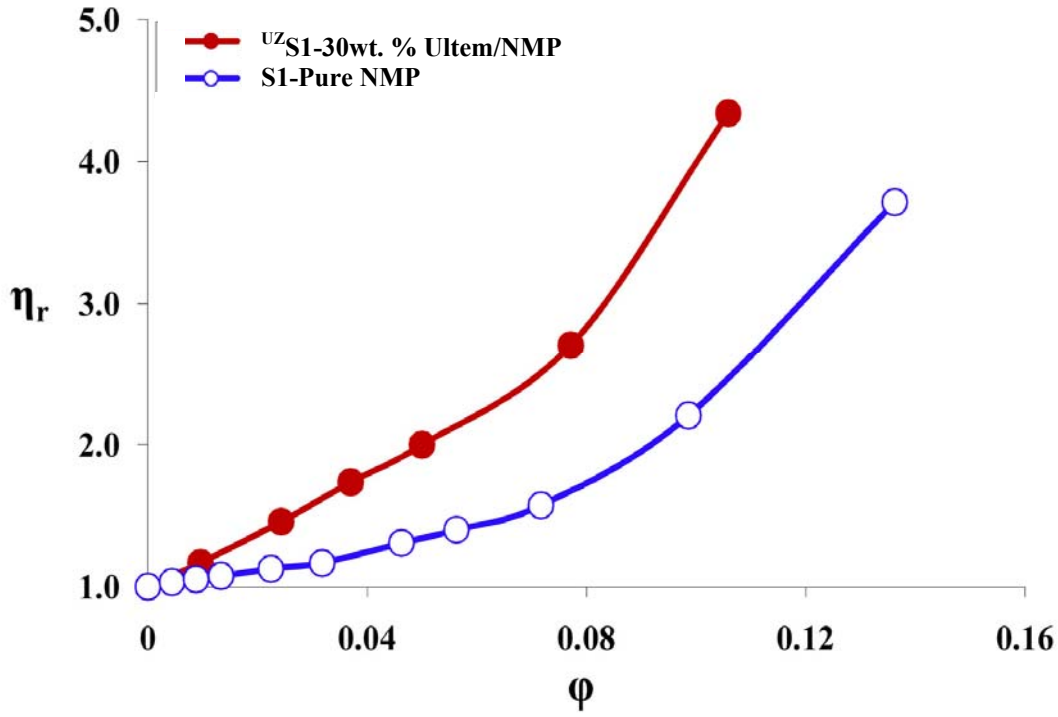

Figure 2.11 Relative viscosity as a function of particles volume fractions for suspension of [UZ] S1 in polymer solution and in pure solvent.

2.6 LTA zeolite particles suspensions in polymer solution

The subject of this final section is to investigate the rheology of zeolite particles in polymer solutions. LTA particles are chosen as the preferred zeolite particles for use in the mixed-matrix membranes (MMMs) because of the requirements of the targeted gas separation application. It is reasonable to expect that the same colloidal and structural forces operative in silica particle suspensions should also be in play in zeolite particle suspensions. LTA particles are hydrophilic, and like silica particles they acquire negative surface charges in NMP solvent with measured zeta potential value of 95 ± 5 mV. The

implication is that the intrinsic viscosity of LTA particles in NMP mediated solutions should be governed by the same forces that were in play for silica particle suspensions. Bare and solvothermally treated (SVT) LTA particles are used in these studies. The details of the solvothermal treatment method are described in the paper by Bae *et al.* [35]. Untreated LTA particles form sufficiently stable suspensions in Ultem/NMP solutions. However, to promote interfacial adhesion between polymer and particles in the final MMMs, SVT particles have been proposed for use in place of untreated (bare) particles. The solvothermal treatment of particles involves the deposition of $Mg(OH)_2$ nano-crystals on particle surfaces. The LTA particles used in this experiment are polydispersed bare LTA and solvothermally treated LTA (SVT LTA). The SEM micrographs of these particles are shown Figure 2.12 (a & b).

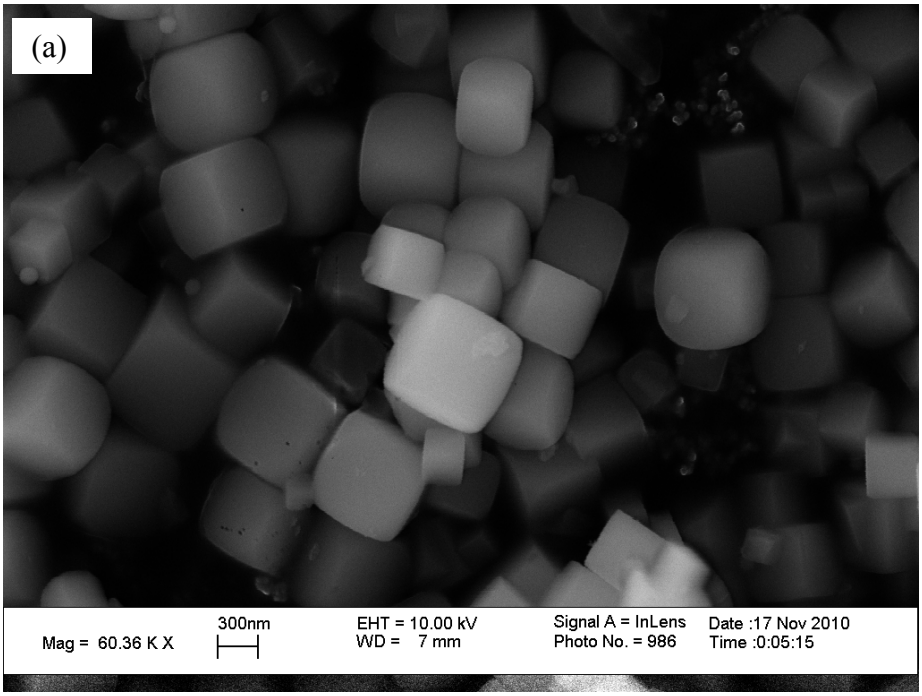

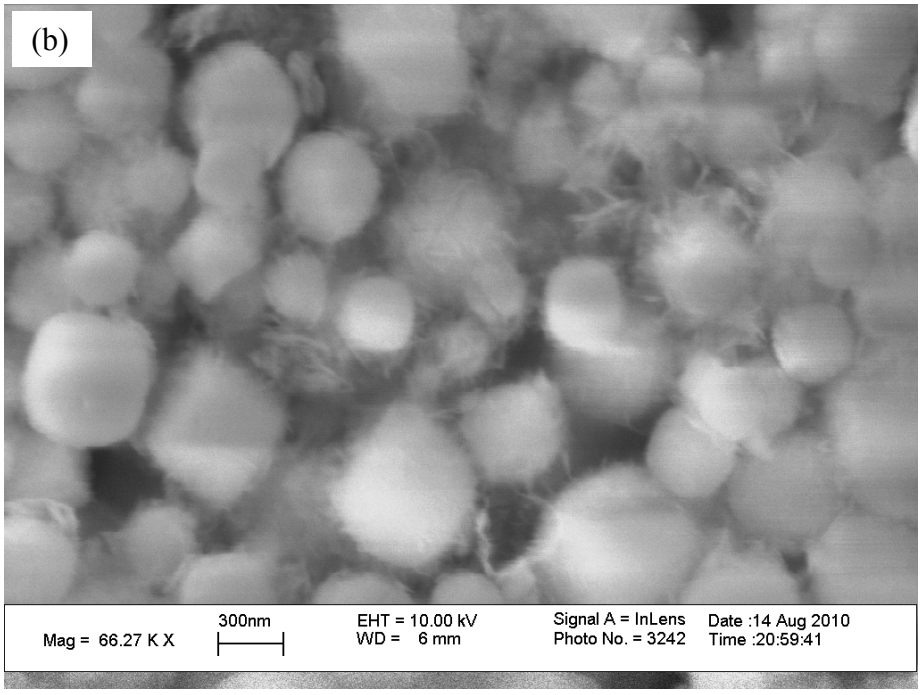

Figure 2.12 SEM image of (a) bare and (b) solvothermally treated LTA 4A.

The relative viscosity of LTA particles suspensions in a 30wt. % Ultem/NMP solution at three different temperatures as a function of particles volume fraction are shown in Figure 2.13. The particles shows anomalous rheological behavior in the sense that the suspension viscosity decreases as the particle concentration is increased from 0.5 to 1 volume percent of particles in solution. It is important to note that these maximums occur at around a relative viscosity of 1.13. It is interesting to note that this viscosity corresponds to particle volume fractions for which the transition between the dilute and the semi-dilute concentrations for hard spheres occurs. This coincidence lead us to believe that the two different regimes of viscosity scaling with particle concentration may be a consequence of charge regulation resulting from overlap of the electric double layer of the LTA particles. At particle concentrations where the double layer starts to overlap, the surface charges decreases with increasing particle concentration due to charge regulation. Such a decrease in surface charge in addition to the increased charge screening described by equation (2.2) with increased particle concentration may be responsible for the humps observed in Figures 2.13 and 2.14.

Figure 2.14 shows that the humps tend to peak at a higher crest with increase in the concentration of the dissolved polymer in solution. This is consistent with our previous observations; when the results in Sections 2.4 and 2.5 are compared for model S1 particles suspensions in pure NMP and 30 wt.% Ultem/NMP solution respectively. It was found that for the case of dissolved macromolecules in solution (*i.e.* suspensions in 30 wt.% polymer solution) the intrinsic viscosity was greater. Thus, one would expect that increases in the concentration of dissolved polymer in solution should result in increased intrinsic viscosities indicated by the higher humps in Figure 2.14.

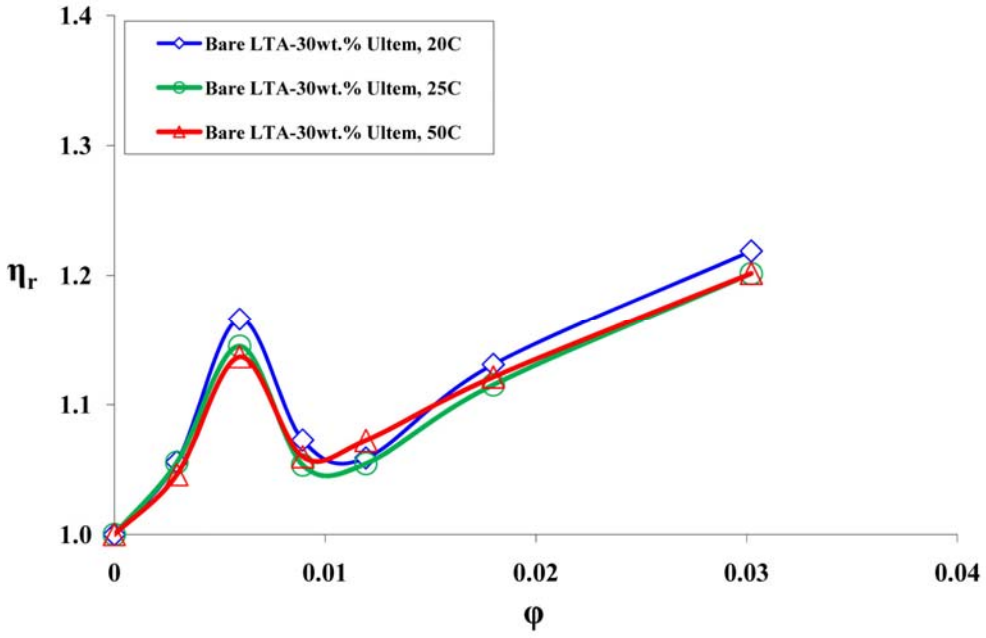

Figure 2.13 Relative viscosity of LTA particles as a function of particles volume fractions at different temperatures in a 30 wt.% Ultem/NMP solution.

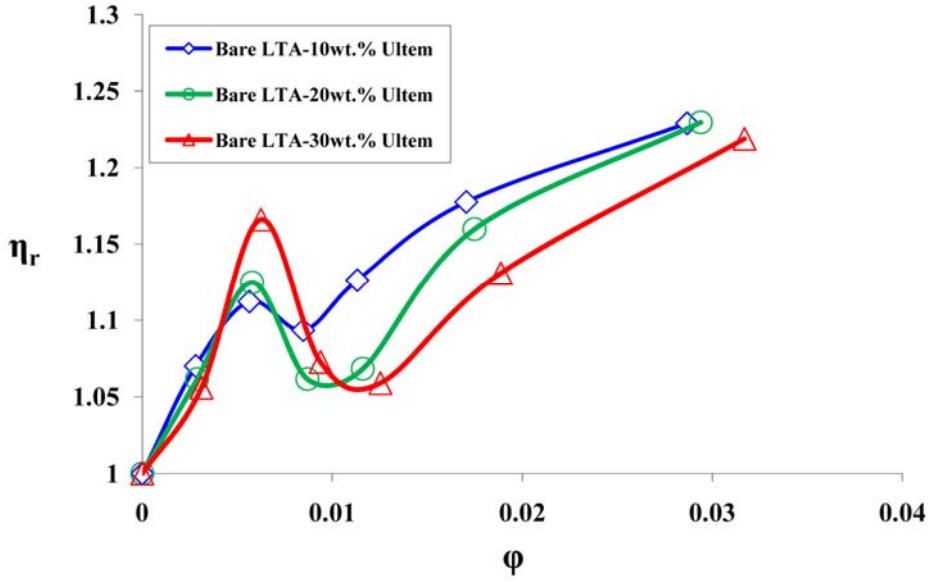

Figure 2.14 Relative viscosity of LTA particles as a function of particles volume fractions in different polymer concentrations at 20 ^{o}C.

Finally, the rheology of SVT LTA particle in a 30 wt.% Ultem/NMP solution as a function of particle volume fraction is reported in Figure 2.15. The rheology of these functionalized particles is important because they are the targeted molecular sieves for use in our finished mixed-matrix membranes. The measured concentrations are from the dilute to concentrated regime; although, concentrated suspensions are the preferred dopes used in the preparation of MMMs. The lesson from our model concentrated silica suspensions in Section 2.4 is that the viscosity of concentrated suspensions can be fully predicted with a Krieger-Dougherty (KD) type model when the *intrinsic viscosity,* $[\eta]$ and *maximum packing fraction,* φ_m are known. The other important finding from that section was that these values are markedly different than the values often quoted for hard spheres. Thus, in order to establish predictive capabilities for SVT LTA particles suspensions viscosities, it is important to determine values for these two parameters. To this end a KD type fit to our experimental data was performed to determine $[\eta]$. As expected, the value of [η] for SVT LTA particles is significantly different than for hard spheres. $[\eta]$ = 7 was determined for SVT LTA particles in 30 wt.% Ultem/NMP compared to the hard spheres predictions of 2.5. The explanation for this deviation is the same as previously explained in this chapter.

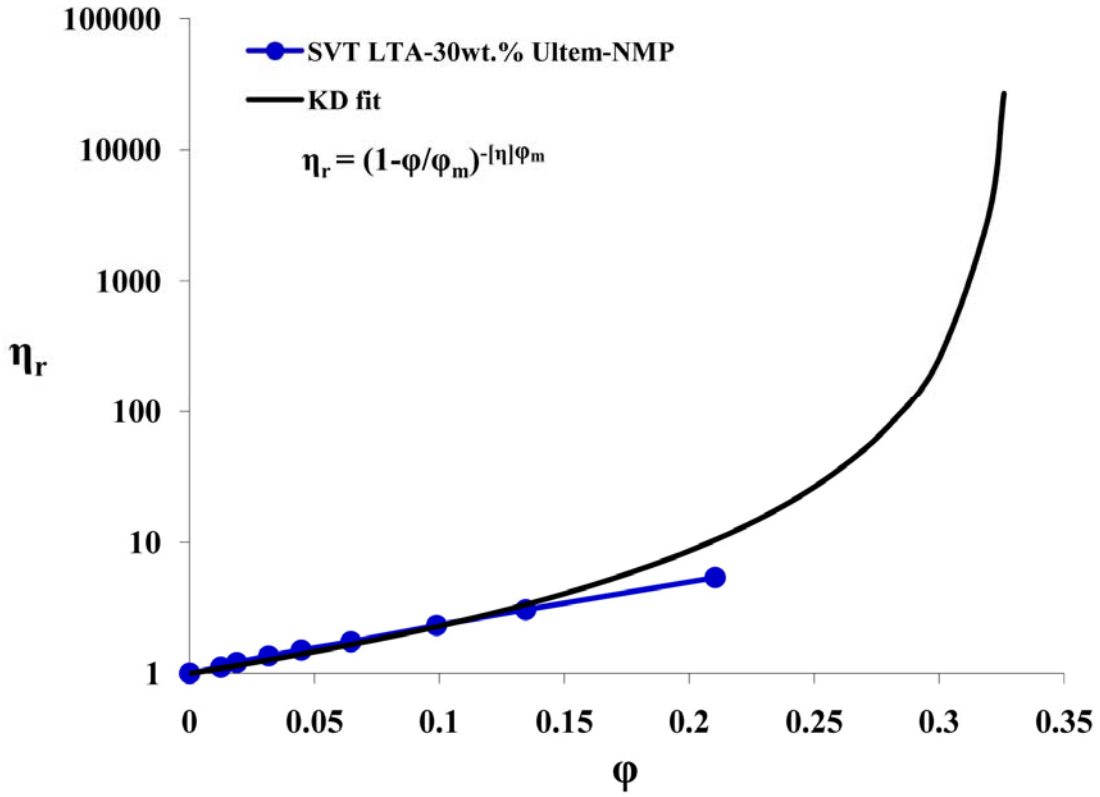

Figure 12.15 Relative viscosity as a function of particles volume fraction for SVT LTA in 30wt. % Ultem solution.

2.7 Conclusions

This chapter progressed from the rheological studies of simple suspension systems to increasingly complex ones. The purpose was to isolate and identify the colloidal and structural forces that determine the viscosity of mixed-matrix membrane dopes. Our studies of simple dilute suspensions of silica spheres in NMP shows that the intrinsic viscosity is influenced by double layer forces. We proposed that the major deviation from Einstein's hard spheres prediction stems from the immobilization of extensive boundary layers around particles. The range of this boundary layer we showed is both tunable by charge-screening ions and water concentration in NMP. In the semi dilute regime, it was found that the suspension viscosities can be very well understood on the basis of the secondary electroviscous models. Both in the semi dilute and concentrated suspensions the effective charged sphere collision diameters are larger than the hard sphere collision diameter of particles. The charged spheres effective collision diameter can be predicted from simple theories of colloidal interactions.

2.8 References

1. Flanigen EM, Bennett JM, Grose RW, Cohen JP, Patton RL, Kirchner RM, Smith JV: **Silicalite, a new hydrophobic crystalline silica molecular-sieve.** *Nature* (1978) **271**(5645):512-516.

2. Fyfe CA, Gobbi GC, Klinowski J, Thomas JM, Ramdas S: **Resolving crystallographically distinct tetrahedral sites in silicalite and zsm-5 by solid-state nmr.** *Nature* (1982) **296**(5857):530-533.

3. Parker LM, Bibby DM, Patterson JE: **Thermal-decomposition of zsm-5 and silicalite precursors.** *Zeolites* (1984) **4**(2):168-174.

4. Labib ME, Williams R: **The effect of moisture on the charge at the interface between solids and organic liquids.** *Journal of Colloid and Interface Science* (1987) **115**(2):330-338.

5. Labib ME: **The origin of the surface-charge on particles suspended in organic liquids.** *Colloids and Surfaces* (1988) **29**(3):293-304.

6. Vanderhoeven PHC, Lyklema J: **Electrostatic stabilization in nonaqueous media.** *Advances in Colloid and Interface Science* (1992) **42**(205-277.

7. Thwala JM, Goodwin JW, Mills PD: **Electrokinetic studies of colloidal silica particles dispersed in non-aqueous media in the presence of a nonionic surfactant, dodecylhexaethylene glycol monoether (c12e6).** *Colloids and Surfaces a-Physicochemical and Engineering Aspects* (2009) **335**(1-3):33-42.

8. Watterson IG, White LR: **Primary electroviscous effect in suspensions of charged spherical-particles.** *Journal of the Chemical Society-Faraday Transactions Ii* (1981) **77**(1115-1128.

9. Zurita L, Carrique F, Delgado AV: **The primary electroviscous effect in silica suspensions - ionic-strength and ph effects.** *Colloids and Surfaces a-Physicochemical and Engineering Aspects* (1994) **92**(1-2):23-28.

10. Booth F: **The electroviscous effect for suspensions of solid spherical particles.** *Proceedings of the Royal Society of London Series a-Mathematical and Physical Sciences* (1950) **203**(1075):533-551.

11. Russel WB: **Low-shear limit of secondary electroviscous effect.** *Journal of Colloid and Interface Science* (1976) **55**(3):590-604.

12. Russel WB: **Rheology of suspensions of charged rigid spheres.** *Journal of Fluid Mechanics* (1978) **85**(MAR):209-232.

13. Russel WB: **Review of the role of colloidal forces in the rheology of suspensions.** *Journal of Rheology* (1980) **24**(3):287-317.

14. Huang RYM, Feng XS: **Studies on solvent evaporation and polymer precipitation pertinent to the formation of asymmetric polyetherimide membranes.** *Journal of Applied Polymer Science* (1995) **57**(5):613-621.

15. Russel WB, Saville DA, Schowalter WR: *Colloidal dispersions.* Cambridge University Press, Cambridge (1989).

16. Vaynberg KA, Wagner NJ: **Rheology of polyampholyte (gelatin)-stabilized colloidal dispersions: The tertiary electroviscous effect.** *Journal of Rheology* (2001) **45**(2):451-466.

17. Imberg A, Evertsson H, Stilbs P, Kriechbaum M, Engstrom S: **On the self-assembly of monoolein in mixtures of water and a polar aprotic solvent.** *Journal of Physical Chemistry B* (2003) **107**(10):2311-2318.

18. Derjaguin B, Kussakov M: **Anomalousproperties of thin polymolecular films v. An experimental investigation of polymolecular solvate (adsorbed) films as applied to the development of a mathematical theory of the stability of colloids.** *Acta Physicochimica Urss* (1939) **10**(1):25-44.

19. Pashley RM: **Hydration forces between mica surfaces in electrolyte-solutions.** *Advances in Colloid and Interface Science* (1982) **16**(JUL):57-62.

20. Read AD, Kitchene.Ja: **Wetting films on silica.** *Journal of Colloid and Interface Science* (1969) **30**(3):391-&.

21. Blake TD, Kitchene.Ja: **Stability of aqueous films on hydrophobic methylated silica.** *Journal of the Chemical Society-Faraday Transactions I* (1972) **68**(8):1435-&.

22. Laven J, Stein HN: **The electroviscous behavior of aqueous dispersions of amorphous silica (ludox).** *Journal of Colloid and Interface Science* (2001) **238**(1):8-15.

23. Adamczyk Z, Jachimska B, Kolasinska M: **Structure of colloid silica determined by viscosity measurements.** *Journal of Colloid and Interface Science* (2004) **273**(2):668-674.

24. Adamczyk Z, Siwek B, Zembala M: **Colloid silica viscosity determined by the particle sedimentation method.** *Bulletin of the Polish Academy of Sciences-Chemistry* (2000) **48**(3):231-242.

25. Dekruif CG, Vanlersel EMF, Vrij A, Russel WB: **Hard-sphere colloidal dispersions - viscosity as a function of shear rate and volume fraction.** *Journal of Chemical Physics* (1985) **83**(9):4717-4725.

26. Honig EP, Punt WFJ, Offermans PHG: **The primary electroviscous effect - measurements on silica sols.** *Journal of Colloid and Interface Science* (1990) **134**(1):169-173.

27. Lyklema J: **Structure of electrical double layer on porous surfaces.** *Journal of Electroanalytical Chemistry* (1968) **18**(4):341-348.

28. Perram JW: **Structure of double-layer at oxide-water interface.** *Journal of the Chemical Society-Faraday Transactions Ii* (1973) **69**(7):993-1003.

29. Perram JW, Hunter RJ, Wright HJL: **Oxide-solution interface.** *Australian Journal of Chemistry* (1974) **27**(3):461-475.

30. Keesman MJ, Offermans PHG, Honig EP: **Silica-gel formation followed by dynamic shear experiments.** *Materials Letters* (1987) **5**(4):140-142.

31. Batchelor GK: **Brownian diffusion of particles with hydrodynamic interaction.** *Journal of Fluid Mechanics* (1976) **74**(MAR9):1-29.

32. Behrens SH, Grier DG: **The charge of glass and silica surfaces.** *Journal of Chemical Physics* (2001) **115**(14):6716-6721.

33. Borkovec M, Behrens SH: **Electrostatic double layer forces in the case of extreme charge regulation.** *Journal of Physical Chemistry B* (2008) **112**(35):10795-10799.

34. Lyklema J: **Adsorption of polymers and correlation with colloidal stability phenomena.** *Chemie Ingenieur Technik* (1970) **42**(12):844-848.

35. Bae TH, Liu JQ, Lee JS, Koros WJ, Jones CW, Nair S: **Facile high-yield solvothermal deposition of inorganic nanostructures on zeolite crystals for mixed matrix membrane fabrication.** *Journal of the American Chemical Society* (2009) **131**(41):14662-14663.

CHAPTER 3

THE RHEOLOGY OF SUSPENSIONS OF POROUS ZEOLITE PARTICLES IN POLYMER SOLUTIONS

3.1 Introduction

It was previously discussed in chapter 1 that the desire for better gas separation efficiencies has led to the development of mixed matrix membranes [1-6] (MMMs). For MMMs, the hollow fiber configuration is generally most suitable because of the high surface area per unit volume it provides for separation and the resulting enhanced productivity. A dual layer mixed matrix hollow fiber membrane possesses an outer annulus selective layer made of zeolite particles dispersed in a polymer matrix, supported by a porous polymeric inner annulus. The dope formulation for the selective layer consists of zeolite particles dispersed in a polymer solution, while the support layer is produced from a neat polymer solution. The spinning of dual layer MMMs dopes into hollow fibers of precise geometry and dimensions requires a good measure and understanding of the rheology of the dope formulations. To our knowledge, there are no reports in the literature were the rheology of porous inorganic particles in polymer solutions is discussed in any detail. This chapter addresses some of the unique ramifications of the presence of porous zeolite particles on the rheology of polymer solutions in general, and more specifically membrane dopes.

The rheology of model hard sphere suspensions has long been a subject of theoretical and experimental investigations. Fundamental and empirical models exist that successfully predict the viscosity of hard spheres suspensions from low to high particle loadings [7-

10]. However, most zeolite particles are not spherical. Particle non-sphericity [11-14] invariably results in additional viscous dissipations not accounted for by hard sphere models. For non-spherical particles with simple prolate or oblate axial symmetry, extensions of hard sphere models can still be used, using the particle aspect ratio as additional parameter [11]. The aspect ratio significantly affects the value of two key parameters: the intrinsic viscosity and the maximum packing volume fraction [11, 12, 15, 16]. For spherical particles, the aspect ratio is unity, while it is greater than 1 for nonspherical particles. In general, as the aspect ratio of particles increases, the intrinsic viscosity increases and the maximum packing fraction decreases; both effects act to enhance the viscosity of a suspension. For hard sphere suspensions, the size of suspended particles itself has no effect on rheology; the volume fraction is the only relevant parameter. The aspect ratio of MFI particles, however, depends on particle size due to unequal growth rates in various directions during the formation of the crystal structure[17, 18]. Based on this peculiar feature of MFI particles, one would expect the viscosity of suspensions of MFI particles to show size dependence. In addition, zeolite particles may possess surface silanol groups or other functional groups that can dissociate and acquire surface charge in aqueous solutions, which leads to a repulsive interparticle potential and enhanced viscosities due to electroviscous effects [19-23]. The emphasis of this paper will not be to account for the deviations listed above, which are fairly well documented in the literature. The goal of this study is to account for deviations from hard sphere behavior that arises from the porous structure of zeolite particles, which enables selective absorption of certain components of the suspending medium.

Specifically, in this paper we report data and semi-empirical models for the viscosity of suspensions of MFI zeolite particles in polymer solutions. As will be shown, the viscosity of zeolite suspensions is poorly predicted by available standard viscosity models. Zeolite particles often have internal pores that are sufficiently large to be accessible to water and other small solvent molecules, while excluding the larger polymer molecules. The selective absorption of solvent molecules from the suspending medium results in concentration changes of both polymers in the suspending phase and particles in the overall suspension, which can lead to dramatic increases in the viscosity of such suspensions. To correctly predict the viscosity of zeolite suspensions in polymer solutions, the quantity of solvent absorbed must first be determined. This can then be used to calculate the correct effective particle volume fraction and effective polymer concentration. We describe in this paper the effect of solvent absorption on the viscosity of zeolite particles in polymer solutions by developing mathematical models to account for solvent absorption. To this end, a solvent absorption parameter, α, was defined and experiments were designed to quantify it. The experimental determination of α is based on direct comparison of the viscosities of porous (calcined) and nonporous (uncalcined) MFI zeolite suspensions in polymeric solutions of polyetherimide (Ultem®) in NMP (N-methylpyrrolidone). This system was chosen because of its relevance for membrane spinning, but the concepts developed in this paper are more broadly applicable.

3.2 Experimental section

3.2.1 Materials

The polymer used in all experiments reported in this study is polyetherimide (Ultem 1000, MW ~ 61,000) purchased from GE plastics. The solvent of choice is NMP (99.95%), purchased from Sigma-Aldrich and used as received.

150 nm pure-silica MFI (shown in Figure 3.1) particles were used in this study. Pure-silica MFI crystals were hydrothermally synthesized using tetraethylorthosilicate (TEOS, Sigma-Aldrich) and tetrapropylammonium hydroxide (TPAOH, 40% in water, Alfa Aesar) as silica source and structure directing agent, respectively. The synthesis is described in Chapter 1 and in more detail in references [24-26]. In order to promote good dispersion of the particles in the polymer solutions, we used silane-treated MFI (ST-MFI) and Ultem-sized MFI (USZ-MFI) instead of untreated pure-silica MFI for our membrane dope preparation. The method of surface functionalization used is described in Chapter 1 and also available in greater detail in the paper by Husain and Koros [27].

Immediately after synthesis, MFI is in the uncalcined, nonporous form with a density of 1.99 $g \cdot cm^{-3}$ [17]. The microporous form is obtained by calcination in air at 500-600 ^{o}C for 8 hours. Calcination is the thermal decomposition of the organic templates to yield the calcined (porous) MFI of a lower density [17].

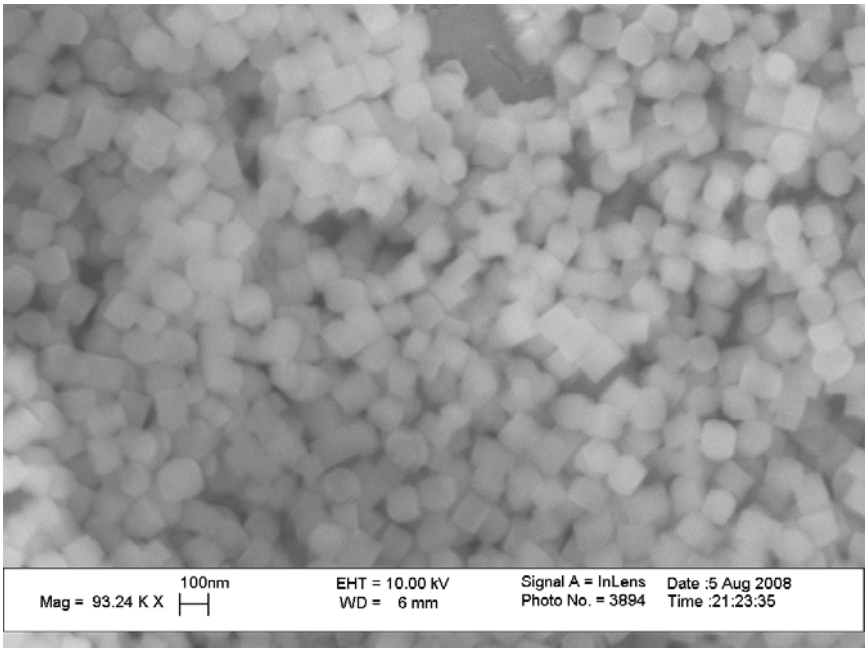

Figure 3.13 SEM micrograph of pure-silica MFI zeolite particles.

3.2.2 Sample preparation

The polymer was dried at 120 ^{o}C for 6 hours before use, while NMP solvent was used without any pretreatment. Polymer solutions were prepared by dissolving calculated amount of dried Ultem polymer in NMP and allowed to fully dissolve on slow roller for at least 72 hours at room temperature before measurements were performed. The suspensions were prepared carefully, following a well-defined protocol to facilitate good dispersion of the particles in a 30 wt.% Ultem/NMP solution. First, the required mass of zeolite was weighed on an analytical balance, and some solvent was added, followed by horn sonication (Biologics Inc., Manassas, VA) 3 to 5 times in 30 second bursts and with at least 1 minute rest intervals between successive steps. The sonication step was used to

break apart agglomerates of fired particles. The next step was a 'priming' step in which a small quantity of pre-prepared polymer solution is added to the sonicated suspension and the mixture is subsequently allowed to mix for 10 - 30 minutes on a slow roller. This step aims to sterically stabilize the suspension against particle aggregation through polymer adsorption. Finally, the remaining amount of polymer is added to the mixture as dried powder to bring the final concentration of all components to the desired dope composition.

3.2.3 Density measurements

The density of calcined MFI particles, ρ_{cal}, was determined by measuring the weight of a fixed volume of MFI before and after calcination, m_{uncal} and m_{cal}, respectively. Using the assumption that the external physical volume occupied by uncalcined and calcined MFI is the same, the density of calcined MFI could be calculated to be 1.76 from the following equation:

$$\rho_{cal} = \frac{m_{cal}}{m_{uncal}} \rho_{uncal} \tag{3.1}$$

The density of polymer solutions was determined with a pycnometer by measuring the weight of known sample volumes. The variation of the density of Ultem/NMP solutions as a function of polymer weight fraction is presented in Figure 3.2. This information is critical for the analysis of suspensions in which the polymer concentration in the suspending medium varies.

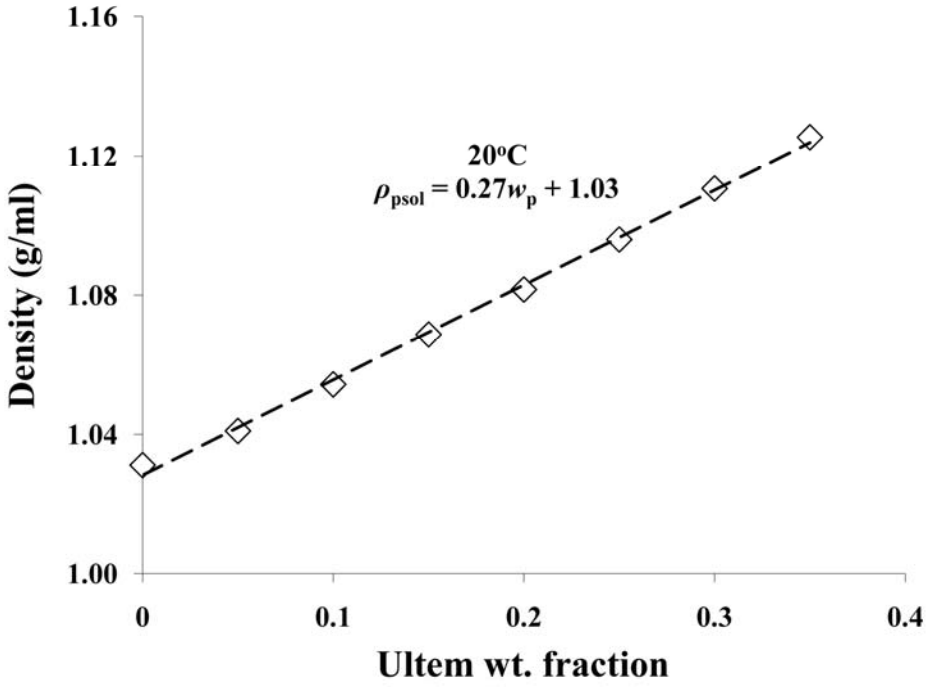

Figure 3.2 Density of Ultem/NMP solutions at 20 ºC as a function of polymer concentration with fitted linear correlation.

3.2.4 Rheological measurements

The shear viscosity of the pure polymer solutions was measured over a range of shear rates (0.1 - 100 s^{-1}) at 20 and 50 ^{o}C with a stress-controlled rheometer (MCR 300, Anton Paar) and Couette geometry (CC10; cup inside diameter 10.845 mm and bob outer diameter 10.000 mm). The viscosities reported for the polymer solutions and zeolite

suspensions in this paper were measured at low shear rates, before the onset of shear thinning, and thus represent the zero shear viscosity. For Ultem/NMP solutions at different polymer concentrations, the viscosity is shown in Figure 3.3. Flow curve measurements were also performed at different MFI particle loadings in suspending media with a nominal concentration of 30 wt.% Ultem in NMP for both uncalcined and calcined MFI particles. The fixed polymer concentration used for these zeolite suspensions represents an optimized dope composition that enables good spinning properties for Ultem/NMP solutions as reported in [28].

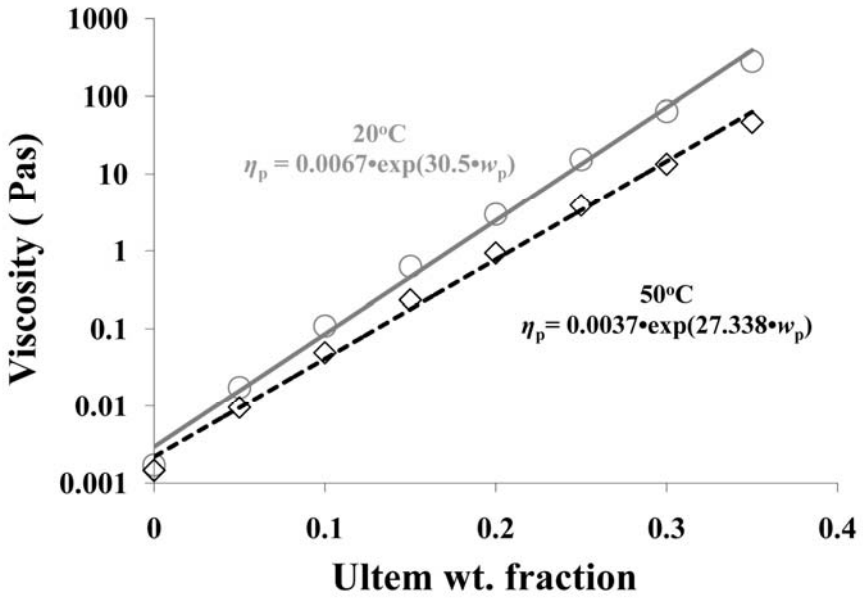

Figure 3.3 Viscosity of Ultem/NMP solutions as a function of polymer concentration at 20 and 50°C with exponential correlation functions.

3.3 Theoretical section

As previous mentioned, calcined MFI zeolite particles have a significant empty pore volume that is in principle accessible to solvent. If solvent molecules are small enough to penetrate into the available pores, then some quantity of solvent is lost from the suspending polymer solution, thereby increasing the polymer concentration. As an additional consequence, the reduced volume of the suspending medium effectively increases the zeolite volume fraction in the suspension. These two concentration changes contribute to a rise in viscosity and it is appropriate to derive model equations for the effective concentrations due to solvent absorption.

3.3.1 Models for effective polymer concentration and zeolite volume fraction

We define a dimensionless fractional absorption parameter, α, as the weight of absorbed solvent (NMP) per unit mass of dry zeolite in suspension. We denote the densities of polymer solution, solvent, zeolite particles and overall suspension as ρ_{psol}, ρ_{solv}, ρ_z and ρ_{susp}, respectively. The weight fraction of zeolite in the suspension is w_z and w_p is the as-prepared nominal weight fraction of polymer in the suspending medium. As a result of solvent absorption, the Ultem (polymer) weight fraction in the continuous phase deviates from the nominal values and must be corrected to $w_{p,eff}$. Similarly, although w_z remains constant, the rheologically more relevant volume fraction of zeolite in the suspension also must be corrected for absorption effects, $\varphi_{z,eff}$. Using this nomenclature, the absorption-corrected polymer weight fraction in the suspending medium can be calculated using

$$w_{p,eff} = \frac{w_p(1-w_z)}{(1-w_z)-\alpha w_z} \tag{3.2}$$

And the absorption-corrected zeolite volume fraction as

$$\varphi_{z,eff} = \frac{w_z}{\frac{\rho_z}{\rho_{susp}} - \alpha w_z \frac{\rho_z}{\rho_{solv}}} \tag{3.3a}$$

The overall suspension density, which varies, can be expressed in terms of other variables:

$$\frac{\rho_z}{\rho_{susp}} = w_z + (1-w_z)\frac{\rho_z}{\rho_{psol}} - \alpha w_z \frac{\rho_z}{\rho_{solv}} \tag{3.3b}$$

Combining equations (3.3a) and (3.3b) leads to the final expression

$$\varphi_{z,eff} = \frac{w_z}{w_z + (1-w_z)\frac{\rho_z}{\rho_{psol}} - 2\alpha w_z \frac{\rho_z}{\rho_{solv}}} \tag{3.3c}$$

As expected, the equations for absorption-corrected concentrations show that the concentration of polymer in the suspending phase and the zeolite particle loading both increase for increasing solvent absorption.

3.3.2 Models for effective viscosities

From the measured viscosity flow curves of different concentrations of Ultem/NMP solutions, a correlation for viscosity as a function of polymer weight fraction at 50°C is expressed in equation (3.4) as expected for concentrated polymer solution viscosities.

$$\eta_p = 0.0037 \cdot e^{27.3 \cdot w_p} \text{ (Pa·s)} \tag{3.4}$$

Hence, using equation (3.2), the corrected effective viscosity of polymer solution after solvent absorption becomes

$$\eta_{p,eff} = 0.0037 \cdot e^{27.3 \cdot w_{p,eff}} = 0.0037 \cdot e^{\left[27.3 \cdot \frac{w_p (1-w_z)}{(1-w_z)-\alpha w_z}\right]} \tag{3.5}$$

This equation can be expressed in a form that shows the relative increase in the viscosity of polymer solution as result of solvent absorption;

$$\frac{\eta_{p,eff}}{\eta_p} = e^{\left[27.3 \cdot \frac{\alpha w_p w_z}{(1-w_z)-\alpha w_z}\right]} \tag{3.6}$$

The Krieger- Dougherty (KD) model for suspensions viscosity is a frequently used model for viscosity prediction for hard sphere suspensions with intrinsic viscosity, [η] and maximum packing fraction, φ_m. There are several models for predicting suspensions viscosity; many of the models however only give good predictions for particular range of particle concentrations. Therefore, we have chosen to use the KD model for our suspension viscosity because of its versatile application to a wide range of particle concentrations and the ready availability of its input parameters (that yields itself readily to easy physical interpretation). The KD model expressed as:

$$\eta_r = \left(1 - \frac{\varphi}{\varphi_m}\right)^{-[\eta]\varphi_m} \tag{3.7}$$

Introducing the absorption-corrected zeolite concentration (equation (3.3c)) into the Krieger Dougherty hard sphere prediction yields the equation below; η and $\eta_{p,eff}$ are respectively the measured suspension viscosity and the effective viscosity of the suspending medium, *i.e.* the polymer solution:

$$\eta_{r,eff} = \frac{\eta_{susp}}{\eta_{p,eff}} = \left[1 - \frac{w_z}{\varphi_m\left(w_z + (1-w_z)\frac{\rho_z}{\rho_{psol}} - 2\alpha\varphi_z\frac{\rho_z}{\rho_{solv}}\right)}\right]^{-[\eta]\varphi_m} \tag{3.8}$$

It should be noted that in experiments the suspension viscosity is naturally compared to the viscosity of the original polymer solution, which gives rise to an apparent relative viscosity, $\eta_{r,\,app}$:

$$\eta_{r,app} = \frac{\eta_{susp}}{\eta_p} = \frac{\eta_{p,eff}}{\eta_p}\left[1 - \frac{w_z}{\varphi_m\left(w_z + (1-w_z)\frac{\rho_z}{\rho_{psol}} - 2\alpha\varphi_z\frac{\rho_z}{\rho_{solv}}\right)}\right]^{-[\eta]\varphi_m} \tag{3.9a}$$

$$\eta_{r,app} = \exp\left(27.3\frac{\alpha w_p w_z}{(1-w_z)-\alpha w_z}\right)\cdot\left[1 - \frac{w_z}{\varphi_m\left(w_z + (1-w_z)\frac{\rho_z}{\rho_{psol}} - 2\alpha\varphi_z\frac{\rho_z}{\rho_{solv}}\right)}\right]^{-[\eta]\varphi_m} \tag{3.9b}$$

Using equation (3.9b) and assuming that porous particles behave as Brownian hard spheres, the effect of solvent absorptions on the viscosity of suspensions of porous particles in a polymer solution can be calculated. The variation of the apparent relative viscosity as a function of particle volume fraction for different values of the absorption parameter α is presented in Figure 3.4. It should be noted that the polymer was assumed to be Ultem at 50°C and an original concentration of 30 wt.%, which are relevant parameters for the system under investigation. The plot shows clearly that the apparent relative viscosity increases strongly with the amount of solvent absorbed. The effect is most severe at high particle loadings since more solvent is absorbed from the continuous phase; the consequence of this is an exponential increase in the viscosity of the polymer

solution according to equation (3.6). The variation of the apparent relative viscosity as a function of polymer concentration at a fixed particle concentration (35 wt.% MFI zeolite) is shown in Figure 3.6 for the same values of α; again, the polymer is assumed to be Ultem dissolved in NMP at 50°C. This graph highlights the fact that the apparent relative viscosity is even more greatly enhanced by solvent absorption at higher polymer concentrations. In the light of these results, it is important to know the value of α as accurately as possible for suspensions of porous particles. In the next section, an experimental determination from rheology measurements will be described.

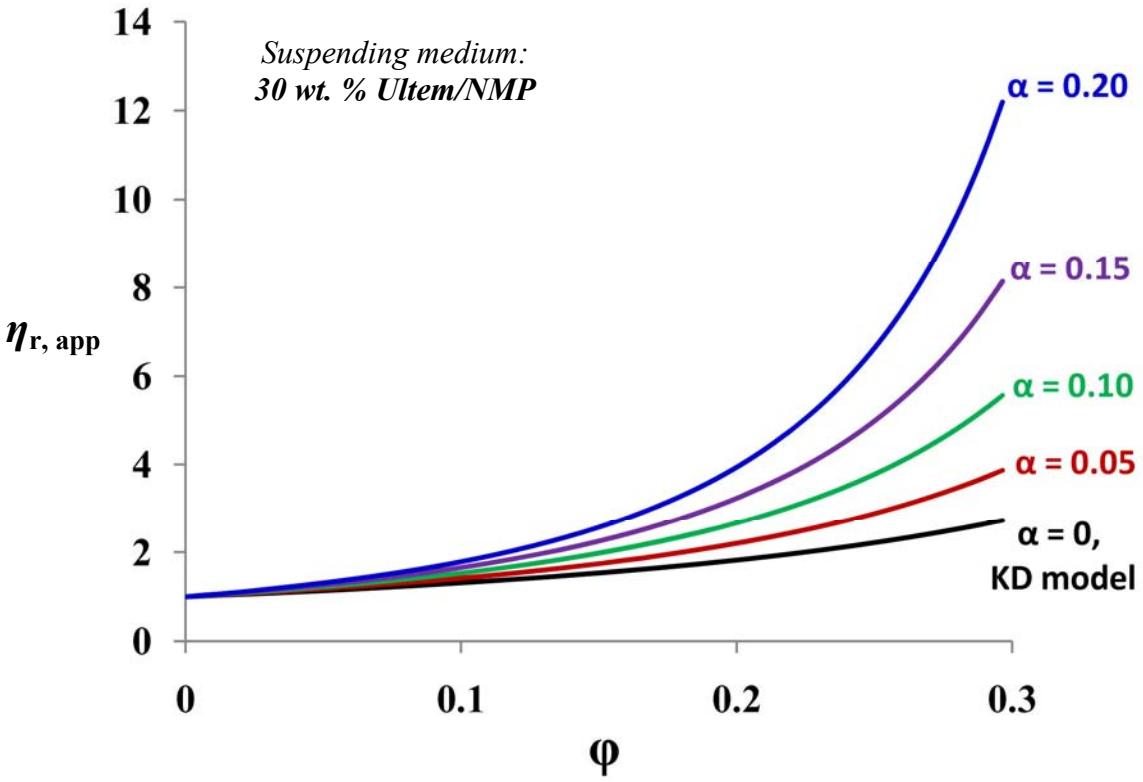

Figure 3.4 The apparent relative viscosity of suspensions of MFI particles in a 30 wt.% Ultem/NMP solution for different values of the absorption parameter *α*.

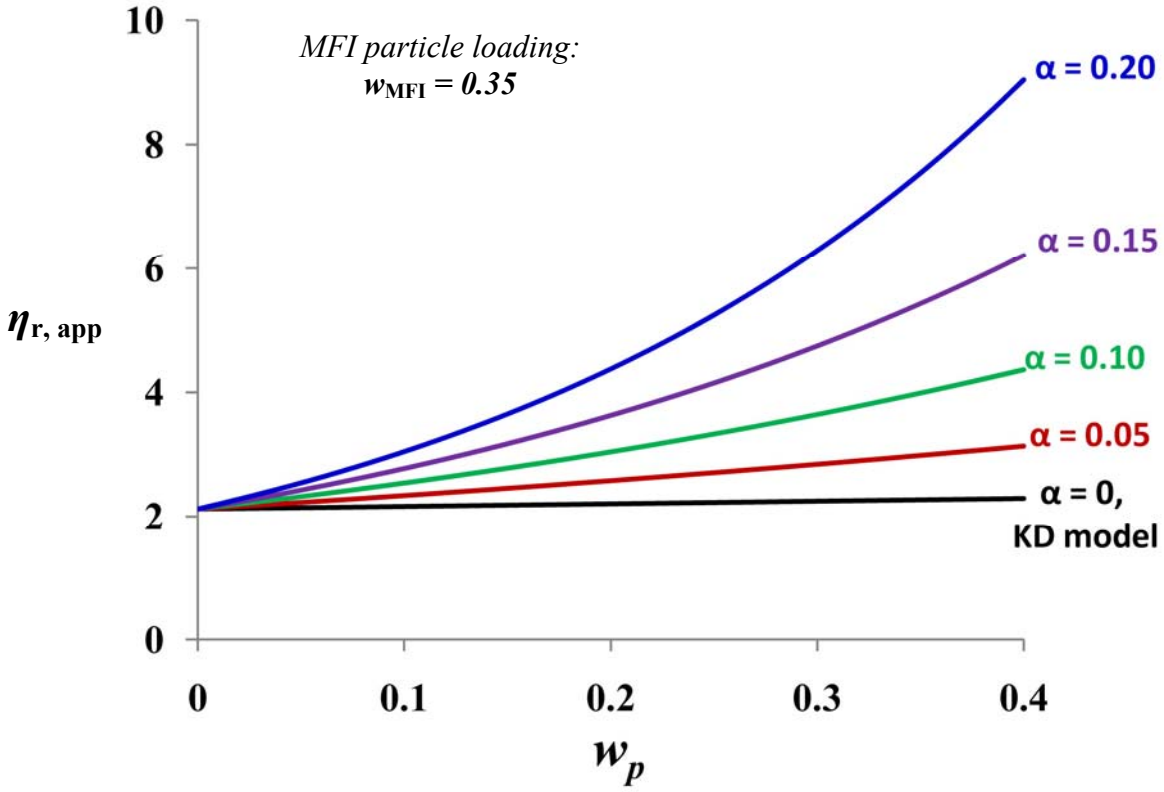

Figure 3.5 The apparent relative viscosity of suspensions with 35 wt.% MFI particles in suspending Ultem/NMP media with varying nominal weight fractions of polymer for different values of the absorption parameter *α*.

3.4 Results and discussion

Figure 3.6 presents experimental data on the apparent relative viscosities of calcined (porous) 150 nm USZ MFI suspensions in 30 wt.% Ultem/NMP solutions as a function of the apparent particle volume fraction, φ_z. This is only an apparent volume fraction because it is calculated based on dry calcined MFI particle density. In reality, the effective volume fraction is greater than the apparent volume fraction due to solvent absorption resulting in a decreased volume of the continuous phase. For comparison, the Krieger-Dougherty hard sphere model prediction is shown in the same figure. It is clear from this graph that there is a great disparity between the two trends. We propose two reasons for this discrepancy between the viscosity of zeolite and hard sphere suspensions. The first and major cause of deviations from hard sphere behavior is the effect described in the previous section: absorption of NMP solvent molecules from the polymer solution into the MFI zeolite pores. The apparent volume fraction of the zeolite suspension as plotted on the horizontal axis of Figure 3.5 is therefore not an accurate depiction of the effective particle volume fractions expressed in equations (3.3a) and (3.3c), but without knowing a, the effective volume fraction cannot be calculated. The apparent relative viscosity in Figure 3.5, calculated as the measured suspension viscosity divided by a 30 wt.% Ultem/NMP solution viscosity, is a combination of increased particle contribution to viscosity plus an additional contribution to the viscosity from the increased polymer concentration above the nominal 30 wt.% Ultem/NMP assumed. The effect is captured in equation (3.9), providing that the particles behave like Brownian hard spheres and that suspending medium does not affect the particle contribution to the viscosity. A secondary cause for the deviations in Figure 3.6 could be that the MFI

zeolite particles do not behave like hard spheres, so that the Krieger Dougherty equation is not an appropriate viscosity model. Although it is known that such non-idealities exist, it is generally not known a priori how strong these affect the suspension viscosity. We therefore devised a strategy to experimentally determine the absorption parameter, α without having to make assumptions about the applicability of the Krieger Dougherty equation.

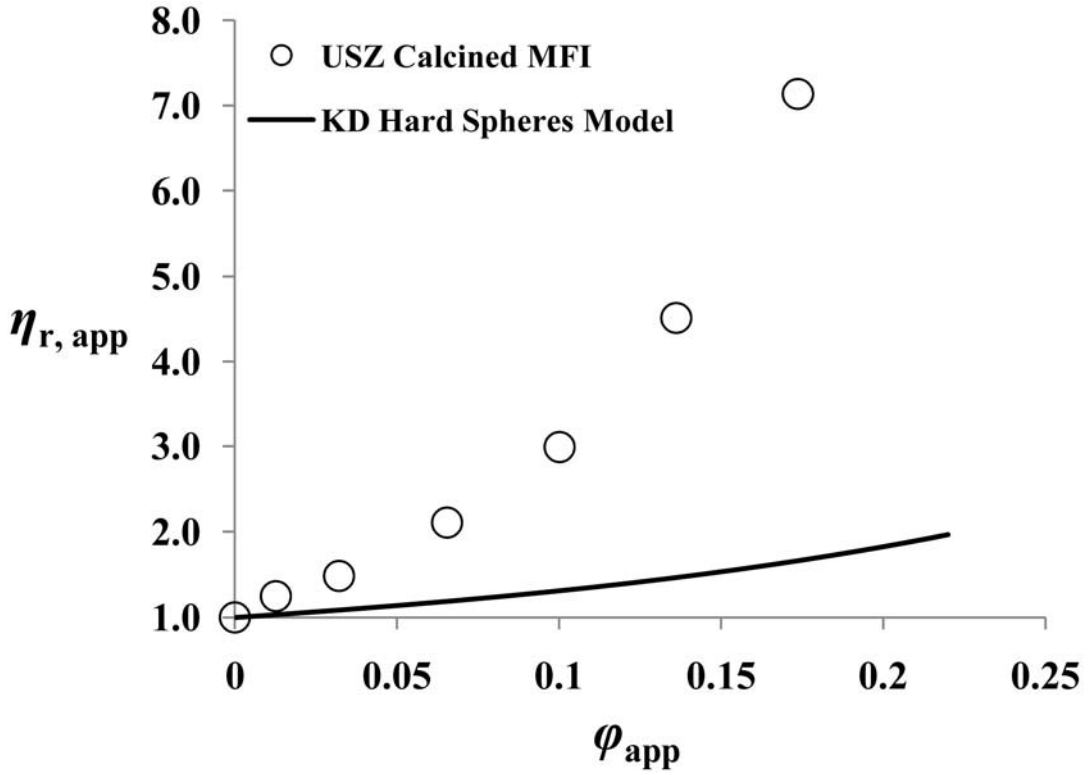

Figure 3.6 Relative viscosity as a function of particle volume fraction. Large deviation between calcined MFI suspension and the Krieger-Dougherty hard sphere model prediction is observed.

Figure 3.7 shows the experimental data that was used to determine the solvent absorption parameter, α for MFI particles. In this approach, a direct comparison of the viscosity of suspensions of comparable concentrations of uncalcined and calcined ST MFI particles in Ultem/NMP solutions was used to estimate the solvent absorption parameter. As expected, in all cases the viscosity of the calcined (porous) zeolite suspensions is greater than the corresponding uncalcined zeolite suspensions due to the absorption of solvent in the suspensions of calcined MFI particles.

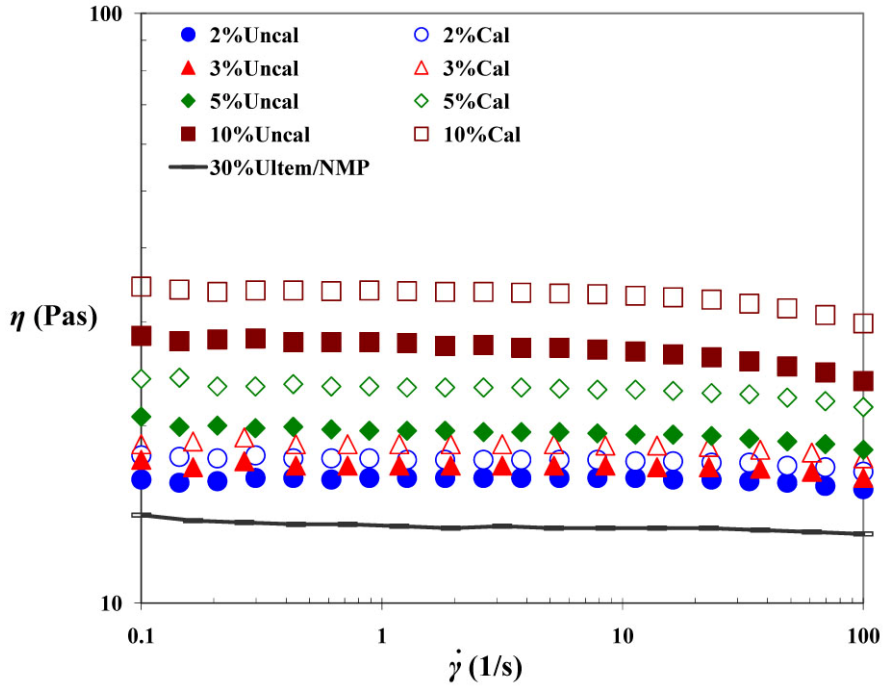

Figure 3.7 Flow curves for polymer solution and suspensions of uncalcined and calcined MFI particles. Open and closed symbols represent porous and non-porous MFI particles respectively, while the different geometric symbols indicate MFI concentration: ● (2 wt.% MFI); ▲ (3 wt.% MFI); ♦ (5 wt.% MFI); ■ (10 wt.% MFI).

In Figure 3.8, the zero-shear apparent relative viscosity is plotted versus particle volume fraction for the uncalcined MFI suspensions, which are non-porous. This data was used to determine empirical fit parameters, β and γ needed to account for deviations from Einstein's and Batchelor's coefficients arising from particle non-sphericity and electroviscous effects. The semi-empirical relationship between the relative viscosity and particle volume fraction for the uncalcined MFI particles suspension from Figure 3.8 is given in equation (3.10).

$$\eta_r = 1 + \beta.\varphi + \gamma.\varphi^2 \tag{3.10}$$

An empirical second order polynomial dependence of relative viscosity on particles volume fraction is used to fit our data for uncalcined MFI suspensions in this range of dilute to semi-dilute concentration of particles. Analysis was carried out in this regime so that the important physical attributes of a suspension (*i.e.* the intrinsic viscosity and the effective collision diameter) are in play and yet not too concentrated that the solution to the mathematical statement to the problem becomes intractable.

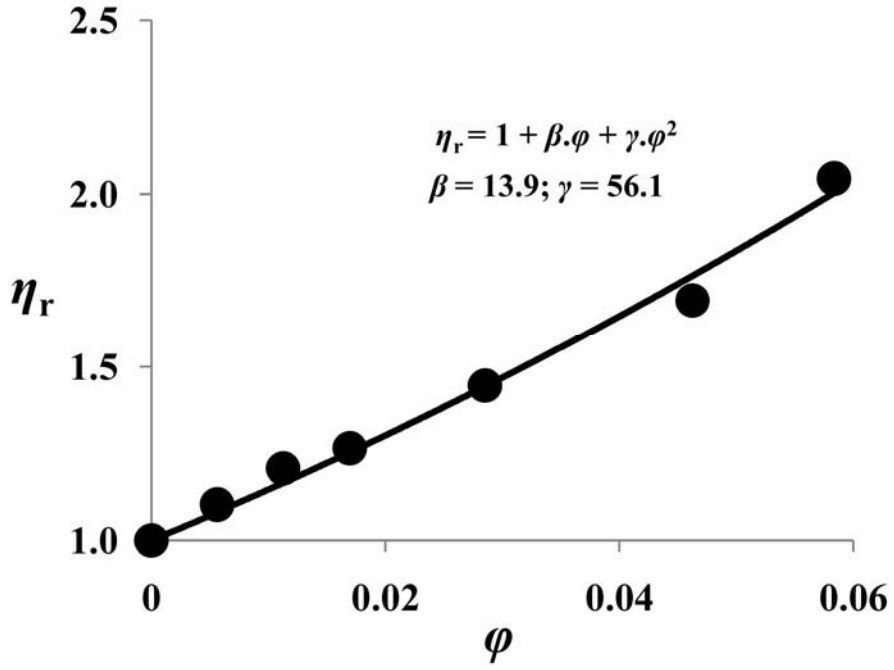

Figure 3.8 A quadratic fit to the relative viscosity versus volume fraction of uncalcined ST MFI particles suspension to determine the intrinsic viscosity, β and the two-body interaction term coefficient, γ for MFI particles.

From the data fit in Figure 3.8, the intrinsic viscosity of uncalcined ST MFI particles is found to be roughly 13.9, much greater than the intrinsic viscosity of 2.5 for hard spheres suspensions. There are a number factors contributing to the observed deviation: (1) the aspect ratio of the MFI particles is not unity; (2) electroviscous effects due to charging of MFI particle surfaces in solution. Together, these effects conspire to significantly increase the intrinsic viscosity of uncalcined MFI in a polymer solution. Similarly, the coefficient of the two-body interaction term is 56.1, which is much greater than the Batchelor value of 6.2 for hard spheres. We believe that this deviation is largely due to secondary electroviscous effects [22].

For the uncalcined MFI suspensions, there is no loss of solvent due to absorption, since the pores of the MFI particles are still occupied by the organic template molecules. Therefore, it is reasonable to expect that the empirical fit obtained for uncalcined MFI particles in Figure 3.8 should also correctly capture the relationship between relative viscosity and particle volume fraction for calcined MFI particles suspensions, provided that the correct effective volume fraction of calcined MFI particles according to equation (3.3) is used. For the calcined MFI particles suspension, the effective relative viscosity can then be expressed as:

$$\eta_{r,eff} = \frac{\eta_{r,app}}{\exp\left(27.338 \frac{w_u w_z \alpha}{1-(1-\alpha) w_z}\right)} = 1 + 13.9\varphi_{z,eff} + 56.1\varphi_{z,eff}^2 \qquad (3.11)$$

Using the expression for $\varphi_{z,eff}$ in equation (3.3c), equation (3.11) can be solved for α as a vector equation, with $\langle \eta_{r,app} \rangle$ and $\langle w_z \rangle$ as input vectors from the measurements on porous, calcined MFI suspensions. Using a suitable optimization scheme in Matlab, the solvent absorption parameter was determined as 0.18. This value is in good agreement with the theoretical pore volume of MFI particles of 0.175 calculated from the information available in [17]. Figure 3.9 shows the how the experimental data of calcined MFI compares with the simulated data after incorporating the determined absorption parameter value, α = 0.18 in equations (3.3c) and (3.11) to correct for solvent absorption. As expected, the experimental result and simulation result show a good agreement.

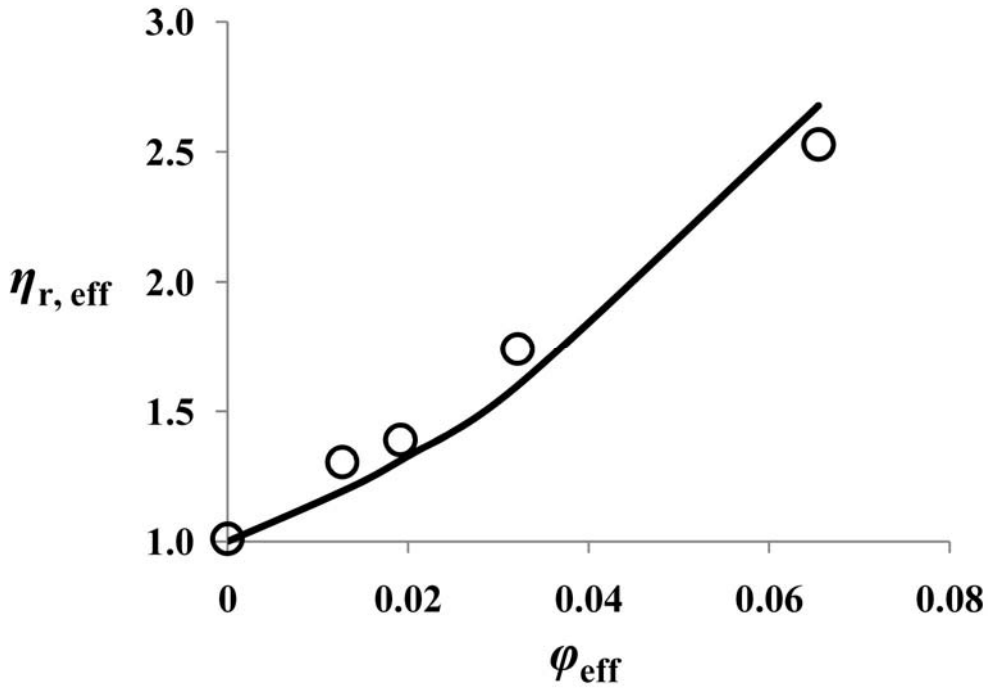

Figure 3.9 Effective relative viscosity versus effective volume fraction for calcined MFI particles suspensions (volume fraction corrected with α = 0.18); line represents model simulations using α = 0.18. Effective relative viscosity only accounts for the effect of porous particles contribution to suspension viscosity.

3.5 Conclusions

We have shown that when solvent molecules are of comparable size to the pore volume windows of porous zeolite particles, the rheology of suspensions of such particles in polymer solutions can drastically be altered by solvent absorption. Absorption of solvent from the suspending medium into porous zeolite particles increases the concentrations of the polymer in the continuous phase and the concentration of dispersed particles. Consequently, such suspensions can have viscosities that significantly exceed model predictions based on non-porous particles. Corrections for these deviations can be achieved by taking into account the changes in polymer and particle concentrations. We present simple models that use a solvent absorption parameter, α, defined as the weight of solvent absorbed per gram of porous zeolite particle to make the necessary corrections. We developed and validated an experimental rheological technique to determine α. The value $\alpha = 0.18$ that was found for MFI zeolites, was found to be in good agreement with the theoretical pore volume available within MFI particles based on the crystal structure. Based on these findings, a model can be proposed to correctly predict the effect of absorption on the viscosity of suspensions of porous particles.

3.6 References

1. Chung TS, Jiang LY, Li Y, Kulprathipanja S: **Mixed matrix membranes (mmms) comprising organic polymers with dispersed inorganic fillers for gas separation.** *Progress in Polymer Science* (2007) **32**(4):483-507.

2. Mahajan R, Koros WJ: **Factors controlling successful formation of mixed-matrix gas separation materials.** *Industrial & Engineering Chemistry Research* (2000) **39**(8):2692-2696.

3. Mahajan R, Koros WJ: **Mixed matrix membrane materials with glassy polymers. Part 1.** *Polymer Engineering and Science* (2002) **42**(7):1420-1431.

4. Mahajan R, Koros WJ: **Mixed matrix membrane materials with glassy polymers. Part 2.** *Polymer Engineering and Science* (2002) **42**(7):1432-1441.

5. Moore TT, Mahajan R, Vu DQ, Koros WJ: **Hybrid membrane materials comprising organic polymers with rigid dispersed phases.** *Aiche Journal* (2004) **50**(2):311-321.

6. Paul DR, Kemp DR: **Diffusion time lag in polymer membranes containing adsorptive fillers.** *Journal of Polymer Science Part C-Polymer Symposium* (1973) 41):79-93.

7. Einstein A: **A new determination of the molecular dimensions.** *Annalen Der Physik* (1906) **19**(2):289-306.

8. Einstein A: **A new determination of the molecular dimensions (vol 19, pg 289, 1906).** *Annalen Der Physik* (1911) **34**(3):591-592.

9. Batchelor GK: **Effect of brownian-motion on bulk stress in a suspension of spherical-particles.** *Journal of Fluid Mechanics* (1977) **83**(NOV):97-117.

10. Krieger IM, Dougherty TJ: **A mechanism for non-newtonian flow in suspensions of rigid spheres.** *Transactions of the Society of Rheology* (1959) **3**(137-152.

11. Mueller S, Llewellin EW, Mader HM: **The rheology of suspensions of solid particles.** *Proceedings of the Royal Society a-Mathematical Physical and Engineering Sciences* (2010) **466**(2116):1201-1228.

12. Jeffery GB: **The motion of ellipsoidal particles in a viscous fluid.** *Proceedings of the Royal Society of London Series a-Containing Papers of a Mathematical and Physical Character* (1922) **102**(715):161-179.

13. Jeffery GB: **The rotation of two circular cylinders in a viscous fluid.** *Proceedings of the Royal Society of London Series a-Containing Papers of a Mathematical and Physical Character* (1922) **101**(709):169-174.

14. Stimson M, Jeffery GB: **The motion of two spheres in a viscous fluid.** *Proceedings of the Royal Society of London Series a-Containing Papers of a Mathematical and Physical Character* (1926) **111**(757):110-116.

15. Kitano T, Kataoka T, Shirota T: **An empirical-equation of the relative viscosity of polymer melts filled with various inorganic fillers.** *Rheologica Acta* (1981) **20**(2):207-209.

16. Pabst W, Gregorova E, Berthold C: **Particle shape and suspension rheology of short-fiber systems.** *Journal of the European Ceramic Society* (2006) **26**(1-2):149-160.

17. Flanigen EM, Bennett JM, Grose RW, Cohen JP, Patton RL, Kirchner RM, Smith JV: **Silicalite, a new hydrophobic crystalline silica molecular-sieve.** *Nature* (1978) **271**(5645):512-516.

18. Fyfe CA, Gobbi GC, Klinowski J, Thomas JM, Ramdas S: **Resolving crystallographically distinct tetrahedral sites in silicalite and zsm-5 by solid-state nmr.** *Nature* (1982) **296**(5857):530-533.

19. Booth F: **The electroviscous effect for suspensions of solid spherical particles.** *Proceedings of the Royal Society of London Series a-Mathematical and Physical Sciences* (1950) **203**(1075):533-551.

20. Russel WB: **Low-shear limit of secondary electroviscous effect.** *Journal of Colloid and Interface Science* (1976) **55**(3):590-604.

21. Vaynberg KA, Wagner NJ: **Rheology of polyampholyte (gelatin)-stabilized colloidal dispersions: The tertiary electroviscous effect.** *Journal of Rheology* (2001) **45**(2):451-466.

22. Watterson IG, White LR: **Primary electroviscous effect in suspensions of charged spherical-particles.** *Journal of the Chemical Society-Faraday Transactions Ii* (1981) **77**(1115-1128.

23. Zurita L, Carrique F, Delgado AV: **The primary electroviscous effect in silica suspensions - ionic-strength and ph effects.** *Colloids and Surfaces a-Physicochemical and Engineering Aspects* (1994) **92**(1-2):23-28.

24. Cheng CH, Bae TH, McCool BA, Chance RR, Nair S, Jones CW: **Functionalization of the internal surface of pure-silica mfi zeolite with aliphatic alcohols.** *Journal of Physical Chemistry C* (2008) **112**(10):3543-3551.

25. Schoeman BJ: **A spectroscopic study of the initial stage in the crystallization of tpa-silicalite-1 from clear solutions.** In: *Progress in zeolite and microporous materials, pts a-c.* 105. Chon H, Ihm SK, Uh YS (Eds), (1997):647-654.

26. Schoeman BJ: **The homogeneous nature of clear tpa-silicalite-1 precursor solutions.** *Microporous Materials* (1997) **9**(5-6):267-271.

27. Husain S, Koros WJ: **Mixed matrix hollow fiber membranes made with modified hssz-13 zeolite in polyetherimide polymer matrix for gas separation.** *Journal of Membrane Science* (2007) **288**(1-2):195-207.

28. Husain S: **Mixed matrix dual layer hollow fiber membranes for natural gas separation.** In: (2006).

CHAPTER 4

MICROFLUIDIC STUDIES OF NONSOLVENT-INDUCED PHASE INVERSION KINETICS OF POLYMER SOLUTIONS

4.1 Introduction

Asymmetric membranes with a dense, selective skin layer and a thick, porous supporting substructure are usually prepared by phase inversion processes from polymeric solutions. Since the creation of the first asymmetric membrane by Loeb and Sourirajan [1], there has been a lot of interest in the formation and application of asymmetric membranes. Despite increased activities in asymmetric membrane production, much is still unknown about the underlying science and the optimization of the process.

Many early investigations focused on the determination of factors that control asymmetric structure formation, with the aim to eliminate the formation of macrovoids [2-6]. Macrovoids are large teardrop-like voids with dimensions ranging from several microns to the thickness of the entire membrane. When present, they can compromise the structural integrity and functionality of a membrane. Efforts at understanding the science underlying membrane structure formation through phase inversion have progressed along two principal directions: one focusing on the thermodynamic aspects and the other on the kinetic aspects of membrane formation. The final asymmetric structure of a membrane is mainly determined by thermodynamics [7], while the average pore size and pore size distribution are largely controlled by the kinetics of phase separation [6,8-10]. Altena and Smolders [7] used an extension of the Flory–Huggins model to three-component systems to predict the miscibility gap of the ternary phase diagram of a membrane forming

system. Using this approach, predictions and experimental measurements of the binodal for membrane forming systems are often found to be in good agreement with theoretical models, provided that good estimates for thermodynamic interaction parameters are available [11].

Experimental measurements and theoretical modeling of the phase separation kinetics of membranes formed by immersion precipitation are both very challenging. Modeling of membrane formation entails the solution of a multi-component mass transfer problem with concentration dependent diffusion coefficients and a moving phase boundary. A number of attempts to model the phase separation kinetics during membrane formation have been reported in literature [6,10,12-20]. Strathmann showed with a simple mass balance that the thickness of the phase separated zone increases linearly with the square root of time, in agreement with experimental observations [6]. The first comprehensive model of the mass transfer processes involved during immersion precipitation of membranes was proposed by Cohen and co-workers [20], although their model was found to contain errors primarily due to steady state assumptions and the neglect of frictional forces between the solvent and nonsolvent. Reuvers and co-workers [12,13] made corrections to the model of Cohen *et al.* and, in addition, proposed methods to estimate the appropriate ternary transport coefficients in their model. They were thus able to predict the full composition path that the membrane forming system experiences during immersion precipitation, all the way to the binodal of the ternary phase diagram. The model is limited because it assumes a constant moving interfacial composition and infinite casting film, which only holds true for very short times. Tsay *et al.* [19] published a rigorous derivation of the diffusion equations that describe immersion precipitation of

membranes, thus relaxing the constant interfacial composition assumption of Reuvers' model. However, this model erroneously predicts faster phase separation kinetics with increasing polymer concentration due to incorrect estimates of ternary diffusion coefficients. Cheng *et al.* [14] incorporated convective contributions to mass transfer from the nonsolvent bath with essential features from the previous models to calculate the composition path up to the spinodal. Due to the challenges encountered with obtaining ternary diffusion coefficients for mass transfer models, other approaches to model immersion precipitation were attempted. In a series of papers, Termonia [15-17] used Monte Carlo type molecular simulations to model immersion precipitation of membranes. Unlike the ternary mass transfer models, this approach does not require a priori knowledge of all pertinent transport parameters. However, the computer processing time and memory needs of the simulation are significant. In light of the numerous challenges associated with modeling phase inversion kinetics, we feel the need to develop an experimental method to reliably measure the kinetics of phase inversion of membrane dopes. To fulfill this need, we have designed, built and tested a microfluidic device to quantify the kinetics of phase separation.

A number of experimental techniques to measure the phase separation kinetics of membrane dopes exist in literature [10,13,21]. Some membrane researchers employed a visual estimate of phase separation time [21], which is somewhat subjective. Other researchers have used light transmission measurements through phase separating samples to monitor precipitation kinetics[13]. Unfortunately, this technique does not offer direct insight into the mechanism of phase separation. Another method commonly reported in membrane literature [10] entails the tracking and recording by video-microscopy of the

phase separation front of dopes placed between two microscopic slides after the introduction of non-solvent. This method is prone to error because of the poorly defined sample geometry and poorly controlled atmosphere.

In this thesis, we report for the first time a microfluidic device for tracking the kinetics of phase separation of membrane dopes that improves on the previous methods. The device provides a well-defined sample geometry and controlled atmosphere for the in situ tracking of the phase separation. In addition, the dimension of the device enables one to measure phase separation kinetics at the length scales encountered in practical membrane formation. To test our device, we measured the phase separation kinetics of PEI (Ultem)/NMP solutions at different polymer concentrations upon contact with an array of nonsolvents. We also report experimental data on membrane solution rheology and nonsolvent thermodynamic interaction parameters to provide a framework for the interpretation of the effective nonsolvent diffusivity, which is used as a measure of the phase separation kinetics (PSK) throughout this work.

4.2 Experimental section

4.2.1 Fabrication and operating principles of microfluidic device for measuring PSK

The microfluidic device used for our phase separation kinetics studies, consists of a 4-way cross channel made from PDMS and microscope glass slides Figures 4.1(a) and (b). The micro-channel has a depth of 100 – 150 μm. The membrane dope channel is 10000 μm long and 500 μm wide. The nonsolvent channel is 6000 μm long and 1000 μm wide. The cross channels are 300 μm wide.

The mold for the PDMS channel was made by photolithographic techniques. The AutoCAD design of our microfluidic channel was printed onto a Chrome photomask manufactured on borofloat substrate (1.1 mm thick; TELIC Co.). A positive SU-8 2100 photoresist (MicroChem Co.) was spin-coated (~150 μm thick) on a silicon wafer (475-575 μm thick; NOVA Electronic Materials Ltd.) and softbaked on a hotplate (Isotemp; Fisher Scientific Inc.) at 65 ^{o}C for 6 minutes and subsequently at 95 ^{o}C for 30 minutes. The photomask was then placed over the photoresist spin-coated wafer and exposed to UV-light (350 mJ/cm^2; OAI Mask Alignment and UV Exposure System; Optical Associates Inc.). The illumination was followed by a post-exposure bake at 65 ^{o}C for 5 minutes and at 95 ^{o}C for 12 minutes. The final mold was formed by immersion in MicroChem's SU-8 developer to remove the uncured resist, followed by isopropyl alcohol rinse and air drying.

Sylgard® 184 silicone elastomer base and curing agent (Dow Corning Co.) were mixed in the weight ratio 10:1 and degassed under vacuum for 60 minutes. The degassed mixture was poured onto the mold and cured at 65^{o}C for at least 10 hours. The cured PDMS with an imprint of the mold (dimensions shown in Figure 4.1b) was peeled from the mold and bonded to microscope glass slides (Figure 4.1(a)) after treatment in an oxygen plasma reactor (PDC-32G; Harrick Plasma). The oxygen plasma treatment makes PDMS more hydrophilic [22-24], which is undesirable for our experiments: in hydrophilic channels, water would prefentially transport along the surface of the channel wall rather than diffuse through the polymer solution, which leads to sidewall-aided nonsolvent transport and an uneven phase separation front. This effect was eliminated by storing microfluidic devices in a dry box for at least 5 days before use in PSK

experiments; during this aging period, the PDMS surface regains its hydrophobic character.

The microfluidic device was placed on an inverted microscope (DM-IRB; Leica) equipped with a low-magnification objective and an analog CCD camera (640 by 480 pixel resolution, 30 Hz frame rate; model 4920; Cohu). PSK experiments were carried out by introducing the polymer solution sample into the dope channel up to the 4-way junction from a manually operated syringe, while flushing dry nitrogen gas through the cross-channel to suppress premature phase separation of the sample due to moisture in the lab environment. After sample loading, the nitrogen gas stream was shut off and video recording was started; 5 μl of water was then introduced into the nonsolvent channel at the rate of 3 μl/s through a syringe pump (KDS210C; KD Scientific Inc.). A typical movie of a PSK experiment lasts ca. 35 seconds (~1000 frames).

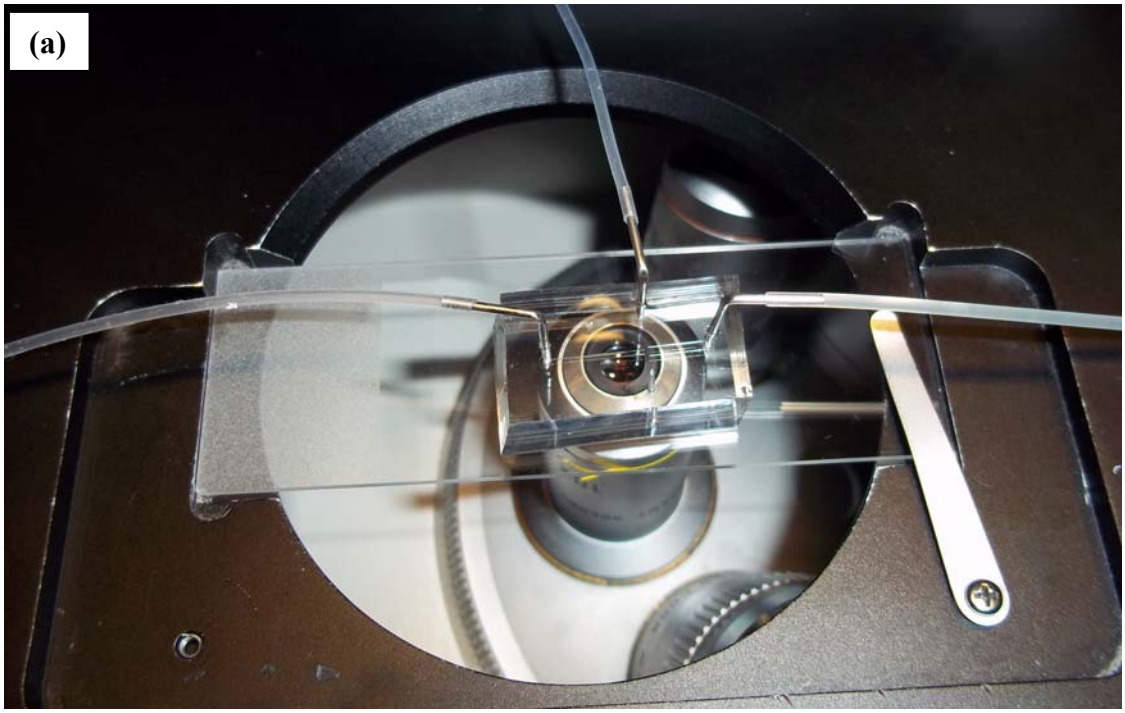

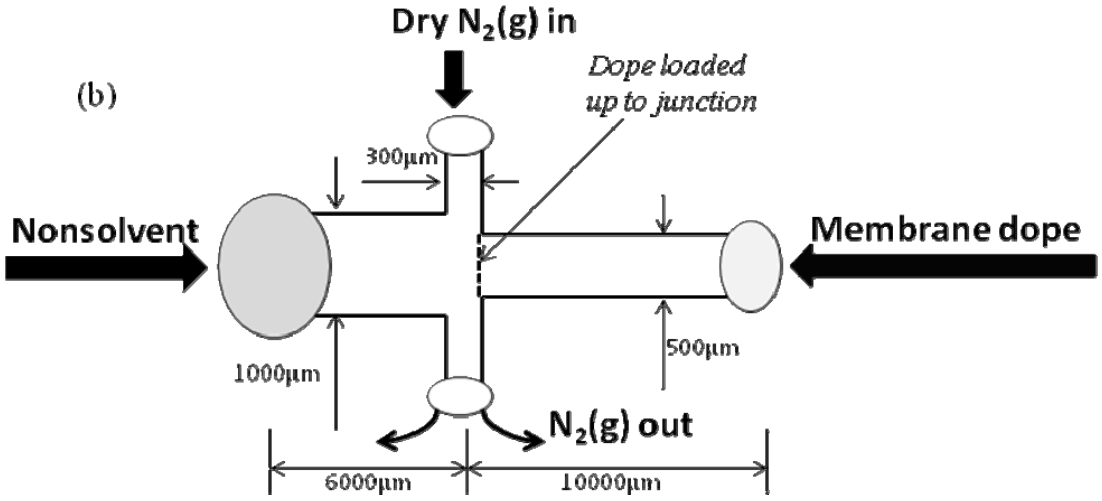

Figure 4.1 (a) Image of integrated set-up and (b) schematic of the PSK microfluidic chip with essential features and dimensions.

4.2.2 Video microscopy, data collection and processing

Videos from the CCD camera were recorded directly onto the hard-drive of a PC with a precision frame grabber (PXC-200; Cyber Optics) and specialized image acquisition software (OpenBox [25]). With a 2.5X objective, the resulting spatial resolution of the set-up was 4.00 μm per pixel. Movies were collected and saved in 8-bit AVI format, with image brightness digitally quantified in the range between 0 and 255. The collected movies were then converted to TIFF format before performing image analysis with the IDL software package (IDL 6.1; ITT Visual Information Solutions). By detecting spatial variations in image brightness, customized IDL code was able to track from frame to frame the position of two interfaces: 1) the phase separation front, and 2) the interface between nonsolvent and polymer solution (see Figures 4.2 and 4.3). This information can then be used to determine the thickness of the phase separated zone as a function of time (see Figure 4. 3).

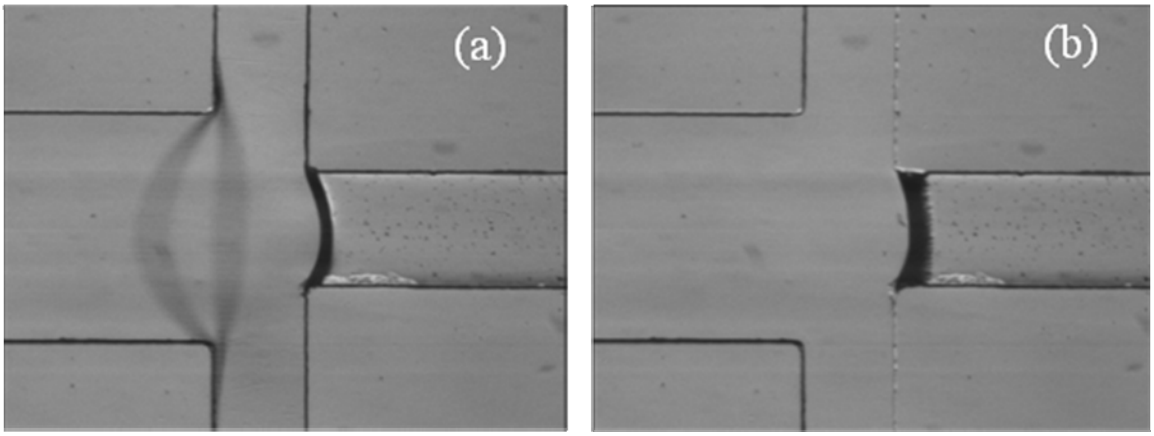

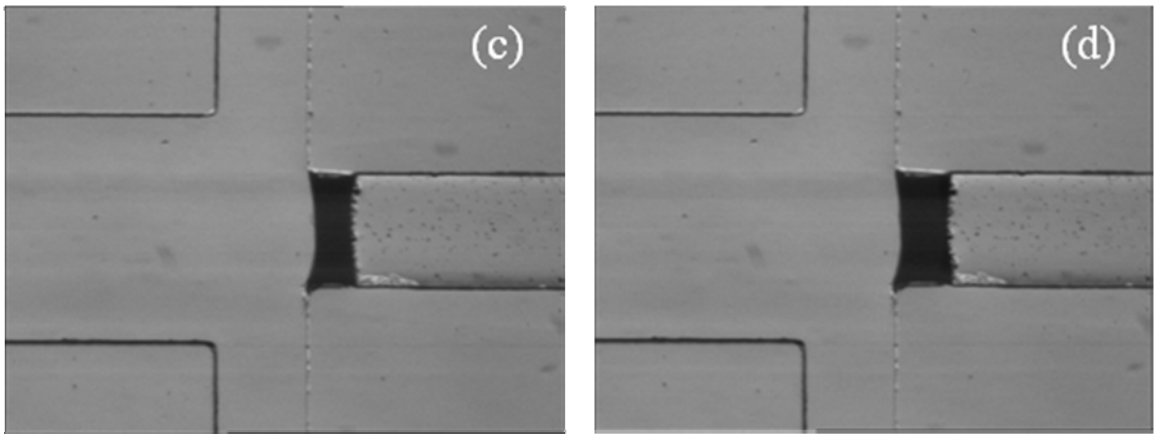

Figure 4.2 Time evolution of phase separated layer for a 30 wt. % Ultem/NMP solution using methanol as nonsolvent: (a) $t = 0$ s (shadows of inflowing nonsolvent are visible), (b) $t = 1$ s, (c) $t = 5$ s, (d) $t = 10$ s.

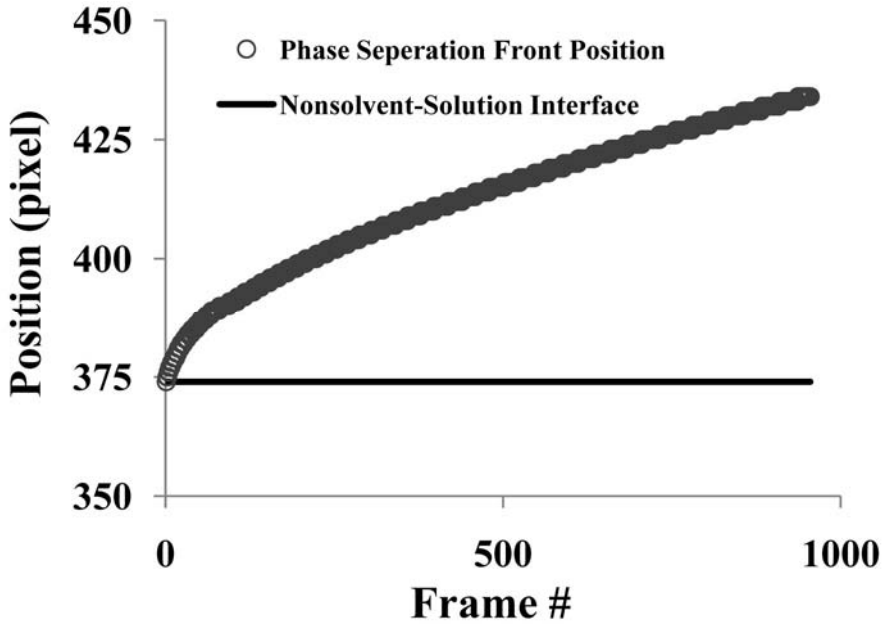

Figure 4.3 Position of the non-solvent dope interface (line) and phase separation front (circles) as a function of frame number (30 frames/s).

4.2.3 Materials and sample preparation

PEI (Ultem® 1000, General Electric) was provided by the research group of professor Koros at Georgia Tech. The polymer was dried under vacuum at 120 ^{o}C for 6 hours before use. The solvent of choice for the Ultem polymer was NMP (99.95% purity grade), purchased from Sigma-Aldrich and used as obtained. DI water was used as the primary precipitating nonsolvent. Other phase inversion inducing nonsolvents and co-solvents used in this work include methanol, ethanol, 2-propanol and acetone. Polymer solutions were prepared by dissolving the required amount of dried polymer in NMP or NMP/ethanol mixtures. Before any testing was done, the solutions were allowed to fully dissolve and equilibrate for at least 72 hours under continuous slow rotation of the sample vial at room temperature.

4.2.4 PSK measurements

The phase separation kinetics of 20, 25, 27.5, 30, 32.5 and 35 wt.% Ultem/NMP solutions were measured in the microfluidic device as described above. At least 3 replicate measurements were carried out for each sample and averages are reported in this thesis. In addition, PSK experiments were performed for solutions of 25, 30 and 35 wt.% Ultem /NMP/ethanol at different ethanol concentrations. Finally, in order to determine the effect of different precipitating nonsolvent on the kinetics of phase separation, PSK measurements were performed and compared for a 30 wt.% Ultem/NMP solution using water, methanol, ethanol, isopropanol and acetone as nonsolvent.

4.2.5 Rheological measurements

The viscosity of the polymer solutions was measured over a range of shear rates (0.1 - 100 s^{-1}) at 25 ^{o}C with a stress-controlled rheometer (MCR 300, Anton Paar) and Couette geometry (CC10; cup inside diameter 10.845 mm and bob outer diameter 10.000 mm). The viscosities reported for the membrane dopes in this thesis were at a shear rate of 0.2 s^{-1}, before the onset of shear-thinning.

4.2.6 Thermodynamic considerations

The cloud points and binodal curve of the ternary phase diagram can be calculated by the method proposed by Altena and Smolders [7]. The ternary diagram can be used to determine the concentration of nonsolvent required for phase separation, C_{ps}. In this work, C_{ps} was determined by preparing several solutions of the polymer at a fixed concentration in nonsolvent-solvent mixtures of varying composition. The lowest concentration of nonsolvent for which the polymer did not dissolve to form a homogeneous solution is reported as C_{ps}. A summary of the effect of interaction parameters on the position of the binodal can be found in the work of Altena and Smolders [7]. Increasing the nonsolvent-solvent interaction parameter χ_{12}, *i.e.* decreasing the miscibility of solvent and nonsolvent, shifts the binodal towards higher values of C_{ps}. The effect of increasing the solvent-polymer interaction parameter χ_{23}, *i.e.* decreasing the solvent quality for the polymer, is to lower C_{ps}. Similar to χ_{23}, an increase in the value of nonsolvent-polymer interaction parameter χ_{13} decreases the amount of nonsolvent necessary for phase separation, C_{ps}. The three binary interaction parameters for the water/NMP/Ultem membrane forming system are available from literature sources

[26,27]. However, in this report we strive to correlate the kinetics of phase separation of polymer solutions with a ternary interaction parameter of the nonsolvent with solvent in the presence of the polymer (*i.e.* $\chi_{1[23]}$). The ternary interaction parameter of nonsolvents (water, methanol, ethanol, isopropanol and acetone) with a 30 wt.% Ultem/NMP solution is approximated using the Flory-Huggins relation for a 3-component system.

$$\chi_{1[23]} = \frac{\nu_1}{RT}\left(\delta_1 - \tilde{\delta}\right)^2 \tag{4.1}$$

Where $\tilde{\delta}$ is the volume-fraction averaged solubility parameter of all components in the solution including the nonsolvent, and δ_1 and ν_1 are respectively the solubility parameter and molar volume of the nonsolvent.

4.3 Results and discussion

4.3.1 Diffusion controlled PSK

For all cases of PSK experiments with Ultem/NMP solutions we found that the thickness of the phase separated region was directly proportional to the square root of the elapsed time as shown in Figure 4.4 for 20, 25, 30 and 35 wt.% Ultem /NMP solutions. This result implies that the kinetics of phase separation of Ultem/NMP solution induced by a nonsolvent (water) can be modeled by a constant effective diffusion coefficient, D_{eff}, of the nonsolvent through the polymer solution. This result is consistent with many experimental studies and mathematical models reported in literature for several different membrane dopes [6,12,20]. For phase separation to occur anywhere in the polymer

solution, the concentration of nonsolvent at that specific location must reach the critical nonsolvent concentration C_{ps} (see section 3.6), which depends on the thermodynamic interactions between the polymer, solvent and nonsolvent. It is expedient to think of D_{eff} as the effective diffusivity of the phase separation front that marks this critical nonsolvent concentration C_{ps}. For one-dimensional diffusion, the relation between the thickness of the phase separated layer, Δx, and time t is then expected to obey the following relation:

$$\Delta x = \left(2 D_{eff}\right)^{1/2} \sqrt{t} \tag{4.2}$$

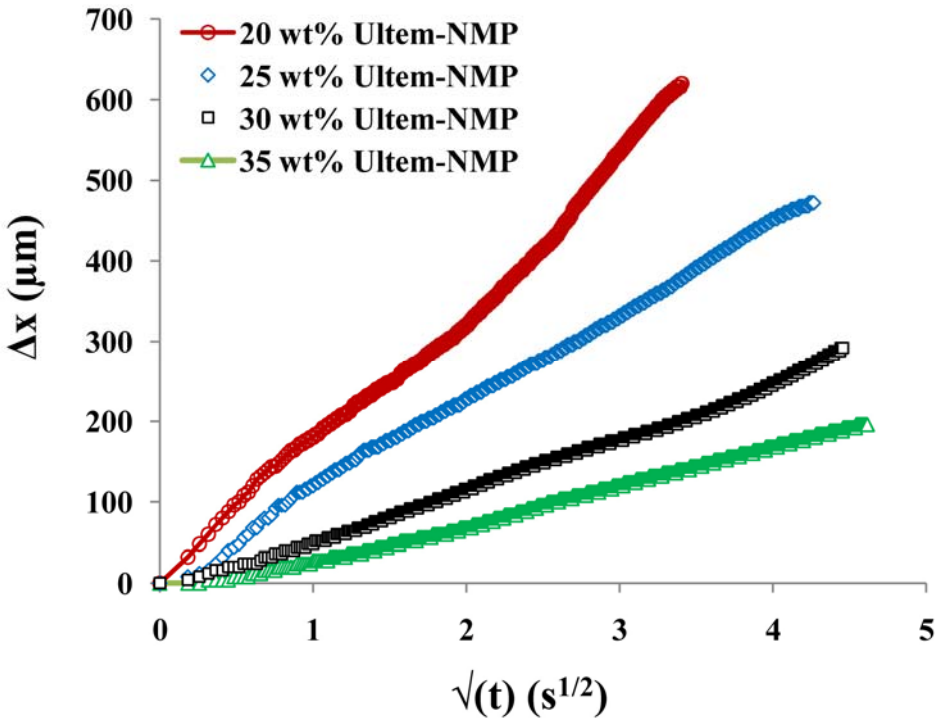

Figure 4.4 Diffusion controlled phase separation for different Ultem/NMP concentrations using water as nonsolvent.

At this point, it is expedient to draw a distinction between D_{eff} and the self-diffusion coefficient of nonsolvent molecules through the polymer solution, D_{self}. An approximate relationship between the two coefficients can be established by modeling the diffusion of nonsolvent into the polymer solution as a semi-infinite transient diffusion problem, which is described by the following PDE:

$$\frac{\partial c_1(x,t)}{\partial t} = D_{self} \frac{\partial^2 c_1(x,t)}{\partial x^2} \tag{4.3}$$

The solution to this problem is available in Crank's book on the mathematics of diffusion [28]. With the boundary conditions appropriate to this case, the solution is:

$$\frac{c_1(0,t) - c_1(x,t)}{c_1(0,t) - c_1(x,0)} = erf\left[\frac{x}{2\sqrt{D_{self}\, t}}\right] \tag{4.4}$$

$c_1 = 0$ at $t = 0$ for $0 < x < \infty$
$c_1 = 1$ at $x = 0$ for $t > 0$
$c_1 = C_{ps}$ at $x = \Delta x$ for $t > 0$

Using these initial and boundary conditions alongside the solution in equation (4.4) yields:

$$1 - C_{ps} = erf\left[\frac{\Delta x}{2\sqrt{D_{self}\, t}}\right] \tag{4.5}$$

Solving equation (4.5) for Δx, and subsequent comparison with equation (4.2) gives the final result:

$$\frac{D_{eff}}{D_{self}} = 2\left[erf^{-1}\left(1 - C_{ps}\right)\right]^2 \tag{4.6}$$

The value of D_{self} can thus be determined from the measured D_{eff} when C_{ps} is known; as an illustration, the result of equation (4.6) is presented graphically in Figure 4.5. The graph illustrates the non-intuitive phenomenon that the phase separation front can diffuse faster than individual non-solvent molecules (D_{eff} /D_{self} > 1), if the critical non-solvent concentration is below 32 wt.%.

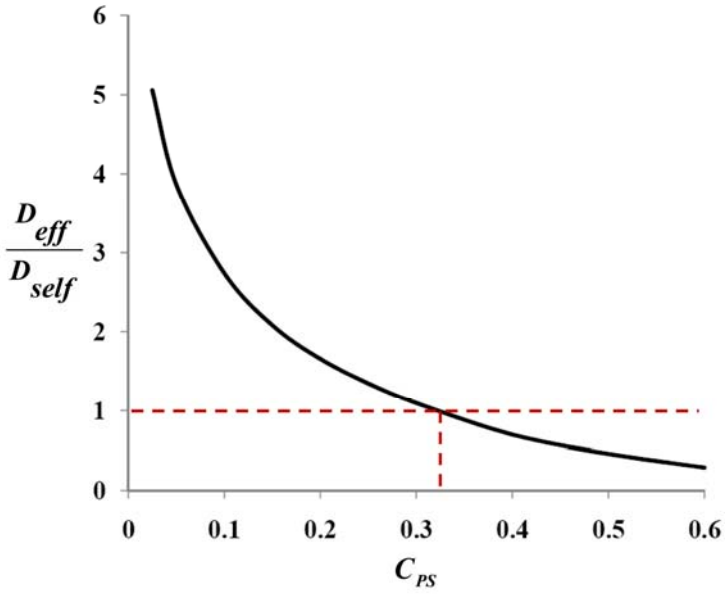

Figure 4.5 D_{eff} /D_{self} as a function of critical nonsolvent concentration for phase separation.

4.3.2 Polymer concentration effects

In our PSK experiments, we observed that the water/NMP/Ultem membrane forming system undergoes instantaneous demixing in agreement with other literature reports [27]. D_{eff} decreases with increasing Ultem polymer concentration (Figure 4.6(a)). Since increases in the polymer concentration also increases the viscosity of the polymer solution, one might expect a decrease in the effective diffusion coefficient for phase separation that is inversely proportional to viscosity, $D \sim 1/\eta$, based on Stokes–Einstein arguments for liquid diffusion. Figures 4.6(a) and (b) indeed show that this scaling holds up to 30 wt.% Ultem/NMP concentrations, for which $\eta \cdot D$ is found to be constant.

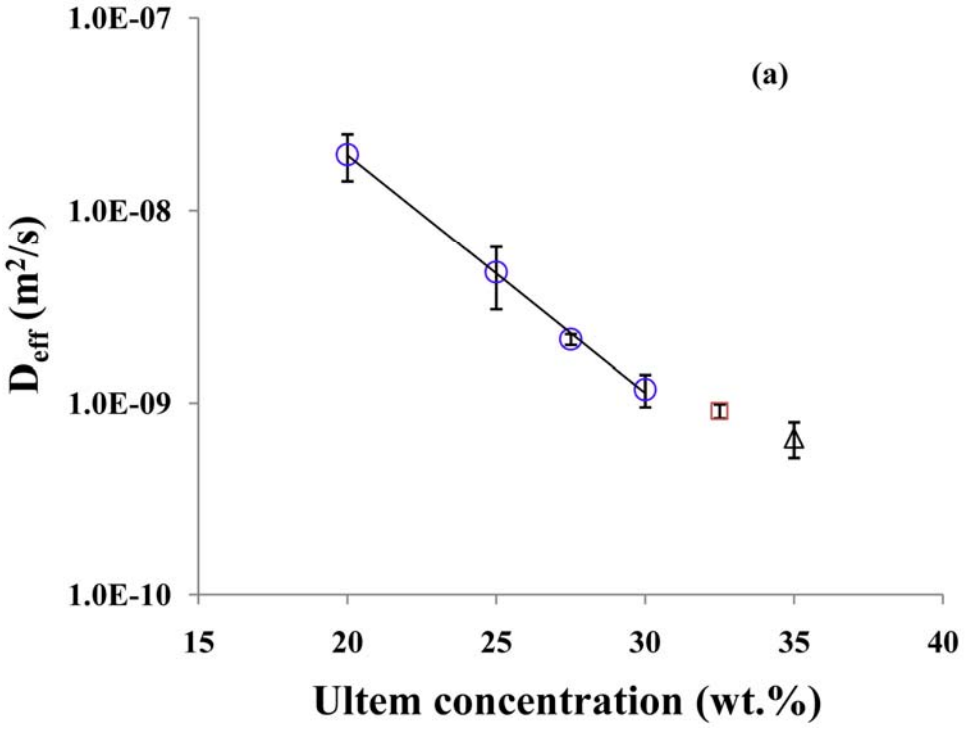

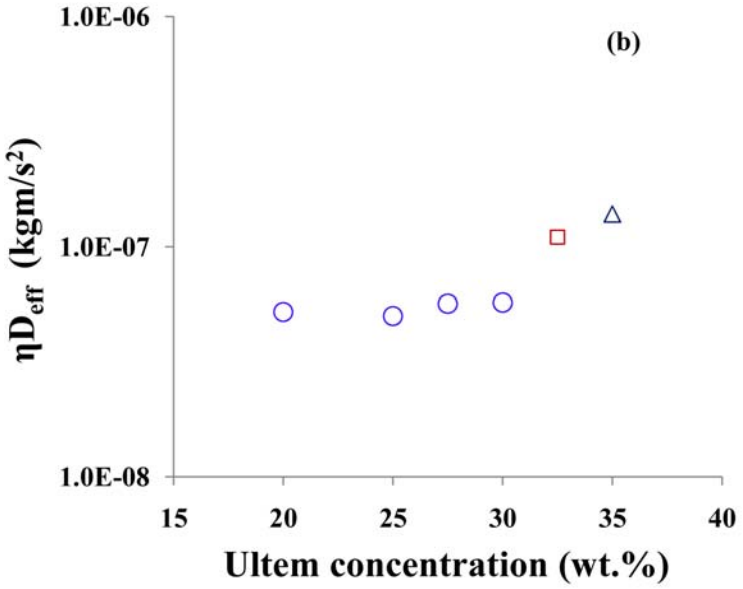

Figure 4.6 Phase separation kinetics in Ultem/NMP solutions as a function of polymer concentration in terms of (a) effective diffusion coefficient and; (b) after normalization with bulk viscosity.

However, even in this inverse proportionality regime of D_{eff} with the measured bulk viscosity of the polymer solution; the Stokes-Einstein equation leads to an underpredicted value of nonsolvent diffusivities by four orders of magnitude assuming water molecules units, 0.2 nm in diameter. This discrepancy can be explained by the fact that nonsolvent molecules do not diffuse through a molecularly homogenous medium, but through a polymer network filled with solvent. As a result, non-solvent molecules experience a viscous drag that is mostly determined by viscosity on the order of the NMP solvent (~2 mPa·s), rather than the averaged bulk polymer solution viscosity (~20,000 mPa·s). Therefore, to correctly interpret D_{eff} (and D_{self}) within the framework of Stokes-Einstein, a microscopic model is needed that takes into account the microstructure of the polymer

solution in relation to the size of the diffusing nonsolvent molecules. In such a model, one can assume that a polymer solution is made up of a three-dimensional network of entangled polymer molecules with a correlation length or characteristic mesh size ξ, filled with solvent molecules. The polymer solution correlation length may then be obtained from De Gennes scaling arguments [29]. Unfortunately, there are no suitable models to evaluate friction losses on the diffusing nonsolvent molecule units within a polymer network. Moreover, the interaction of the diffusing nonsolvent molecules with the polymer segments and solvent molecules introduce additional sources of complication into such a model approach. In the face of these challenges we shall not pursue such a microscopic model for PSK in this thesis any further. However, in the next section we investigate the effect of nonsolvent interaction with the components of the polymer solution. At concentrations greater than 30 wt.% Ultem, the effective diffusion coefficient exceeds the trend predicted at lower concentrations (Figures 4.6(a) and (b)). This is in part due to the observation that the amount of nonsolvent (water) required for phase separation decreases at a faster rate at polymer concentrations above 30 wt.% as shown in Table 4.1. This significant decrease in C_{ps} in combination with the fact that low C_{ps} values correspond to larger increases in D_{eff} according to Figure 4.5 may partly account for the observed deviation.

Table 4.1 C_{ps} values for different concentrations of Ultem/NMP solution.

Polymer concentration (wt. %)	C_{ps} **(wt. %)**
20.0	3.20
25.0	3.08
30.0	2.99
32.5	2.65
35.0	2.58

4.3.3 Solvent quality effects

The quality of NMP as solvent for Ultem can be decreased by the addition of nonsolvent for Ultem as a co-solvent with NMP in the dope. For this study, ethanol is used as the cosolvent. Figure 4.7 shows that kinetics of phase separation increases with increasing ethanol concentration. It should be noted that the bulk viscosity of Ultem/NMP solutions is increased by adding ethanol (Figure 4.7(b)). This increase in PSK for a dope with increased viscosity seems counterintuitive within the framework of the Stokes-Einstein relation in which one would expect the diffusivity to decrease with increasing dope viscosity. This finding indicates that PSK may not be solely governed by the dope rheology. An explanation for this observation is because the inclusion of ethanol as a cosolvent in the dope increases the disparity in solubility parameters between the polymer and the NMP/ethanol (solvent/cosolvent) mixture. Consequently, the effective interaction parameter $\chi_{1[23]}$ according to equation (4.1) increases. Thus a lower critical nonsolvent

concentration for phase separation C_{ps} [7] is required. As shown in Figure 4.5, a decreased amount of water necessary to induce phase separation can increase the effective diffusivity of the phase separated front, even if the self-diffusion coefficient may be lowered slightly. Figure 4.7(c) shows the ratio of the effective diffusivity in a solution with known ethanol concentration to the effective diffusivity in ethanol-free dope versus ethanol weight fraction in the liquid phase. This plot reveals that ethanol inclusion in membrane dopes accelerates phase separation kinetics faster in the 35wt. % Ultem/NMP solution. The observed behavior is consistent with the results of Figure 4.6. This observation is due to the smaller C_{ps} values and much greater entanglement at this polymer concentration as explained in Section 4.3.2.

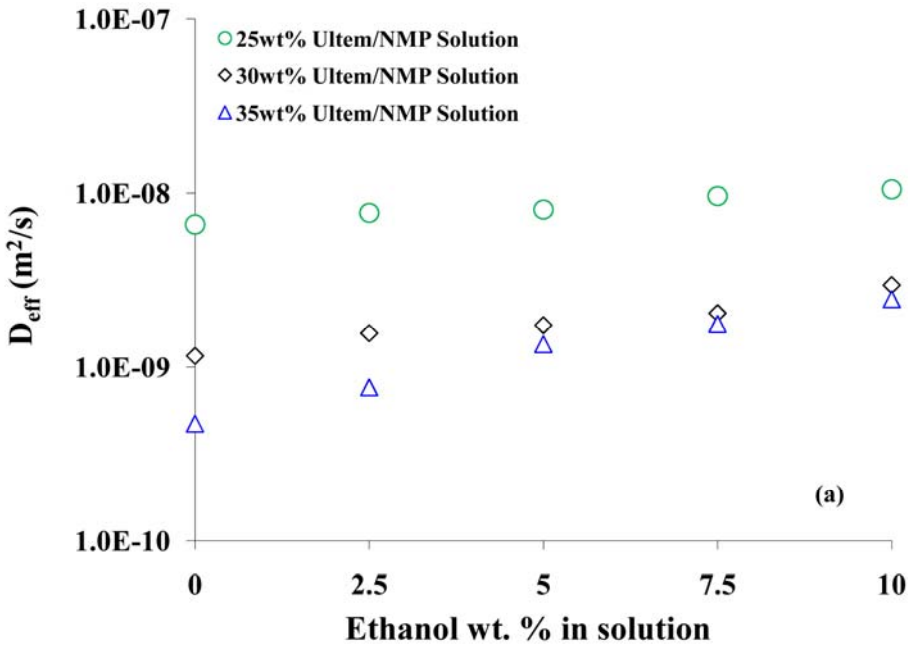

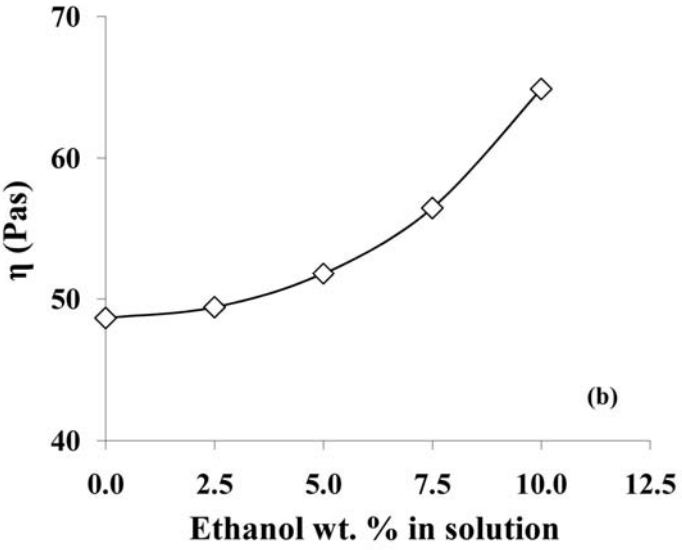

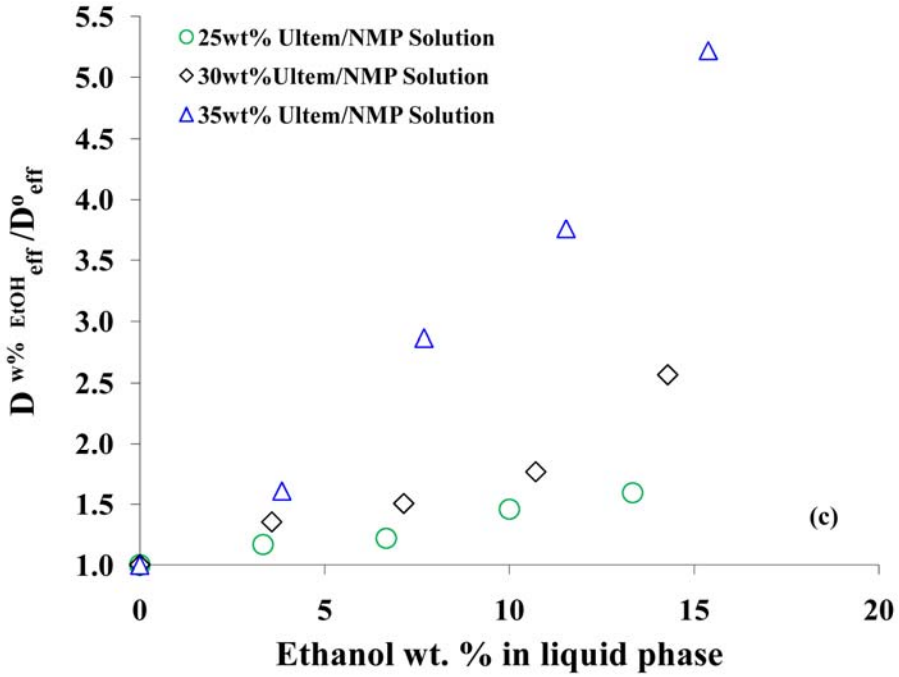

Figure 4.7 (a) Phase separation kinetics for different polymer concentrations as a function of ethanol nonsolvent concentration in the dope; (b) dope viscosity as a function of ethanol co-solvent concentration in 30 wt.% Ultem solutions; (c) ratio of effective diffusivity in solutions with ethanol to the effective diffusivity in ethanol-free solutions versus ethanol concentration in the NMP/ethanol liquid phase.

4.3.4 Nonsolvent-polymer solution interaction parameter effects

The effect of using different nonsolvents on the phase separation kinetics (PSK) was studied by comparing the effective diffusion coefficient D_{eff} for five different nonsolvents 30 wt.% Ultem/NMP dopes. The PSK is fastest for water and progressively slower for higher alcohol homologues as shown in Figure 4.8. In this series, isopropanol, the largest nonsolvent molecule tested, is only roughly a factor of 1.5 larger than water, the smallest nonsolvent molecule. The size disparities alone can therefore not account for the factor 10 difference between the effective diffusivities of isopropanol and water.

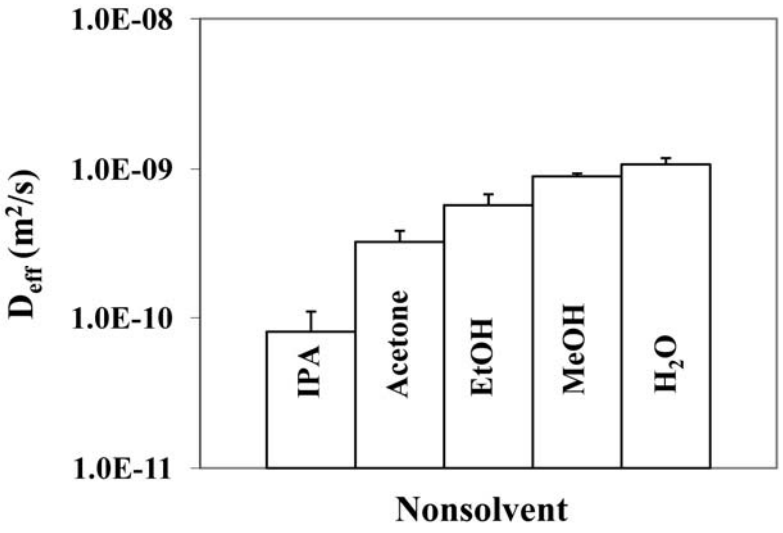

Figure 4.8 Effective diffusivity of phase separation for different nonsolvents in 30 wt.% Ultem/NMP solutions.

In order to investigate the variations in D_{eff} for the different nonsolvents, we correlated D_{eff} with $\chi_{1[23]}$, the interaction parameters of the nonsolvent with the solvent in the presence of the polymer. $\chi_{1[23]}$ was calculated using equation (4.1) and the results are shown in Table 4.2. When the effective diffusivity is plotted against $\chi_{1[23]}$ (Figure 4.9(a)), the alcohols show a good correlation between D_{eff} and $\chi_{1[23]}$ while, water and acetone seem to be poorly aligned in this plot. However, from Table 4.2 it can be seen that C_{ps} value varies significantly for water, acetone and the alcohols. On the other hand a fairly constant concentration of 12.5 wt.% of nonsolvent in dope induces phase separation when an alcohol is the nonsolvent. This explains why the alcohols are well aligned in Figure 4.9(a). The effect of different concentration of nonsolvent required for phase separation is corrected by plotting D_{self} (in place of D_{eff}) against interaction parameter as shown in Figure 4.9(b). D_{self} can be calculated as described earlier from equation (4.6) or estimated from Figure 4.5.

Table 4.2 C_{ps} and interaction parameter values for different nonsolvents in a 30 wt.% Ultem/NMP solution.

Nonsolvent	C_{ps} **(wt. %)**	$\chi_{1[23]}$
Water	3.00	4.0
Methanol	12.0	0.39
Ethanol	12.5	0.090
Acetone	28.0	0.19
Isopropanol	12.5	$5.0 \cdot 10^{-5}$

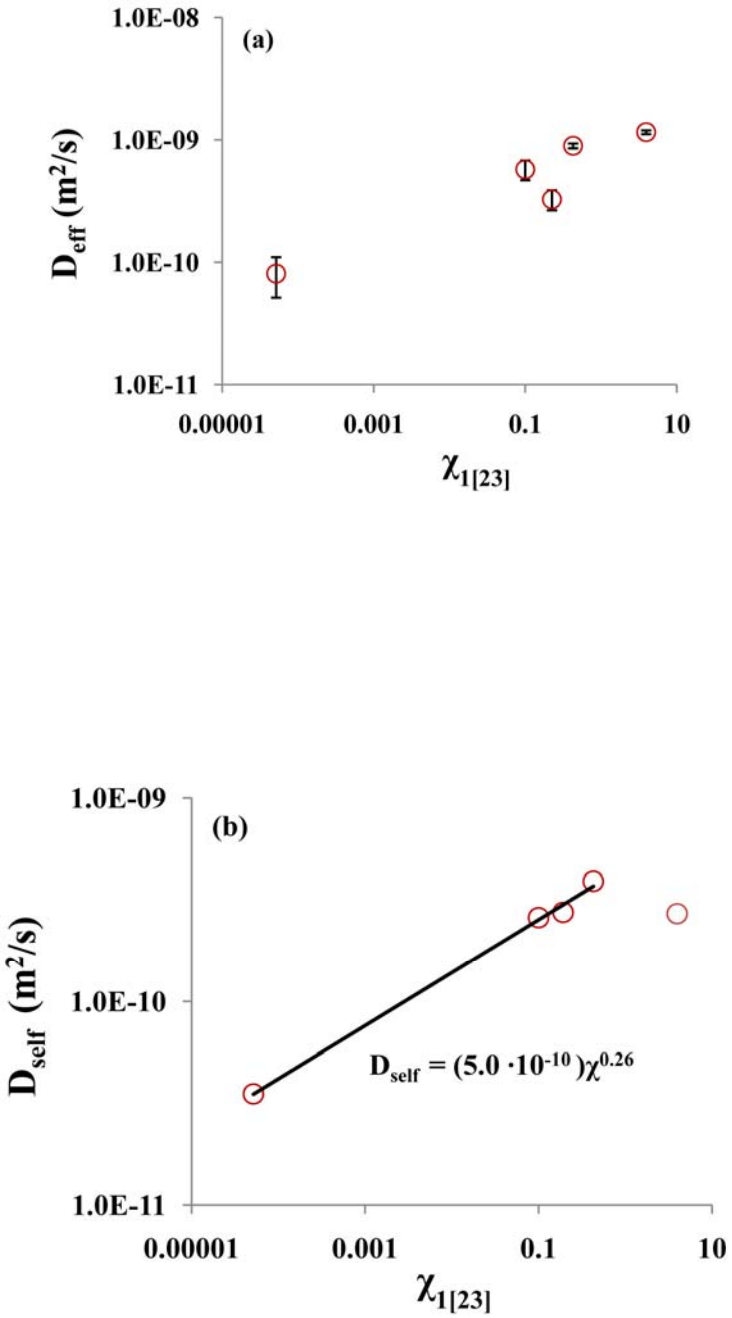

Figure 4.9 (a) D_{eff} and (b) D_{self} plotted against interaction parameter for various nonsolvents in 30 wt.% Ultem/NMP solutions.

Figure 4.9(b) shows that when D_{self} is plotted against the interaction parameter, a better correlation is obtained, since the acetone data is now aligned with the alcohols. Unfortunately, water is the outlier in this new framework; a possible explanation for this deviation is the well-known formation of the complex [NMP-$(H_2O)_2$] between NMP and water [30-32]. This complex formation is due to hydrogen bonding associative interaction which is not accounted for by the Flory-Huggins relation that was used to calculate the interaction parameters. We expect that this hydrogen bonding associative interactions may result in a decrease of the interaction parameter predicted by equation (4.1) because water-NMP hydrogen bonding mediated associative interactions likely leads to reduced nonsolvent activity in the mixture.

4.4 Conclusions

We described the construction, development and operation of a novel microfluidic device used for the measurement of the kinetics of phase inversion that occurs when a polymer solution is brought into contact with a nonsolvent. We believe that this device is an improvement on previously available methods because of good data reproducibility evident from the experimental error bars and better control of the atmosphere in our microfluidic channel. In addition, the devices are inexpensive. We reported experimental data to demonstrate the use of our device to measure the kinetics of phase inversion of polymer solutions. It was found that phase separation kinetics (PSK) is well described by a one-dimensional diffusion process with a constant effective diffusivity for the Ultem/solvent/nonsolvent systems tested. The PSK slows down with increasing polymer concentration. Attempts to correlate D_{eff} with the polymer solution bulk viscosity

revealed large discrepancies between the observed D_{eff} and theoretical predictions. These findings reveal that the microstructure of the polymer solution in relation to the size of the diffusing nonsolvent molecules is highly important in concentrated polymer solutions. Furthermore, the role of thermodynamics on the kinetics of phase separation was explored by *(a)* changing the solvent quality and *(b)* using different nonsolvents to induce phase inversion. In the former case, the solvent quality was decreased by adding cosolvent to the polymer solution, and this resulted in faster PSK. In the latter case, it was shown that PSK can be correlated with the interaction parameter, $\chi_{1[23]}$. Semi-quantitative rationalizations were offered to explain the trends we obtained for the variation of D_{eff} with polymer solution bulk viscosity and nonsolvent interaction parameters. In summary, we have shown that PSK of polymer solutions is controlled by the polymer solution microstructure and thermodynamic interaction of the component molecules of the polymer solution and nonsolvent.

In addition to the model systems investigated in this thesis, we expect that the new device will be valuable for screening the phase separation kinetics of membrane dopes with more complex compositions, including highly volatile components, viscosity modifying additives and particulates like zeolite particles for mixed-matrix membranes. For these systems, there are currently no meaningful kinetic models and other experimental methods may prove challenging. Our microfluidic device presents an effective screening tool that can be used to optimize membrane dope formulations and processing conditions during hollow fiber spinning.

4.5 References

1. Loeb S, Sourirajan S: **Sea water demineralization by means of an osmotic membrane.** In: Ser. 38. Adv. Chem., (1962):117.

2. Frommer MA, Matz R, Rosentha.U: **Mechanism of formation of reverse osmosis membranes - precipitation of cellulose acetate membranes in aqueous solutions.** *Industrial & Engineering Chemistry Product Research and Development* (1971) **10**(2):193-196.

3. Frommer MA, Lancet D: **Mechanism of membrane formation .5. Structure of membranes and its relation to their preparation conditions.** *Abstracts of Papers of the American Chemical Society* (1971) NSEP):32.

4. Matz R: **Structure of cellulose-acetate membranes .1. Development of porous structures in anisotropic membranes.** *Desalination* (1972) **10**(1):1-15.

5. Frommer MA, Messalem RM: **Mechanism of membrane formation .6. Convective flows and large void formation during membrane precipitation.** *Industrial & Engineering Chemistry Product Research and Development* (1973) **12**(4):328-333.

6. Strathmann H, Kock K, Amar P, Baker RW: **Formation mechanism of asymmetric membranes.** *Desalination* (1975) **16**(2):179-203.

7. Altena FW, Smolders CA: **Calculation of liquid liquid-phase separation in a ternary-system of a polymer in a mixture of a solvent and a nonsolvent.** *Macromolecules* (1982) **15**(6):1491-1497.

8. Strathmann H, Kock K: **Formation mechanism of phase inversion membranes.** *Desalination* (1977) **21**(3):241-255.

9. Bokhorst H, Altena FW, Smolders CA: **Formation of asymmetric cellulose-acetate membranes.** *Desalination* (1981) **38**(1-3):349-360.

10. Kang YS, Kim HJ, Kim UY: **Asymmetric membrane formation via immersion precipitation method .1. Kinetic effect.** *Journal of Membrane Science* (1991) **60**(2-3):219-232.

11. Karimi M, Albrecht W, Heuchel M, Kish MH, Frahn J, Weigel T, Hofmann D, Modarress H, Lendlein A: **Determination of water/polymer interaction parameter for membrane-forming systems by sorption measurement and a fitting technique.** *Journal of Membrane Science* (2005) **265**(1-2):1-12.

12. Reuvers AJ, Vandenberg JWA, Smolders CA: **Formation of membranes by means of immersion precipitation .1. A model to describe mass-transfer during immersion precipitation.** *Journal of Membrane Science* (1987) **34**(1):45-65.

13. Reuvers AJ, Smolders CA: **Formation of membranes by means of immersion precipitation .2. The mechanism of formation of membranes prepared from the system cellulose-acetate acetone water.** *Journal of Membrane Science* (1987) **34**(1):67-86.

14. Cheng LP, Soh YS, Dwan AH, Gryte CC: **An improved model for mass-transfer during the formation of polymeric membranes by the immersion-precipitation process.** *Journal of Polymer Science Part B-Polymer Physics* (1994) **32**(8):1413-1425.

15. Termonia Y: **Monte-carlo diffusion-model of polymer coagulation.** *Physical Review Letters* (1994) **72**(23):3678-3681.

16. Termonia Y: **Fundamentals of polymer coagulation.** *Journal of Polymer Science Part B-Polymer Physics* (1995) **33**(2):279-288.

17. Termonia Y: **Molecular modeling of phase-inversion membranes - effect of additives in the coagulant.** *Journal of Membrane Science* (1995) **104**(1-2):173-179.

18. McHugh AJ, Tsay CS, Barton BF, Reeve JL: **Comments on a model for mass-transfer during phase inversion.** *Journal of Polymer Science Part B-Polymer Physics* (1995) **33**(15):2175-2179.

19. Tsay CS, McHugh AJ: **Mass-transfer modeling of asymmetric membrane formation by phase inversion.** *Journal of Polymer Science Part B-Polymer Physics* (1990) **28**(8):1327-1365.

20. Cohen C, Tanny GB, Prager S: **Diffusion-controlled formation of porous structures in ternary polymer systems.** *Journal of Polymer Science Part B-Polymer Physics* (1979) **17**(3):477-489.

21. Wallace DW, Staudt-Bickel C, Koros WJ: **Efficient development of effective hollow fiber membranes for gas separations from novel polymers.** *Journal of Membrane Science* (2006) **278**(1-2):92-104.

22. Owen MJ, Smith PJ: **Plasma treatment of polydimethylsiloxane.** *Journal of Adhesion Science and Technology* (1994) **8**(10):1063-1075.

23. Bhattacharya S, Datta A, Berg JM, Gangopadhyay S: **Studies on surface wettability of poly(dimethyl) siloxane (pdms) and glass under oxygen-plasma treatment and correlation with bond strength.** *Journal of Microelectromechanical Systems* (2005) **14**(3):590-597.

24. Bodas D, Khan-Malek C: **Hydrophilization and hydrophobic recovery of pdms by oxygen plasma and chemical treatment - an sem investigation.** *Sensors and Actuators B-Chemical* (2007) **123**(1):368-373.

25. Keller M, Schilling J, Sackmann E: **Oscillatory magnetic bead rheometer for complex fluid microrheometry.** *Review of Scientific Instruments* (2001) **72**(9):3626-3634.

26. Zeman L, Tkacik G: **Thermodynamic analysis of a membrane-forming system water n-methyl-2-pyrrolidone polyethersulfone.** *Journal of Membrane Science* (1988) **36**(119-140.

27. Albrecht W, Weigel T, Schossig-Tiedemann M, Kneifel K, Peinemann KN, Paul D: **Formation of hollow fiber membranes from poly(ether imide) at wet phase inversion using binary mixtures of solvents for the preparation of the dope.** *Journal of Membrane Science* (2001) **192**(1-2):217-230.

28. Crank J: **The mathematics of diffusion.** In: Clarendon Press, Oxford, (1975).

29. Degennes PG: **Dynamics of entangled polymer-solutions .1. Rouse model.** *Macromolecules* (1976) **9**(4):587-593.

30. Assarsso.P, Eirich FR: **Properties of amides in aqueous solution .I. .A. Viscosity and density changes of amide-water systems .B. An analysis of volume deficiencies of mixtures based on molecular size differences (mixing of hard spheres).** *Journal of Physical Chemistry* (1968) **72**(8):2710-2719.

31. Hong PD, Huang HT: **Effect of polymer-solvent interaction on gelation of polyvinyl chloride solutions.** *European Polymer Journal* (1999) **35**(12):2155-2164.

32. Imberg A, Evertsson H, Stilbs P, Kriechbaum M, Engstrom S: **On the self-assembly of monoolein in mixtures of water and a polar aprotic solvent.** *Journal of Physical Chemistry B* (2003) **107**(10):2311-2318.

CHAPTER 5

STUDIES OF THE EFFECT OF DISPERSED PARTICLES ON THE PHASE SEPARATION KINETICS OF MEMBRANE DOPES

5.1 Introduction

Mixed-matrix membranes (MMMs) [1-8] have attracted a lot academic and industrial interest lately due to the great potentials it promises. The development of MMMs to deliver on its promises has however been slow. The major challenges encountered in the efficient development of MMMs are associated with some the paradigm shifts associated with its development and processing.

Some of the challenges encountered in incorporating particles into a polymer matrix, which must be addressed during the development of commercially viable MMMs, are briefly reiterated here. First, the particles have to be kept well-dispersed without aggregation in a polymer solution. Secondly, adequate interfacial adhesion must exist between the dispersed particles and the polymer matrix phase [8] in the finished MMM products. Thirdly, dispersed particles can significantly alter the thermodynamics and phase inversion in membrane dopes. In spite of the important role of PSK on the final structure of a membrane, the effect of dispersed particulates on PSK is yet to be explored in any detail. Therefore, we feel that the science of MMMs formation will greatly benefit from a study of the effect of dispersed particles on the phase separation kinetics of membrane dopes. An analogous study for neat polymer solutions was the subject of Chapter 4.

In this chapter, the focus would be to isolate the effect of dispersed particles on the PSK of polymer solutions. First the effect of particles on the thermodynamic quality of the membrane dopes would be investigated, followed by PSK measurements using the technique developed and described in Chapter 4. The effect of various physicochemical properties of particles on the PSK, such as (1) hydrophilicity, (2) porosity and (3) size are investigated in this chapter. These studies, to our knowledge, constitute the first of its kind in the open literature; and so it is necessarily foundational.

5.2 Materials and methods

Two aqueous silica sols are the sources of the silica particles used in the studies described in this Chapter: (i) a commercial product of Nissan Chemical America (Houston, TX) with mean particle size of 100 nm and (ii) a commercial product of Bangs Lab (Fisher, IN) with mean particle size of 320 nm. The dried forms of the particles are obtained by centrifugation of the sols to collect the particles at 9000 rpm for (i) and 7000 rpm for (ii) for 10 minutes. This is followed by a washing step by re-suspensions in DI-water and collection by centrifugation. Next the particles are re-suspended in isopropyl alcohol (ACS grade) and collected by centrifugation at 5000 to 7000 rpm for 5 to 10 minutes depending on particle size. Finally the particles are dried at 110-120 ^{o}C for at least 10 hours. The Ultem-sized forms of the 100 nm and 320 nm silica were used in these studies. The Ultem-sizing of particles [7] involves the chemical grafting of Ultem macromolecules to the particle surface, as was described in detail in Section 1.4. In addition, Ultem-sized calcined 150 nm MFI particles (USZ-MFI) were also used as dispersed particles. Finally, bare and solvothermally treated (SVT) LTA particles were

used in this study because LTA particles are the target molecular sieves for the finished MMM desired applications. The details of the solvothermal treatment method are described in the paper by Bae *et al.* [9].

The Ultem sizing of silica and MFI particles was necessary to ensure that stable suspensions with respect to aggregation could be prepared. In contrast, untreated bare LTA particles form sufficiently stable suspensions in NMP/Ultem solutions to enable PSK measurements. However, to promote interfacial adhesion between polymer and particles in the final membrane, SVT particles have been proposed for use in MMMs in place of untreated (bare) particles. The solvothermal treatment of particles involves the deposition of $Mg(OH)_2$ nano-crystals on particle surfaces. It was developed as a high yield method to match the performance of Grignard treated (GT) particles, which were developed by research efforts in the Koros group for MMM applications [10,11]. Both Ultem-sizing and solvothermal modification of particles increase the hydrophobicity of particles due to the decrease in surface silanol groups.

The polymer used in these experiments was again Ultem®, the solvent is NMP, and DI water is the nonsolvent. The suspensions were prepared to facilitate good dispersion of particles in a 30 wt.% Ultem/NMP solution. The methods used here for experimentation are described in detail in Chapter 4, where the phase separation kinetics of polymer solutions was measured. The experimentation, data collection and analysis remain the same as in this chapter; the key difference is that particles were added to the membrane dopes. The concentration of nonsolvent in MMMs dope required for phase separation is again termed C_{ps}, which was determined by titrating a fixed amount of membrane dope against small quantities of nonsolvent at a time until sample becomes irreversibly turbid.

The lowest amount of nonsolvent for which the membrane dope remained irreversibly turbid was used to calculate C_{ps}.

5.3 Effect of particles on membrane dope thermodynamics

The primary emphasis in this chapter is to study the effect of addition of particles to membrane dopes on the kinetics of phase separation. However, the focus of the current section is to first study the effect of particles on the equilibrium thermodynamics of the membrane dopes. In Chapter 4, it was shown that the thermodynamics of the components of a polymer solution and the phase inversion inducing nonsolvent play an important role in the kinetics of phase inversion. Therefore it is appropriate in the present study to precede the experiments on PSK with a study on the thermodynamics of phase separation. In Chapter 4, it was also shown that the effect of membrane dope components on the thermodynamics can be quantified in terms of C_{ps}. To assess the effect of particle addition on the thermodynamic quality of a MMMs dopes with respect to water (the phase separation–inducing nonsolvent), C_{ps} values are reported for suspensions of different particles types in Ultem/NMP solutions in Table 5.1. The C_{ps} values reported are approximate since they determined by visual turbidity measurements. The measurements are within ±0.20 wt.% error of the average values reported in Table 5.1. The first two rows of Table 5.1 show the C_{ps} values for pure Ultem/NMP solutions without dispersed particles. This implies there is very little change in C_{ps} value over this range of polymer concentration as discussed in Chapter 4.

Table 5.1 Effect of dispersed particles on C_{ps} values for Ultem/NMP suspensions of particles using water as nonsolvent.

Dispersed phase	**Suspending phase**	**Particle loading (wt. %)**	C_{ps} **(wt. %)**
None	20 wt.% Ultem/NMP	0	**3.20**
None	30 wt.% Ultem/NMP	0	**3.00**
Bare LTA	20 wt.% Ultem/NMP	1	**3.62**
Bare LTA	20 wt.% Ultem/NMP	2	**3.64**
Bare Silica	30 wt.% Ultem/NMP	1	**3.34**
USZ Silica	30 wt.% Ultem/NMP	1	**3.30**
USZ MFI	30 wt.% Ultem/NMP	2	**2.66**
USZ MFI	30 wt.% Ultem/NMP	5	**2.64**

A comparison of the C_{ps} values for bare LTA particles suspended in a 20 wt.% Ultem/NMP solution with the results for pure polymer solutions reveals that LTA particles cause an increase in C_{ps} value for the pure 20 wt.% Ultem/NMP polymer solution. This result can be interpreted as the presence of LTA particles enhancing the tolerance of the polymer solution to water, the nonsolvent in this experiment. A possible explanation may be due to the hydrophilic nature of LTA, which allows it to selectively

adsorb water from the mixture, thus decreasing the amount of water available in the mixture for phase separation by liquid-liquid demixing. Consequently, LTA increases the tolerance of the dope to water as experimentally observed in Table 5.1.

Silica particles are nonporous and less hydrophilic than LTA. It is reasonable to expect that the tolerance for water in a polymer solution suspension of silica particles should be less than for suspensions of LTA particles. A comparison of the C_{ps} value for silica particles suspended in a 30 wt.% Ultem/NMP solution reveals that silica particles do cause an increase in C_{ps}, albeit to a lesser extent than for LTA particles. C_{ps} value for USZ-silica particles are similar to bare silica particles because a relatively small proportion of the hydrophilic silanol groups on silica are capped after Ultem-sizing. This assertion is supported by the fact that the measured zeta potential values for bare and USZ-silica in NMP (which is a function of the number of acidic silanol groups on particle surface) was shown to be similar in Section 2.1.

Finally, a comparison of the C_{ps} value for USZ-MFI particles suspended in a 30 wt.% Ultem/NMP solution and the corresponding pure polymer solution reveals that MFI particles cause a decrease in C_{ps} value. This finding indicates that the inclusion of MFI particles in the dope decreases the tolerance for nonsolvent (water). The observation can be explained by the fact that MFI is relatively hydrophobic and prefers to adsorb organic molecules like NMP rather than water. In Chapter 3, it was shown that MFI has large enough window to allow absorption of NMP into its internal pores, thereby raising the polymer concentration in solution. Finally, it was shown in Chapter 4 that increasing the polymer concentration in Ultem/NMP solutions results in a decrease in C_{ps}, especially above 30 wt.% polymer.

5.4 Effect of particles on the PSK of membrane dopes

In this section, the effect of dispersed particles on phase separation in a membrane is studied. It is expedient to systematically isolate the important physicochemical properties of dispersed particles which affect the PSK of MMM dopes. Each of these important parameters is isolated and discussed one after the other in this section.

In the preceding section, it was shown that the chemical nature (*i.e.* hydrophobic or hydrophilic) of the particles with respect to the other components of the membrane forming system affects the minimum nonsolvent concentration required for phase separation for the system, C_{ps}. From Chapter 4 it is known that C_{ps} plays a key role in determining phase separation kinetics, because it defines how much nonsolvent is needed. However, C_{ps} does not determine how fast the nonsolvent is being transported. Therefore, in this section we will investigate the phase separation kinetics in order to identify the effect of particles on mass transfer in the membrane dopes during phase inversion.

First, we looked at the addition of silica spheres, which are monodisperse non-porous spheres. Figure 5.1 show the effective PSK diffusivities for suspensions as a function of the particle concentration for 100 nm and 320 nm USZ-silica. For the 100 nm particles, there was an initial decrease in PSK rate at low particle concentrations and then an increase at concentrations greater than 3 wt.%. On the other hand, the addition of 320 nm particles results in a monotonic decrease of the effective diffusion coefficient at all concentrations investigated. This surprising result suggests that there are competing effects. We anticipated that presence of non-porous particles in the dope would be a reduction of non-solvent diffusivity due to physical hindrance; this is indeed observed for

the larger USZ-silica particles. The unexpected upturn for 100 nm particles must be a size effect and we hypothesize that surface diffusion of water along the relatively hydrophilic silica surface is the underlying mechanism. The smaller 100 nm particle possess 3.2 times more surface area per unit volume than the 320 nm particles. Apparently, surface diffusion can overcome the physical hindrance of solid particles, provided that the surface area per unit volume is large enough, thereby enhancing the phase separation kinetics. Note that at 10 wt.% loading of 100 nm particles, the effective diffusion coefficient is faster than for the pure polymer solution.

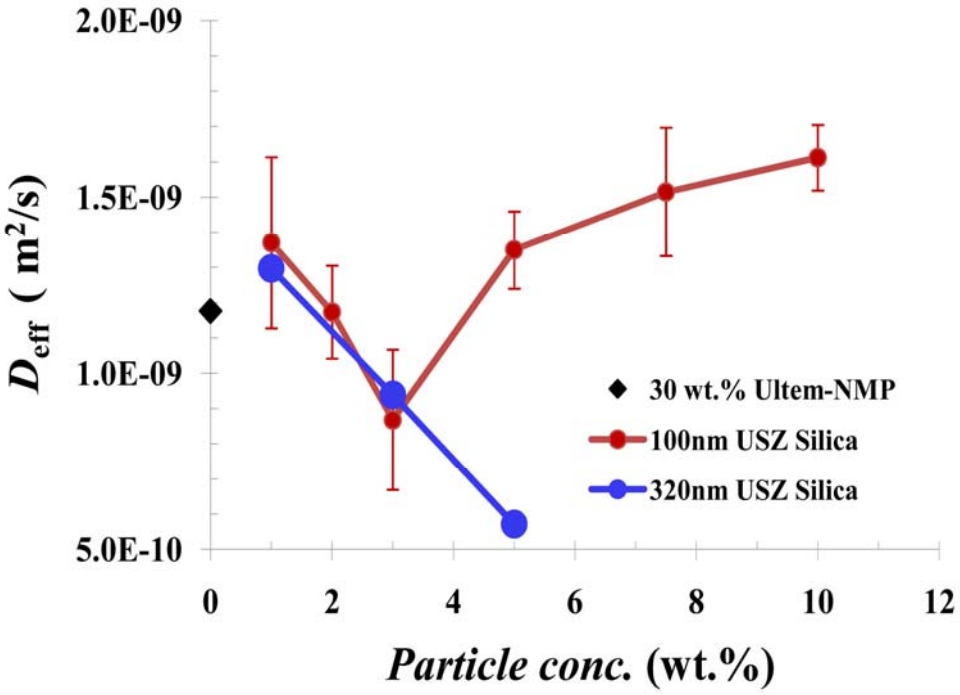

Figure 5.14 PSK as a function of particle concentration in 30 wt.% Ultem/NMP solutions, using water as the nonsolvent, for 100 nm and 320 nm USZ-silica particles.

While the silica particles were solid, the zeolite particles used for mixed matrix membranes are invariably porous. The zeolite particles used here are LTA and MFI zeolite particle. From the rheological studies in Chapter 2 and Chapter 3, we found that NMP solvent is absorbed into the pore spaces of MFI, while no such effect was found for LTA particles. LTA particles are however known to be hydrophilic, adsorbing water molecules that are smaller than NMP molecules. It is therefore conceivable that LTA is porous to water but not to NMP. The implications of porosity on PSK can be quite pronounced. Figure 5.2 shows PSK as function of particle concentration for bare and SVT LTA particles in comparison to the 320 nm silica particles in 30 wt. % Ultem/NMP solutions. The average particle size of LTA particles is comparable to 320nm silica. The graph shows that adding porous LTA particles to the membrane dope enhances the phase separation rate while the solid silica particles retard PSK. This result can be explained based on the fact that LTA being porous to diffusing water molecules provide additional internal surface area for nonsolvent diffusion that is not available in nonporous silica particles.

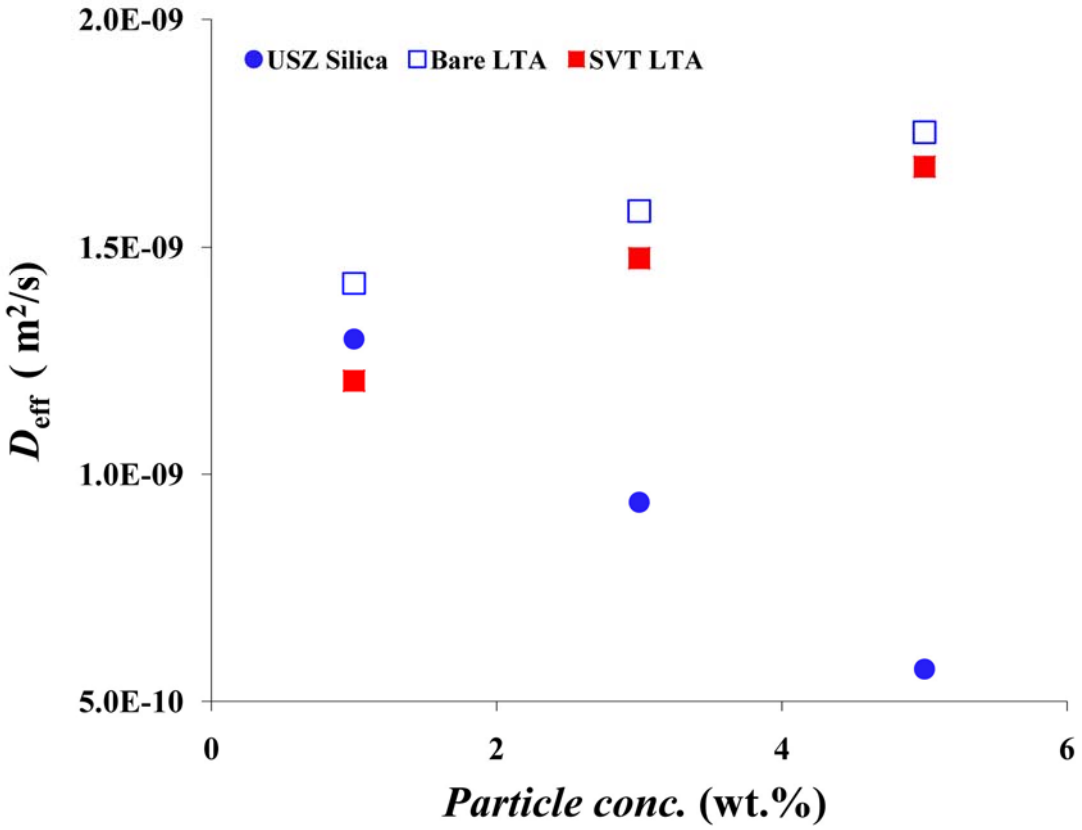

Figure 5.15 PSK as a function of particle concentration in 30 wt.% Ultem/NMP solutions, using water as the nonsolvent, for USZ-silica, bare and SVT-LTA particles.

Figure 5.3 shows effective diffusivities of phase separation for USZ-MFI, bare LTA and USZ silica particles in 30 wt.% Ultem/NMP solutions as a function of particle concentration. The emphasis here is to compare the PSK of porous MFI zeolite particles with the results for porous LTA zeolite particles. It can be seen that although MFI zeolites are porous, they actually suppress PSK instead of accelerating it like porous LTA particles. This behavior can be explained based on the differences in chemical nature of the two porous zeolites. MFI absorbs NMP when suspended in Ultem/NMP solutions, as

we established in Chapter 3. The implication of the internal pore sites being filled up with NMP molecules is that it precludes nonsolvent diffusion through the MFI particles. Consequently, the effect of MFI particles on PSK resembles the trend observed for nonporous silica particles.

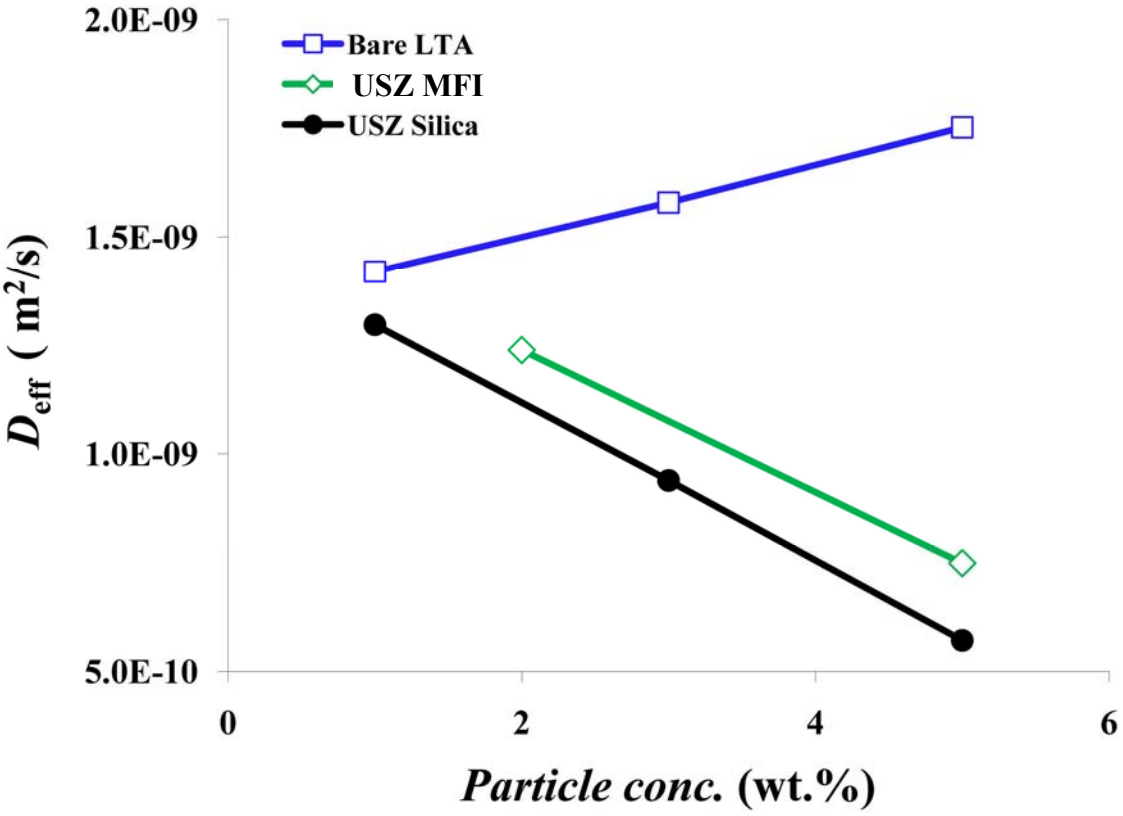

Figure 5.16 PSK as a function of particle concentration in 30 wt.% Ultem/NMP solutions, using water as the nonsolvent, for bare LTA, USZ–MFI and USZ-silica particles.

5.5 Conclusions

Our studies show that the incorporation of zeolite particles into membrane dopes changes both the thermodynamics and the kinetics of phase separation of the dope when it comes into contact with a nonsolvent.It was found that the equilibrium thermodynamics of the dope is altered based on the degree of hydrophilicity of the zeolite particles with respect to water as nonsolvent. When the particles are hydrophilic they make the membrane dopes more tolerant to water (the nonsolvent) with respect to phase separation and vice versa. This tolerance can be quantified in terms of the C_{ps} value which in turn affects the kinetics of phase separation.

The ultimate effect of particles on PSK is more subtle, because mass transfer plays a role in addition to equilibrium phase behavior. It was found that PSK can be enhanced by dispersing particles with smaller sizes. This we found was due to the increased surface area furnished by smaller particles for enhanced surface diffusion. It was also found that in the case of LTA with hydrophilic pore walls there is much greater surface area available for surface diffusion so that PSK is greatly enhanced. For porous MFI zeolite particles whose pore volume is filled up due to the selective adsorption of solvent from the suspending polymer solution rendering the pore wall surface unavailable, it was found that PSK is decreased just like for a solid nonporous particle.

This report constitutes a foundational study on the effect of zeolite particles on the PSK of MMM dopes. We hope this report would incentivize experimentalists and theoreticians to conduct more investigations in this relatively infantile aspect of synthetic membranes development.

5.6 References

1. Mahajan R, Koros WJ: **Factors controlling successful formation of mixed-matrix gas separation materials.** *Industrial & Engineering Chemistry Research* (2000) **39**(8):2692-2696.

2. Mahajan R, Koros WJ: **Mixed matrix membrane materials with glassy polymers. Part 1.** *Polymer Engineering and Science* (2002) **42**(7):1420-1431.

3. Mahajan R, Koros WJ: **Mixed matrix membrane materials with glassy polymers. Part 2.** *Polymer Engineering and Science* (2002) **42**(7):1432-1441.

4. Kulprathipanja S: **Mixed matrix membrane development.** In: *Advanced membrane technology.* 984. Li NN, Drioli E, Ho WSW, Lipscomb GG (Eds), (2003):361-369.

5. Husain S: **Mixed matrix dual layer hollow fiber membranes for natural gas separation.** In: (2006).

6. Chung TS, Jiang LY, Li Y, Kulprathipanja S: **Mixed matrix membranes (mmms) comprising organic polymers with dispersed inorganic fillers for gas separation.** *Progress in Polymer Science* (2007) **32**(4):483-507.

7. Husain S, Koros WJ: **Mixed matrix hollow fiber membranes made with modified hssz-13 zeolite in polyetherimide polymer matrix for gas separation.** *Journal of Membrane Science* (2007) **288**(1-2):195-207.

8. Liu JQ, Bae TH, Qiu WL, Husain S, Nair S, Jones CW, Chance RR, Koros WJ: **Butane isomer transport properties of 6fda-dam and mfi-6fda-dam mixed matrix membranes.** *Journal of Membrane Science* (2009) **343**(1-2):157-163.

9. Bae TH, Liu JQ, Lee JS, Koros WJ, Jones CW, Nair S: **Facile high-yield solvothermal deposition of inorganic nanostructures on zeolite crystals for mixed matrix membrane fabrication.** *Journal of the American Chemical Society* (2009) **131**(41):14662-14663.

10. Shu S, Husain S, Koros WJ: **A general strategy for adhesion enhancement in polymeric composites by formation of nanostructured particle surfaces.** *Journal of Physical Chemistry C* (2007) **111**(2):652-657.

11. Shu S, Husain S, Koros WJ: **Formation of nanostructured zeolite particle surfaces via a halide/grignard route.** *Chemistry of Materials* (2007) **19**(16):4000-4006.

CHAPTER 6

CONCLUDING REMARKS

6.1 Conclusions

The research described in this thesis has resulted in the following major contributions and achievements:

Rheology

- We have developed models to account for effects of solvent absorption on the viscosity of suspensions of porous particles in polymer solutions; the concepts can be combined with any viscosity model that successfully describes the particle contribution to suspension viscosity as a function of particle volume fraction (*i.e.* Krieger-Dougherty).
- We proposed and validated an experimental method to quantify the amount of solvent absorbed in zeolite suspensions by directly comparing the rheology of suspensions of porous and non-porous zeolite particles.
- We also found that electroviscous effects control the rheology of suspensions of siliceous and zeolite particles in aqueous and other polar solvents in the semi-dilute and concentrated regime.
- Our results show that the intrinsic viscosity of siliceous particles in NMP varies with salt contents and the type of medium. It was impossible to explain the observed anomalous rheology based on the dry volume of the particles. We found that boundary layers of significant thickness exist around siliceous particles

suspended in NMP and that they dictate the rheology of dilute suspensions of siliceous particles in NMP.

Phase separation kinetics (PSK)

- A novel microfluidic device was designed and constructed that enables quantitative measurements of the kinetics of phase separation during the formation of polymer based membranes by a wet phase inversion process.
- The microfluidic device was successful employed to investigate the phase separation kinetics of Ultem/NMP/water membrane forming systems.
- From our phase separation kinetics studies it was found that the membrane dope solution microstructure and thermodynamic interactions between the components of the membrane forming system are the key control parameters.
- We propose for the first time an order of magnitude estimate for PSK that uses the self-diffusion coefficient of the nonsolvent in the solvent and a measure for the thermodynamic interactions (C_{ps}) in an adapted version of a Fickian 1-D transient diffusion model.
- Studies conducted on the effects of dispersed particles on the PSK of membrane dopes revealed that the degree of hydrophilicity, pore window size and the available surface area for transport are the important features of suspended particulates that affect PSK. Our experiments showed that PSK is slowed down by the addition of MFI zeolites to dopes, while the addition of LTA particles enhances PSK. In the case of MFI, the internal pore surface is not available for surface diffusion, because its pores are filled with NMP solvent absorbed from the medium. In contrast, LTA particles possess very large surface area for surface

diffusion, arising from both the internal pore surfaces and external surface, and thus PSK is enhanced by a factor of 1.7 at a modest 5 wt.% loading of LTA particles.

These major contributions are described in greater details in the next two subsections.

6.1.1 Conclusions from Rheology studies

We presented data and predictive models for the shear rheology of suspended zeolite particles in polymer solutions. It was found that zeolite suspensions have relative viscosities that dramatically exceed the Krieger-Dougherty predictions for hard sphere suspensions. Our investigations show that the major origin of this discrepancy is the selective absorption of solvent molecules from the suspending polymer solution into the zeolite pores. This effect raises both the polymer concentration in the suspending medium and the particle volume fraction in the suspension. Consequently, both the viscosity of the polymer solution and the particle contribution to the suspension viscosity are greatly increased. We propose a predictive model for the viscosity of porous zeolite suspensions by incorporating a solvent absorption parameter, α, into the Krieger-Dougherty model. We experimentally determined the solvent absorption parameter by comparing viscosity data for suspensions of porous and non-porous MFI zeolite particles. Our result (α = 0.18) is in good agreement with the theoretical pore volume of MFI particles, which corresponds to $\alpha = 0.175$.

In our quadratic fit to the viscosity data of semi-dilute concentrations of uncalcined MFI in polymer solutions we found a very high intrinsic viscosity and a second-order interaction coefficient that cannot be explained solely on the basis of the nonsphericity of

MFI particles. We investigated this observation in more detail by studying the rheology and structural properties of model suspensions of spherical silica particles in NMP solvent with and without added salts, water and dissolved polymer. The simplified model systems enabled us to isolate the contributions of various components, which resulted in some insightful findings. First of all, we found that the silica particles are highly charged in NMP; one consequence is a very high intrinsic viscosity, and that the intrinsic viscosity is lowered significantly by addition of dissolved salt, in agreement with the hypothesis of electrostatic screening effects. However, the experimental results could not be predicted on the basis of simple theories for primary electroviscous effects[1,2] in aqueous suspensions. Our investigation further showed that by increasing the concentration of water in the suspending NMP medium, we could greatly change the intrinsic viscosity. This result suggested the presence of specific interactions arising from the interplay between hydrogen bonding, intermolecular forces and the colloidal forces of the components of the suspension. We propose that the specific interactions are manifested in the form of an immobilized boundary layer around the particles. In the semi-dilute concentration regime, secondary electroviscous effects seem to control the rheology. This is manifested in the form of an effective collision diameter greater than the hard sphere diameter of the particles. Prediction of the effective collision diameter from simple theories on the secondary electroviscous effect[3,4] is in good agreement with our experimental observation. In conclusion, the rheological implications of charged siliceous particles and the low salt concentrations in NMP mediated suspensions are such that the effective collision diameters of the particles are much larger than the dry particle

size. This effect we demonstrated can be predicted by electroviscous models in semi-dilute and concentrated systems.

6.1.2 Conclusions from PSK studies

We described the construction, development and operation of a novel microfluidic device used for the measurement of the kinetics of phase inversion that occurs when a polymer solution is brought into contact with a nonsolvent bath. We believe that this device is a significant improvement on previous methods because of good data reproducibility (evident from the small experimental error bars) and much improved control of the atmosphere in which the phase separation occurs in our microfluidic channel. In addition, the devices are inexpensive. We reported experimental data to demonstrate the use of our device to measure the kinetics of phase inversion of polymer solutions. It was found that phase separation kinetics (PSK) is well described by a one-dimensional diffusion process with a constant effective diffusivity for all PEI/solvent/nonsolvent systems tested, with and without added particles. The PSK slows down with increasing polymer concentration; PSK decreases by a factor of 30 between 20 wt.% and 35 wt.% Ultem/NMP solutions. Attempts to correlate D_{eff} with the polymer solution bulk viscosity revealed large discrepancies between the observed D_{eff} and theoretical predictions. These findings reveal that the microstructure of the polymer solution in relation to the size of the diffusing nonsolvent molecules is the important factor that determines PSK in concentrated polymer solutions. The practical significance of this is that, an estimate for D_{eff} is determined by the solvent viscosity and not the bulk viscosity of the polymer solution. Furthermore, the role of thermodynamics on the kinetics of phase separation

was explored by *(a)* changing the solvent quality through the addition of a small amount of nonsolvent as co-solvent (up to 15 wt.% ethanol in NMP) and *(b)* using different nonsolvent (water, methanol, ethanol, IPA and acetone) to induce phase inversion. In the former case, the addition of co-solvent to the polymer solution resulted in faster PSK and this effect increases with the polymer concentration in solution. It was found that the addition of a modest 10 wt.% ethanol to a 35 wt.% Ultem/NMP solution increases the effective diffusion coefficient by a factor 4. In the latter case, it was shown that PSK can be correlated with the thermodynamic interaction parameter between the components in the ternary polymer/solvent/nonsolvent system, $\chi_{1[23]}$. Semi-quantitative rationalizations were offered to explain the trends we obtained for the variation of D_{eff} with polymer solution bulk viscosity and nonsolvent interaction parameters. In conclusion, we have shown that PSK of polymer solutions is controlled by the polymer solution microstructure and thermodynamic interaction of the component molecules of the polymer solution and nonsolvent.

The efficient development of mixed matrix hollow fiber membranes for gas separations by phase inversion of polymer solutions with added zeolite particles requires understanding of the effects of the new solid component on the phase separation kinetics, which is critical for large-scale processing. Our studies show that the incorporation of zeolite particles into membrane dopes changes both the thermodynamics (position of the binodal in the phase diagram) and the kinetics of phase separation (effective nonsolvent diffusivity) of the dope when the composite dope comes in contact with the nonsolvent.

Our studies show that the thermodynamics of the dope is altered based on the degree of hydrophilicity of the zeolite particles with respect to water as nonsolvent. When the

particles are hydrophilic, they make the membrane dopes more tolerant to water (the nonsolvent) with respect to phase separation and vice versa. This tolerance can be quantified in terms of the minimum nonsolvent concentration needed to induce phase separation, C_{ps}, which in turn affects the kinetics of phase separation.

The ultimate effect of particles on PSK is a little more subtle. It was found that PSK can be enhanced in suspensions with particles of smaller sizes. We hypothesize that this effect is due to the increased surface area furnished by smaller particles, resulting in enhanced surface diffusion of nonsolvent along the particles. It was also found that in the case of LTA, which is porous and has hydrophilic pore walls, there is a much greater surface area available for surface diffusion so that PSK is more strongly enhanced than for non-porous hydrophilic silica. For porous MFI zeolite particles, whose pore volume is filled up due to the selective adsorption of solvent from the suspending polymer solution, it was found that PSK is decreased just like for a solid nonporous particle; the filling of pores with solvent hinders nonsolvent diffusion through the pores.

6.2 Recommendations

The research described in this thesis has resulted in answers to many questions it set out to investigate, but in the process, some other promising research questions have been identified.

1. In my work on correlating the polymer solution microstructure and components thermodynamics with the PSK of polymer solutions, we identified promising correlations. I believe it may be possible to generalize our concepts to any arbitrary nonsolvent/solvent/polymer combination. We found that PSK is controlled by *(a)* the

thermodynamic interaction parameters and *(b)* the microstructure (mesh size) of polymer in the concentrated solution. It was impossible to determine the exact PSK scaling with the polymer solution microstructure[5] because we did not perform experiments with different MWs of the same polymer at a fixed concentration, which would be the logical next step. Such experiments would enable the correlation of PSK with the hindrance factor on diffusing nonsolvent due to the presence of dissolved macromolecules in solution.

2. During the preparation of asymmetric membranes, membrane spinning researchers prefer to use a dry inversion phase, during which a volatile component of the membrane dope vaporizes, before the wet phase inversion stage that was the focus in this thesis. In this two-step process, the topmost layer of the skin is already formed during the dry phase[6-8] due to a local increase in polymer concentration. Although this method of phase inversion was not investigated in my thesis, I believe that the microfluidic PSK device developed in this thesis can be adapted to study the effects of controlled solvent evaporation on PSK. In this function, the microfluidic device would be pre-saturated with the vapor of the volatile solvent component of the membrane dope. After the sample is loaded, a switch valve maybe used to continuously flush the microfluidic device with dry air at low flow rates. Subsequently the thickness of the phase inverted zone resulting from solvent evaporation is tracked as a function of time.
3. In Chapter 1, I went to great lengths to argue that the PSK and thermodynamics of membrane dopes kinetics can be used to tune the structures formed in phase inversion membranes. For gas separation membranes, which were the focus of my thesis, there

is not sufficient incentive to control the pore size distribution, because the selectivity of the membrane originates primarily from the skin layer which is formed by gelation. However, for membranes like MF and UF membranes, the pore size regime exploited for separation is much larger than in GS membranes. The range of pore sizes used in UF and MF membranes[9-11] can be formed by nucleation and growth. I believe that studies on the control of pore sizes by a careful analysis of the role of PSK and thermodynamics of the membrane dope components data on the pore size distribution would greatly advance the science of porous structure formation in membranes.

4. Macrovoids[12] are known to compromise the structural integrity of membranes. The PSK device developed in this thesis may be used to empirically correlate numerical PSK values, viscosity and some measure of thermodynamics (e.g. interaction parameters values or C_{ps} values described in this thesis) with membranes in which there are no macrovoids. To achieve this purpose: one should measure the viscosity, PSK values, C_{ps} values (and/or calculate interaction parameters) and obtain SEM images of immersion precipitation membrane films made from (a) hydrophobic polymer (b) hydrophilic polymer of comparable MW, at different polymer concentrations in a fixed solvent/nonsolvent pair. From a match, of the four parameters with the incidence of macrovoids formation, it may be possible to set semi-quantitative guidelines for the elimination of macrovoids.

6.3 References

1. Watterson IG, White LR: **Primary electroviscous effect in suspensions of charged spherical-particles.** *Journal of the Chemical Society-Faraday Transactions Ii* (1981) **77**(1115-1128.

2. Booth F: **The electroviscous effect for suspensions of solid spherical particles.** *Proceedings of the Royal Society of London Series a-Mathematical and Physical Sciences* (1950) **203**(1075):533-551.

3. Russel WB: **Low-shear limit of secondary electroviscous effect.** *Journal of Colloid and Interface Science* (1976) **55**(3):590-604.

4. Russel WB: **Review of the role of colloidal forces in the rheology of suspensions.** *Journal of Rheology* (1980) **24**(3):287-317.

5. Degennes PG: **Dynamics of entangled polymer-solutions .1. Rouse model.** *Macromolecules* (1976) **9**(4):587-593.

6. Broens L, Altena FW, Smolders CA, Koenhen DM: **Asymmetric membrane structures as a result of phase-separation phenomena.** *Desalination* (1980) **32**(1-3):33-45.

7. Wijmans JG, Baaij JPB, Smolders CA: **The mechanism of formation of microporous or skinned membranes produced by immersion precipitation.** *Journal of Membrane Science* (1983) **14**(3):263-274.

8. Mulder MHV, Hendrikman JO, Wijmans JG, Smolders CA: **A rationale for the preparation of asymmetric pervaporation membranes.** *Journal of Applied Polymer Science* (1985) **30**(7):2805-2820.

9. Broens L, Koenhen DM, Smolders CA: **Mechanism of formation of asymmetric ultrafiltration and hyperfiltration membranes.** *Desalination* (1977) **22**(1-3):205-219.

10. Koenhen DM, Mulder MHV, Smolders CA: **Phase separation phenomena during formation of asymmetric membranes.** *Journal of Applied Polymer Science* (1977) **21**(1):199-215.

11. Broens L, Altena FW, Smolders CA, Koenhen DM: **Asymmetric membrane structures as a result of phase separation phenomena.** *Desalination* (1980) **32**(33-45.

12. Smolders CA, Reuvers AJ, Boom RM, Wienk IM: **Microstructures in phase-inversion membranes .1. Formation of macrovoids. 73**:Abs 259-275.

APPENDIX A

DERIVATION OF EQUATIONS FOR SOLVENT ABSORPTION IN POROUS PARTICLES SUSPENSIONS

A. Model for increased polymer concentration

Using a basis of 1g zeolite suspension

We define fractional adsorption parameter, $\alpha = \dfrac{\text{weight of adsorbed solvent}}{\text{weight of dry zeolite}}$

Density of zeolite: ρ_z

Density of zeolite suspension: ρ_{susp}

Weight fraction of zeolite in suspension: w_z

Weight fraction of suspending medium in suspension: $1 - w_z$

Weight fraction of polymer in suspending medium (before absorption): w_p

Weight fraction of polymer in suspension: $w_p\left(1 - w_z\right)$

Weight fraction of solvent in suspension: $(1-w_z)(1-w_p)$

After solvent absorption

Weight of solvent absorbed in zeolite particles: $\alpha \cdot w_z \cdot m_{susp}$

Weight of solvent left in suspending phase: $(1-w_p)(1-w_z) \cdot m_{susp} - \alpha \cdot w_z \cdot m_{susp}$

Corrected Ultem weight fraction in suspending phase:

$$w_{p,eff} = \frac{w_p(1\text{-}w_z)}{w_p(1\text{-}w_z) + (1\text{-}w_p)(1\text{-}w_z)\text{-}\alpha w_z} = \frac{w_p(1\text{-}w_z)}{(1\text{-}w_z)\text{-}\alpha w_z}$$

B. Density of suspension from measured polymer solution density

Densities of suspension and zeolite particles are ρ_{susp} and ρ_Z respectively

$$\rho_{susp} = \frac{1}{[\text{vol. of polymer solution}]+[\text{vol. of zeolite in solution}]\text{-}[\text{vol. of absorbed solvent}]}$$

$$\frac{\rho_{susp}}{\rho_z} = w_z + (1-w_z)\frac{\rho_z}{\rho_{psol}} - \alpha w_z \frac{\rho_z}{\rho_{solv}}$$

C. Model for Increased Zeolite concentration

Weight of absorbed NMP: $\alpha \cdot w_z \cdot m_{susp}$

Volume of absorbed NMP: $\frac{\alpha \cdot w_z \cdot m_{susp}}{\rho_{solv}}$

Volume of particles: $\frac{w_z \cdot m_{susp}}{\rho_z}$

Volume of suspension: $\frac{m_{susp}}{\rho_{susp}}$ Effective zeolite volume fraction:

$$\varphi_{z,eff} = \frac{\left(w_z \cdot m_{susp} / \rho_z\right)}{\left(m_{susp} / \rho_{susp}\right) - \left(\alpha \cdot w_z \cdot m_{susp} / \rho_{solv}\right)} = \frac{w_z}{\frac{\rho_z}{\rho_{susp}} - \alpha w_z \frac{\rho_z}{\rho_{solv}}}$$

$$\varphi_{z,eff} = \frac{w_z}{w_z + \left(1 - w_z\right)\frac{\rho_z}{\rho_{psol}} - 2\alpha w_z \frac{\rho_z}{\rho_{solv}}}$$

VITA

Kayode Olanrewaju was born in Kaduna, Nigeria, as a fifth child in a family of seven children. He had primary and secondary school education in Lagos, Nigeria. He obtained a BS in chemical engineering from New Mexico Institute of Mining and Technology in May, 2006. He completed a PhD dissertation in chemical engineering at the Georgia Institute of Technology under the supervision of Dr. Victor Breedveld in December, 2010. He loves scientific research because he gets to learn from the laws of nature how things work, and how to implement novel functionalities and create new things. In addition to his research activities in the area of the rheology of complex fluids, colloidal interactions, polymer physics and gas separation membranes he play tennis and soccer, listen to a fair bit of music and political commentaries.